Feasibility of EcoGrout

Modelling of in-situ calcite precipitation and CO_2 degassing in porous medium

Master Thesis

Faculty of Geosciences
Utrecht University

By

J. H. van Lopik

Supervisors

prof. dr. ir. S.M. Hassanizadeh

dr. N. Hartog

dr. A. Marsman

Universiteit Utrecht

Deltares
Enabling Delta Life

Abstract

EcoGrout is a new method to strengthen and stabilize unconsolidated sediments in the subsurface. This method is based solely on chemically induced calcite precipitation. In situ precipitation of calcite will result in cementation of the grain particles during the EcoGrout process. Consequently, it will also decrease the porosity and thereby the permeability of the soil. The basic application of Ecogrout involves use of a solution with a designated degree of calcite saturation and CO_2 pressure by the use of calcium chloride ($CaCl_2$), sodium bicarbonate ($NaHCO_3$) and pH adjustments to control both the amount and rate of calcite precipitation. This modelling study explores the conditions under which precipitation amounts and rates can be controlled and prevent clogging in the vicinity of the injection point, whilst ensuring sufficient radii of influence for the Ecogrout treatment. To analyze this EcoGrout process, a model for multiphase flow of multiple gas-components and water (STOMP-WNE) with a reactive batch chemistry module (ECKEchem) is used. This model is extended to account for porosity and permeability alteration over time during calcite precipitation. Also a kinetic equation for degassing of CO_2 proposed by Zhao et al. (2011) is implemented.

Simulation of an injection pulse with an EcoGrout solution at calcite equilibrium at a pCO_2 of 5.1 atm was done to investigate the behavior of CO_2 degassing in the porous medium and its effect on calcite precipitation. Several cases with different mechanical properties, kinetic properties or EcoGrout solution configurations are presented to investigate its sensitivity on CO_2 degassing and calcite precipitation.

Precipitation of calcite is controlled by the degassing of CO_2. Due to degassing of CO_2 the alkalinity and pH increase. Consequently, the injected EcoGrout solution becomes supersaturated with respect to calcite and calcite precipitation starts. Since the pore volume reduction obtained from one injection pulse is low, many injections are required to obtain the required cementation within the soil. Large injection radii can be achieved when the injection pressure is higher than the pCO_2 of the solutions and no degassing occurs during the injection. In addition, the degassing rates of CO_2 are sufficiently low that injection at CO_2 supersaturation is also feasible.

Notation

Roman symbols

A	effective surface area of the mineral [m^2/m^3
a_i	aqueous activity of species i [mol/m^3]
a_j	aqueous activity of defined equilibrium species j [mol/m^3]
b_i	kinetic equation stoichometric coefficient of species i
C_i	concentration of species i [mol/m^3]
$C_{tc\,j}$	concentration of total component species j [mol/m^3]
$C_{tk\,j}$	concentration of total kinetic species j [mol/m^3]
D	hydrodynamic dispersion coefficient [m^2/s]
Da	Damkölher number [-]
D_m	diffusion coefficient [m^2/s]
d_{50}	median grain diameter [m]
E_a	activation energy [J/mol]
e_i	stochiometric coefficient of equilibrium species i
f_i	conservation equation stoichometric coefficient of species i
g	gravity constant equals 9.81 [m^2/s]
H	Henry's constant [atm]
IAP	ion activity product [mol^2/L^2]
ICP	ion concentration product [mol^2/L^2]
k	kinetic rate constant [s^{-1}]
k_b	backward kinetic rate coefficient
k_{calc}	kinetic rate constant for the precipitation-dissolution reaction [mol/ m^2 s]
k_{calc}'	lumped kinetic rate constant for the precipitation-dissolution reaction [mol/m^3 s]
$K_{eq\,j}$	equilibrium constant of equilibrium equation j
k_f	forward kinetic rate coefficient
k_g	kinetic rate constant for the degassing-dissolution reaction [s^{-1}]
K_H	Henry's constant [L atm/mol]
k_l	average mass transfer coefficient between the liquid-gaseous phase [m^3/ m^2s]
k_{ref}	kinetic rate constant for the precipitation-dissolution reaction at reference temperature [mol/ m^2 s]
k_{rl}	relative aqueous permeability [-]
k_{rg}	relative gas permeability [-]
k_{ry}	relative permeability for phase y [-]
K_{sp}	solubility product of calcite [mol^2/L^2]
m	dimensionless van Genuchten fitting parameter (1-1/n) [-]
m_i	mass source rate for species i [mol/m^3 s]
m_y	mass source rate for phase y [kg/s]
n	dimensionless van Genuchten fitting parameter [-]
N_{cn}	Number of conservation equations
N_{eq}	Number of equilibrium equations
$N_{eq\,j}^{s}$	Number of equilibrium species in equilibrium equation j
N_{kn}	Number of kinetic equations
$N_{tc\,j}^{s}$	Number total component species

$N_{tk\,j}^{R}$	Number kinetic reactions associated with total kinetic species j
$N_{tk\,j}^{s}$	Number total kinetic species
P_c	gas-aqueous capillary pressure [Pa]
P_g	gaseous pressure [Pa]
P_g^j	gaseous pressure of component j [Pa]
P_l	aqueous pressure [Pa]
P_y	aqueous pressure for phase y [Pa]
Pe	Peclet number [-]
R	gas constant equals 8.314 [J/ K mol]
$R_{tc\,j}$	produced moles of component species j from kinetic reaction j [mol/m^3 s]
$R_{tk\,j}$	produced moles of kinetic species j from kinetic reaction j [mol/m^3 s]
R_k	kinetic reaction rate of reaction k
Re	Reynolds number [-]
s_{el}	effective aqueous saturation [-]
s_{et}	effective total saturation [-]
s_g	gaseous saturation [-]
s_l	aqueous saturation [-]
s_m	irreducible aqueous saturation [-]
s_n	saturation of the non-wetting phase [-]
Sh'	Sherwood number [-]
T	temperature [K]
T_{ref}	reference temperature for the precipitation-dissolution reaction [K]
u	semi-empirical constant for the precipitation-dissolution reaction [-]
V_l	aqueous Darcy velocity vector [m/s]
V_y	Darcy velocity vector for phase y [m/s]
w	semi-empirical constant for the precipitation-dissolution reaction [-]
z	depth [m]

Greek symbols

α	van Genuchten fitting parameter [1/m]
α_l	effective surface area of the gas-water interface [m^2/m^3]
β_k	kinetic equation reaction rate coefficient of reaction k
ΔG	Gibbs free energy of the overall reaction [J/mol]
Δx	grid spacing of the model [m]
θ_d	diffusive porosity [-]
κ	intrinsic permeability [m^2]
μ_y	kinematic viscosity for phase y [Pa s]
ρ_g^j	gas density of component j [kg/m^3]
ρ_y	density for phase y [kg/m^3]
Ω_{calc}	calcite saturation index [-]
ω_g^j	gas mass fraction for component j [-]
ω_y^j	mass fraction for component j in phase y [-]

Index

1. Introduction

Throughout the world, insufficient support of unconsolidated soils in many geotechnical applications are of major concern, like unstable soils at hill slopes, around excavation sites and beneath buildings and roads. Many methods to strengthen and stabilize the subsurface are known to obviate these kind of problems. Grouting is a popular method for a wide range of geotechnical applications. During grouting, voids in the soil are filled with grout mixture to displace the water or gas in the pores. The aim of grouting is to improve the ground conditions by increasing the cohesion and the strength of the soil, or to control the groundwater flow by reducing porosity and permeability (Powers et al., 2007). Grouting can be used for different geotechnical purposes, e.g. protection of an excavation site, soil stabilizing for road or embankments or reducing contaminant displacement. The chosen method of grouting can be determined from the desired cementation of the soil and the soil characteristics itself.

A wide range of grouting methods is proposed and used by geotechnical engineers (Byle et al., 1995):

- Compaction grouting: a stiff mortar is injected to displace the soil instead of filling the voids in the soil with grout. This reduces the porosity and increases the density of the soil.
- Jet grouting: grout mixtures are injected at high pressure on the order of 35-40 Mpa to physically disrupt and mix the soil with the injected grout mixture.
- Soil mixing: mechanical mixing of soil with mortar by using an auger and paddle arrangement.
- Fracture grouting: fluid grout is injected at high pressure with the intention to fracture the soil. The produced lenses of hardened grout increase the strength and stiffness of the soil.
- Permeation grouting: grout mixtures are injected at low pressure and permeate through the voids in the soil. In this case no significant displacement or fracturing of the soil occurs. Grout mixtures are composed of cement or chemicals like sodium silicate, acrylamides, polyurethanes or epoxies (Kazemian et al., 2010) .

These grouting methods all have their limitations and disadvantages. In many cases mortar or cement is used, but the production of these products consumes a lot of energy and has a negative impact on the environment (Van Oss et al., 2003). Also chemical grout mixtures, especially acrylamides and polyurethane, can be very toxic and environmentally harmful. Another disadvantage is the cost of the chemical grout mixtures, which range up to $72 per m^3 of soil.

The hardening time of a chemical grout mixture must match with the method of injection. When the grout hardens too fast, the required area that needs to be grouted will not be reached. But when the grout hardens too slow, the grout will be spread too thinly and the desired soil strength in the injection area will not be reached. This means that the kind of grouting method determines the injection radius. Silicate and acrylic based grouts are commonly used in the process of chemical grouting of sandy soils. Depending on the conductivity, the effective injection radius of these chemicals is limited within the range of 0.3 to 1.0 m.

Grouting methods based on induced calcite precipitation in the subsurface might be a good alternative. *Biogrouting* was suggested as such a method and is based on bacterial activity in the soil. Calcium chloride ($CaCl_2$) and urea ($CO(NH_2)_2$) solutions are injected into the soil after the bacterium *Sporosarcina pasteurii* is added in the porous medium. The bacterium contains urease enzymes, which hydrolyze the urea into carbonate (CO_3^{2-}) and ammonium (NH_4^+) ions. These produced carbonate ions react with the calcium ions and form the precipitate calcium carbonate ($CaCO_3$). However, the by-product ammonium chloride (NH_4Cl) is formed and needs to be removed (Van Paassen et al., 2010, Van Wijngaarden et al., 2011 and Van Wijngaarden et al., 2012). The disadvantage of this method is the dependence on microbial growth. Bacteria may form cluster colonies, causing local enhanced precipitation of calcite at the colony site and less precipitation at areas with low bacteria concentration. Also local insufficient nutrient supply for the bacteria in the porous medium might be an obstacle for uniform calcite precipitation, because less microbial growth will result in less production of calcium carbonate in the soil. We can obviate this by using different methods based on nonmicrobial-induced carbonate precipitation.

The rate limiting step in the above mentioned method is the formation of carbonate ions from urea by bacteria. For a method solely based on chemical reaction reactions, the rate limiting step for calcite precipitation must be low enough to obtain sufficient injection radii and prevent clogging during injection. The *EcoGrout* method is in development by Deltares and it is based solely on the chemical reaction processes of calcite precipitation in soils and caves by degassing of CO_2. For example, the overall reaction that drives the dissolution of calcite by natural shallow groundwater and precipitation of calcite in caves occurs by the following reversible reaction (Appelo et al., 2005):

$$Ca^{2+} + 2HCO_3^- \leftrightarrow CaCO_3 + CO_2(g) + H_2O \qquad \text{(Eq. 1)}$$

The degassing of CO_2 from such groundwaters results in calcite precipitation. Using EcoGrout solutions with high CO_2 concentrations that keep a considerable amount of calcite in solution, degassing will result in enhanced calcite formation within the voids of the soil. These EcoGrout solutions are mixtures of calcium chloride ($CaCl_2$) and sodium bicarbonate ($NaHCO_3$) and are injected in an open groundwater system. This results in the following reaction:

$$Ca^{2+} + 2HCO_3^- \rightarrow CaCO_3(s)\downarrow + CO_2(g)\uparrow + H_2O \qquad \text{(Eq. 2)}$$

CO_2 degassing will occur as long as the CO_2 pressure is higher than the system (hydrostatic) pressure. The precipitation of calcite will cause an in-situ increase in stiffness and strength of the soil and a decrease in permeability.

At a certain injection rate, the rate of the EcoGrout reaction process will determine the radius of influence in the porous medium. Initial injection concentrations of calcium and bicarbonate as well as the hydrostatic pressure in the porous medium will have a large control on the reaction mechanism and rate. Also, EcoGrout solutions can be oversaturated, undersaturated or in equilibrium with respect to calcite and aqueous CO_2. The reaction described by Eq. 2 describes calcite precipitation driven by CO_2 degassing from a solution initially in equilibrium with respect to calcite. Studies have shown that degassing from water supersaturated with CO_2 is relatively slow (Zhao et al., 2011). Analyzing different scenarios

can be used to check whether application for geotechnical engineering is feasible or not under various conditions. Initially, experimental studies have suggested the use of calcium chloride ($CaCl_2$) and sodium bicarbonate ($NaHCO_3$) solutions with a molar ratio of 1:2. Calcite precipitation rates were far too high and resulted in clogging in the vicinity of the injection point and consequently in insufficient injection radii (Van der Star et al., 2012). Calcite precipitation solely controlled by degassing of CO_2 from EcoGrout solutions close to calcite equilibrium and initially high pCO_2 values might obviate these problems, since CO_2 degassing rates are low. This study will mainly focus on the precipitation of calcite solely controlled by CO_2 degassing.

One of the main advantages of the EcoGrout method is that the reactants are not expensive. Sodium bicarbonate is known as ordinary baking-soda, and calcium chloride is a by-product of making sodium carbonate during the Solvay process. This process involves making sodium carbonate from sodium chloride and calcium carbonate by several reaction steps. The by-products of the EcoGrout reaction are sodium (Na^+) and chloride (Cl^-) and therefore only increased salinity might be an issue.

Since cementation of the soil and permeability reduction are the main objective in the EcoGrout process, it is necessary to obtain a good understanding of the process. To obtain a better understanding of parameters which play an important role in the EcoGrout process, a model was built which combines these parameters. In this study the following aspects were investigated:

- The concentration of the injected calcium bicarbonate solutions and the transport of these and other formed aqueous species.
- The chemical reactions in the groundwater carbonate system.
- The rate limiting kinetics of degassing that controls the process of calcite precipitation.
- The precipitation of calcite and its effects on porosity and permeability.
- Multiphase flow of formed gaseous CO_2 in the aqueous phase to investigate the transport behaviour of degassed CO_2 in porous media.

Multiphase flow modelling of multiple-component gasses and water was done with the *Subsurface Transport Over Multi Phases, Water-N component gas-Energy* (STOMP-WNE) code. A module which accounts for Equilibrium-Conservation-Kinetic Equation Chemistry and Reactive Transport (ECKEChem) was used to describe the batch chemistry (White et al., 2005). In this study the batch chemistry results of the STOMP simulator were compared to results obtained with the model PHREEQC for Windows for validation. The PHREEQC database *PHREEQC.dat* was used for modelling the batch chemistry of EcoGrout solutions and contains the thermodynamic data for aqueous species and gas and mineral phases (Parkhurst et al., 1999).

2. Theoretical background

EcoGrout aims to be a method of sufficient soil reinforcement and permeability reduction due to calcite precipitation from an injection mixture of dissolved sodium carbonate ($NaHCO_3$) and calcium cloride ($CaCl_2$). Therefore, a thorough understanding of carbonate equilibria and the kinetic reaction that controls the calcite precipitation is required to describe the EcoGrout reaction mechanism.

2.1 Dissolved carbonate equilibria

Inorganic carbon in water exists in four distinct species: aqueous carbon dioxide ($CO_2(aq)$) and its three products of hydration reactions, carbonic acid (H_2CO_3), bicarbonate (HCO_3^-) and carbonate (CO_3^{2-}). In the presence of gaseous CO_2, dissolved aqueous CO_2 exchanges with gaseous CO_2:

$$CO_2\,(g) \leftrightarrow CO_2\,(aq) \qquad \text{(Eq. 3)}$$

The balance reaction between gaseous and aqueous CO_2 in water is described by Henry's law. It states that the solubility of gaseous CO_2 in water is proportional to the partial pressure of gaseous CO_2 above the water interface under equilibrium conditions:

$$K_H = pCO_2/a_{CO_2(aq)} \qquad \text{(Eq. 4)}$$

The value for Henry's constant (K_H) is given in table 1. The solution is supersaturated with aqueous CO_2 if $CO_2(aq) > pCO_2/K_H$. If $CO_2(aq) < pCO_2/K_H$, the solution is undersaturated with regard to aqueous CO_2

Carbonic acid is formed by association between water and aqueous CO_2.

$$CO_2(aq) + H_2O \leftrightarrow H_2CO_3 \qquad \text{(Eq. 5)}$$

The carbonic acid and aqueous CO_2 concentrations are combined, because only a small fraction of the aqueous CO_2 dissociates to carbonic acid at equilibrium and it is difficult to distinguish both species analytically. Therefore the total aqueous CO_2 concentration is assumed to be the sum of carbonic acid and aqueous carbon dioxide, $[CO_2] = [CO_2(aq)] + [H_2CO_3(aq)]$.

During dissociation of aqueous CO_2 and water, two protons are released by two reaction steps to form respectively bicarbonate and carbonate ions.

$$CO_2\,(aq) + H_2O \leftrightarrow HCO_3^- + H^+ \qquad \text{(Eq. 6)}$$

$$CO_2\,(aq) + H_2O \leftrightarrow CO_3^{2-} + 2H^+ \qquad \text{(Eq. 7)}$$

As for every acid-base reaction, the dissociation of water in protons and hydroxides is important:

$H_2O \leftrightarrow OH^- + H^+$ (Eq. 8)

These reversible reactions are described by their equilibrium constants (*see table 1*). Note that the activities of the species are used instead of the concentrations. The activities are calculated from the species concentrations with the extended Debye-Hückle equation in PHREEQC (*see A.1*). The distribution of the dissolved carbonate species, CO_2(aq), HCO_3^- and CO_3^{2-}, can be described as a function of the pH. The fraction between the carbonate species and the total carbonate species at a given pH can be calculated when the equilibrium constants are known (*see Fig. 1*). For pH values between 6.3 and 10.3, bicarbonate is the most abundant carbonate specie in water. With a pH value lower than 6.3, or higher than 10.3, the dominant carbon species are aqueous CO_2 or carbonate respectively (Appelo et al., 2005).

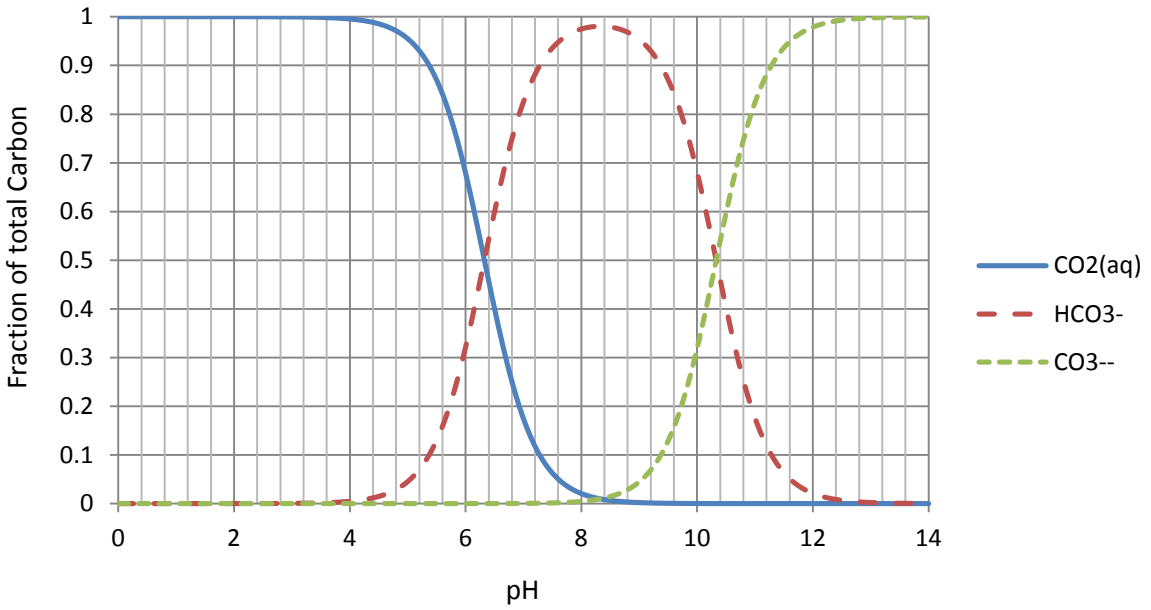

Fig. 1. *Aqueous carbon dioxide, bicarbonate and carbonate species fractions of total dissolved carbon as function of pH.*

Carbonate ions react with cations present in the water to form solid carbonate minerals. EcoGrout focuses on the precipitation of calcite due to reaction with calcium (Ca^{2+}) ions. The dissolution and precipitation of calcite is described as a reversible reaction.

$CaCO_3(s) \leftrightarrow Ca^{2+} + CO_3^{2-}$ (Eq. 9)

Generally, the solubility of a solid mineral is described as the mass of the mineral, which can dissolve in a given volume of the solvent. The activity of solid phase is, by convention, equal to one and the solubility product of calcite yields:

$$K_{sp} = \frac{\left(a_{Ca^{2+}}\, a_{CO_3{}^{2-}}\right)}{a_{CaCO_3}} = \frac{\left(a_{Ca^{2+}}\, a_{CO_3{}^{2-}}\right)}{1} \quad \text{(Eq. 10)}$$

The solubility product of calcite (K_{sp}) is given in table 1. However, a given solution may not be in equilibrium with calcite. The ion activity product (IAP) is used to describe the actual activities of the solution in the same form as the solubility product:

$$IAP = (a_{Ca^{2+}}\, a_{CO3^{2-}}) \qquad \text{(Eq. 11)}$$

Sometimes the concentrations of the calcium and carbonate ions are used to describe calcite solubility product (K_{sp}') and the ion concentration product (ICP) of calcite. The ratio between IAP and the solubility product of calcite are used to determine whether a solution is in equilibrium, undersaturated or supersaturated with reference to the calcite mineral. This ratio is called the saturation index (Ω_{calc}):

$$\Omega_{\mathrm{calc}} = \frac{IAP}{K_{sp}} \qquad \text{(Eq. 12)}$$

The saturation index of calcite is frequently expressed as the log value of Ω_{calc} in the literature (e.g. SI in PHREEQC (Parkhurst et al., 1999)). Using Eq. 12, a value of one implies a solution in equilibrium with the calcite mineral. If the IAP is lower than the solubility product, the saturation index is lower than one, which means undersaturation with regard to calcite. Supersaturation with respect to calcite implies a saturation index higher than one.

In shallow groundwater systems the pCO_2 is constant because equilibrium between aqueous CO_2 in the groundwater and gaseous CO_2 in the atmosphere is maintained. An overall equilibrium reaction for calcite precipitation and dissolution for these open $CaCO_3$-CO_2-H_2O systems is deduced from Eqs. 3 and 6-9:

$$Ca^{2+} + 2HCO_3^- \leftrightarrow CaCO_3(s) + CO_2(g) + H_2O \qquad \text{(= Eq. 1)}$$

Alternatively, transport of CO_2 between the natural groundwater system and the atmosphere can be slow or nonexsistent. Under these conditions the $CaCO_3$-CO_2-H_2O system is considered to be closed and the total amount of carbon remains constant. This implies that the pCO_2 of the groundwater can alter if the configuration of the carbonate system changes:

$$Ca^{2+} + 2HCO_3^- \leftrightarrow CaCO_3(s)\downarrow + CO_2(aq) + H_2O \qquad \text{(Eq. 13)}$$

The reaction process described by above mentioned reactions (Eqs. 3, 6-9) does not fully describe all aqueous reactions involved. Association between available cations, e.g. calcium and sodium, and anions, e.g. hydroxide, carbonate and bicarbonate, occurs and several aqueous complexes are formed. The formation of these complexes may have a considerable effect on the carbonate system at a given pH. The equilibrium constants for formation of these complexes are obtained from the PHREEQC database (*see table 1*). A major contribution of $CaHCO_3^+$ ions in the Ca-H_2O-CO_2 system can be assumed at low pH and high pCO_2 and the contribution of aqueous $CaCO_3$ complexes is negligible (Arakaki et al., 1995). In this study the formation of $CaHCO_3^+$ complexes is taken into account.

The equilibrium values shown in table 1 vary with temperature. The temperature range for shallow groundwater is 5-15 ^{0}C. The calcite solubility product and the equilibrium constants for bicarbonate and carbonate dissociation are hardly effected in this temperature range, but

Henry's constant decreases with a factor 0.53 with decreasing temperature, resulting in a K_H value of 15.5 L atm/mol at 5 ^{0}C, compared to 29.41 L atm/mol at 25 ^{0}C (*PHREEqc.dat)*. In this study a constant temperature of 25 ^{0}C is assumed for all equilibrium constants..

Table 1. *Equilibrium constants for the modelled reactions at a temperature of 25 ^{0}C (PHREEQC.dat)*

Reaction	Equilibrium	Log(K_{eq})
$H_2O \leftrightarrow OH^- + H^+$	$K_w = (a_{H+})(a_{OH^-})$	-14
$CO_2(aq) + H_2O \leftrightarrow HCO_3^- + H^+$	$K_1 = (a_{HCO_3^-})(a_{H+}) / (a_{CO_2(aq)})$	-6.352
$CO_2\,(aq) + H_2O \leftrightarrow CO_3^{2-} + 2H^+$	$K_2 = (a_{CO_3^{2-}})(a_{H+})^2 / (a_{CO_2(aq)})$	-16.681
$CO_2\,(g) \leftrightarrow CO_2\,(aq)$	$K_H = pCO_2/(a_{CO_2(aq)})$	1.468
$CaCO_3(s) \leftrightarrow Ca^{2+} + CO_3^{2-}$	$K_{sp} = (a_{Ca^{2+}})(a_{CO_3^{2-}})$	-8.48
$Ca^{2+} + H_2O \leftrightarrow CaOH^+ + H^+$	$K_{eq} = (a_{CaOH^+})(a_{H+}) / (a_{Ca^{2+}})$	-12.78
$Ca^{2+} + CO_3^{2-} \leftrightarrow CaCO_3$	$K_{eq} = (a_{CaCO_3}) / (a_{Ca^{2+}})(a_{CO_3^{2-}})$	3.224
$Ca^{2+} + CO_3^{2-} + H^+ \leftrightarrow CaHCO_3^+$	$K_{eq} = (a_{CaHCO_3^+}) / (a_{Ca^{2+}})(a_{CO_3^{2-}})(a_{H+})$	11.435
$Na^+ + H_2O \leftrightarrow NaOH + H^+$	$K_{eq} = (a_{NaOH})(a_{H+}) / (a_{Na^+})$	-14.18
$Na^+ + CO_3^{2-} \leftrightarrow NaCO_3^-$	$K_{eq} = (a_{NaCO_3^-}) / (a_{Na^+})(a_{CO_3^{2-}})$	1.27
$Na^+ + HCO_3^- \leftrightarrow NaHCO_3$	$K_{eq} = (a_{NaHCO_3}) / (a_{Na^+})\,(a_{HCO_3^-})$	-0.25

2.2 Kinetic equations

At a certain injection rate, the radius of influence of a given EcoGrout mixture in the soil is mainly determined by the kinetic rate of the whole reaction process and the injection pressure controlling the advective solute transport. Slow kinetics keep a solution at non-equilibrium conditions for longer times. The reaction rate of calcite formation must be considerably lower than the advective transport rate to attain the desired radius of influence. High precipitation rates with respect to flow rates will result in a small radius of influence and clogging in the vicinity of the injection point. The most ideal case is solute transport without any precipitation of calcite until the injection pulse stops. This condition can be achieved when the calcite precipitation is entirely dependent on CO_2 degassing and the injection pressure is higher than the CO_2 pressure. The Damkölher number is used to relate the kinetic rate to the advective transport flux:

$$Da = \frac{reaction\ rate}{advective\ mass\ transport\ rate} = \frac{k * \Delta x}{V} \qquad \text{(Eq. 14)}$$

If the Damkölher number is lower than one, the advective transport will be the limiting case for species transport. If the Damkölher number is higher than one, the kinetics will be limiting. This implies that at high Da values a lower radius of influence is expected, when kinetics largely limit the solute transport (Kühn, 2004). Note that the kinetic reaction rate constant in this equation yields only for simple first order kinetics and that for n^{th}-order or more complex kinetic reactions, e.g. calcite precipitation-dissolution, different relationships for the Damkölher number have to be determined (Knapp, 1989).

The rate limiting step of in the whole reaction process will control the reaction rate of calcite precipitation. If the goal is to maximize the radius of influence, than the Damköhler numbers should be as low as possible. This could be achieved by increasing the injection rate or by slowing the kinetic process. The reaction that controls calcite precipitation in a $CaCO_3$-CO_2-H_2O solution depends on the concentration of the different species and the physical

conditions of the system, e.g. mass transfer of aqueous CO_2 to gaseous CO_2 (Zhao, et al., 2011), formation of aqueous CO_2 from bicarbonate ions (Dreybrodt et al., 1997 and Guo et al., 2007) and precipitation of the calcite mineral itself (Morse et al., 2007 and Noiriel et al., 2011).

2.2.1 Calcite precipitation kinetics

A kinetic relationship for precipitation or dissolution of calcite can be described by using the saturation index of calcite. A general equation is introduced by Steefel et al. (1994):

$$\frac{dCaCO_3(s)}{dt} = k_{calc} A \left[\exp\frac{(\Delta G)^w}{RT} - 1\right]^u = k_{min} A[{\Omega_{calc}}^w - 1]^u \qquad \text{(Eq. 15)}$$

Where the temperature dependence of the reaction rate constant is described by the Arrhenius equation:

$$k_{calc} = k_{ref}[-\frac{E_a}{R}\left(\frac{1}{T} - \frac{1}{T_{ref}}\right)] \qquad \text{(Eq. 16)}$$

Equation 15 is normally used for slow calcite precipitation kinetics, assuming surface controlled growth of the mineral. Therefore the effective surface area of the calcite mineral (A [m^2/m^3]) is taken into account. An EcoGrout mixture that is initially in equilibrium with calcite at high CO_2 pressure, becomes highly supersaturated with regard to the calcite mineral only after CO_2 degassing occurs. This is due to increasing CO_3^{2-} concentrations during the degassing of CO_2. Under these conditions the rates of calcite precipitation cannot exceed the rate of CO_2 degassing. Depending on the kinetic balance between CO_2 degassing and calcite precipitation, a certain degree of supersaturation with respect to calcite maintained. Depending on the available reactive calcite surface area, calcite precipitation may occur as calcite crystal. However, at higher supersaturation heterogeneous calcite crystal nuclei will be formed in the aqueous phase. This implies that different effective surface areas, in this case the critical radius of the nuclei, should be taken into account. The semi-empirical constant u and the kinetic rate constant depend on whether calcite precipitation occurs by diffusion controlled growth, spiral growth at dislocations, homogenous or heterogeneous nucleation (Noiriel et al., 2011, Morse et al., 2007 and Molins et al., in press).

During nucleation processes the reactive surface area of calcite particles is unknown and therefore the reaction rate constant and effective surface area are lumped:

$$\frac{dCaCO_3(s)}{dt} = k_{calc}'[{\Omega_{calc}}^w - 1]^u \qquad \text{(Eq. 17)}$$

For polynuclear growth mechanisms high u^{th} order are found in the literature. E.g.: Sheikholeslami et al. (2003) determined u values increasing from 4.28 to 5.48 with increasing NaCl concentrations from 0.5 to 1.5 mol/L, whilst using low calcium carbonate solutions. Kinetic precipitation rates (k_{min}') between 1.23e-7 and 7.87e-11 mol/m^3 hr were found. Lioliou et al. (2007) have found u = 3, w = 1/2 and a k_{min}' = 1e-5 mol/m^3 hr at constant calcite saturation index of 1.2. Studies at saturation indices ranging from 36 to 131 used more complex polynuclear mechanism growth equations (e.g. Rosa, S. et al, 2011).

2.2.2 CO2 degassing kinetics

The rate of CO_2 degassing cannot be described by simple first order kinetics. Only when the aqueous phase is supersaturated with respect to aqueous CO_2, mass transfer from the aqueous to the gas phase is expected. Many kinetic rate equations for degassing from supersaturated liquids are proposed (e.g. Kashchiev, et al., 1993). Zhao et al. (2011) have used pore network simulation data to analyze the kinetics of gaseous CO_2 formation from water supersaturated with CO_2. They used a system pressure of 1.1 atm and modelled degassing of CO_2 from water supersaturated with CO_2 at a pCO_2 of 3.3 atm. A relation between macroscopic rate coefficients and gas saturation was found. The predicted rate coefficients are in good agreement with empirical rates, but the amount of simulation results is limited. An empirical mass transfer equation for nonaqueous phase liquid (NAPL) dissolution from regions with high initial liquid NAPL phase (Nambi et al., 2003) describes the mass transfer from aqueous to gaseous CO_2 in these simulations. The kinetic transfer of aqueous CO_2 to gaseous CO_2 depending on the saturation of CO_2 in water is described:

$$\frac{dCO_2(g)}{dt} = k_l \alpha_l ([CO_2] - \mathrm{P_l}/\mathrm{K_H}) \qquad \text{(Eq. 18)}$$

This equation describes kinetic degassing of CO_2 if $CO_2(aq) > P_l/K_H$, implying water is supersaturated with aqueous CO_2. If $CO_2(aq) < P_l/K_H$, water is undersaturated with aqueous CO_2, implying kinetic dissolution of gaseous CO_2 in the aqueous phase.

The parameters for the average mass transfer coefficient between the liquid and gaseous phase (k_l) and effective surface area of the gas-water interface (α_l) are hard to determine separately, because there are no physical estimates of the specific surface area of the gas bubbles. Therefore a lumped mass transfer coefficient (k_g) is determined. This lumped mass transfer coefficient is related to a modified Sherwood number (Sh'), which is a dimensionless value that shows the ratio of convective mass transport to diffusive mass transport between the fluid and the surface boundary:

$$k_g = \frac{Sh' D_m}{d_{50}^2} \qquad \text{(Eq. 19)}$$

The Sherwood number is correlated to the Reynolds number (Re) and the non-wetting saturation (S_n), which is in our case the gas saturation. Nambi et al. (2003) correlated these parameters over a range of non-wetting saturations from 0.01 to 0.35:

$$Sh'_{Nambi} = 37.15\, Re^{0.61} S_n^{1.24} \qquad \text{(Eq. 20)}$$

Zao et al. (2011) showed that pore network modelling predictions on the modified Sherwood number for CO_2 degassing from supersaturated water is consistent with the modified Sherwood relationship determined by Nambi et al. (2003) if the gas saturation is lower than 0.12. The correlation between the determined lumped mass transfer coefficient and the gas saturation is shown in Fig. 2.

At low gas saturation values the lumped mass transfer coefficient decreases with increasing gas saturation. These values are determined in a pore network simulation with a grid size of 100*100 nodes and 50 nucleation nodes. At these nucleation nodes the heterogeneous nucleation of CO_2 gas bubbles is simulated (Zhao et al., 2011 and Enouy et al., 2010)

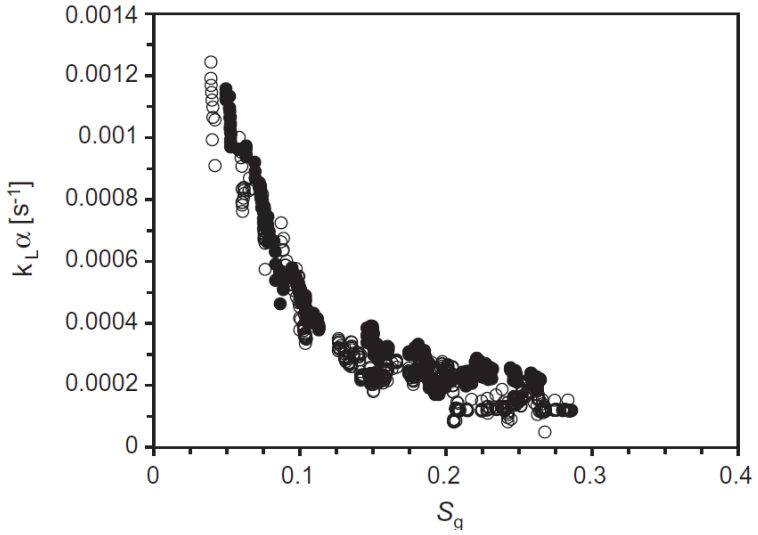

Fig. 2. *Dependence of lumped mass transfer coefficient on gas saturation (Zhao et al. 2011)*

2.3 EcoGrout solutions at calcite equilibrium

In this study an EcoGout solution at equilibrium with respect to calcite at a given pCO_2 is used. The species assemblage of an EcoGrout mixture in equilibrium with calcite can be calculated from the PHREEQC database. In table 2 the species assemblages are shown when a mixture of 0.1875 mol/L $CaCl_2$ and 0.375 mol/L $NaHCO_3$ reacts in a closed system until calcite equilibrium is reached with and without taking in account the salinity of the solution. Table 2.1 shows the species assemblage when formation of sodium complexes is taken into account. Modelling the injection of this species assemblage into porous medium is complex due to the large amount of needed equilibrium reactions for the batch chemistry. Therefore also the assemblage without taking in account the sodium complexes is calculated in PHREEQC and used for the model setup.

Table 2. *EcoGrout species assemblage at calcite equilibrium with no CO_2 degassing. Species assemblage 1 accounts for formed sodium complexes and assemblage 2 only for calcium complexes.*

Species assemblage	**1**
pCO2 [atm]	5.24E+00
pH [-]	5.59E+00
Species	**Concentration [mol/L]**
CO2	1.61E-01
HCO3-	4.36E-02
CO3-2	2.34E-06
Ca+2	2.22E-02
CaHCO3+	3.30E-03
CaCO3	5.03E-06
CaOH+	5.16E-10
Na+	3.70E-01
NaHCO3	4.09E-03
NaCO3-	3.75E-06
NaOH	6.04E-10

Species assemblage	**2**
pCO2 [atm]	5.03E+00
pH [-]	5.56E+00
Species	**Concentration [mol/L]**
CO2	1.69E-01
HCO3-	3.29E-02
CO3-2	9.70E-07
Ca+2	1.49E-02
CaHCO3+	3.00E-03
CaCO3	5.50E-06
CaOH+	5.18E-10

During the EcoGrout process the mixture is injected in porous media at a high injection pressure. The injection pressure must be higher than the pCO_2 of the injected mixture to prevent instantaneous degassing during injection. At the end of the injection pulse, the system pressure drops to hydrostatic pressure. If the hydrostatic pressure is lower than the pCO_2 of the solution, kinetic degassing starts because the solution becomes supersaturated with respect to aqueous CO_2 (*see Eq. 18*). The removal of CO_2 will gradually increase the pH and thereby the concentration of carbonate ions. Consequently, the solution becomes supersaturated with respect to calcite and calcite precipitation starts. Studies have shown that the expected partitioning of ^{13}C and ^{12}C between dissolved carbonate species and solid calcite does not occur, because calcite is formed rapidly after degassing of CO_2 (e.g. Michaelis et al., 1985). Therefore we can assume that the rate limiting step in this process is the degassing of CO_2 and calcite precipitation kinetics are sufficiently fast.

PHREEQC is used to calculate calcite equilibrium at given pCO_2 values. Starting with the species assemblage shown in table 2 the calcite solubility decreases with decreasing pCO_2 at calcite equilibrium. At a pCO2 of 5.03 atm, the initial total dissolved calcium concentration in the solution is 0.018 mol/L, if we assume injection of the species assemblage as shown in table 2.2. Degassing lowers the pCO_2 of the solution until a total gas pressure is reached that equals the hydrostatic pressure of 1.1 atm (equal to 1.4 m below the groundwater table) at equilibrium conditions. Consequently, the calcium solubility is reduced and the total dissolved calcium concentration is 0.0097 mol/L (*see Fig. 3*). This implies that for this specific case the potential for calcite precipitation is 0.0083 mol/L. Note that for injection at larger depths the pCO_2 reduction due to degassing will be lower and thereby the net calcite precipitation will also be reduced. This study will focus on EcoGrout injection at a depth of 1.4 m below the groundwater table, implying that the pCO_2 of the solution is lowered to 1.1 atm by CO_2 degassing.

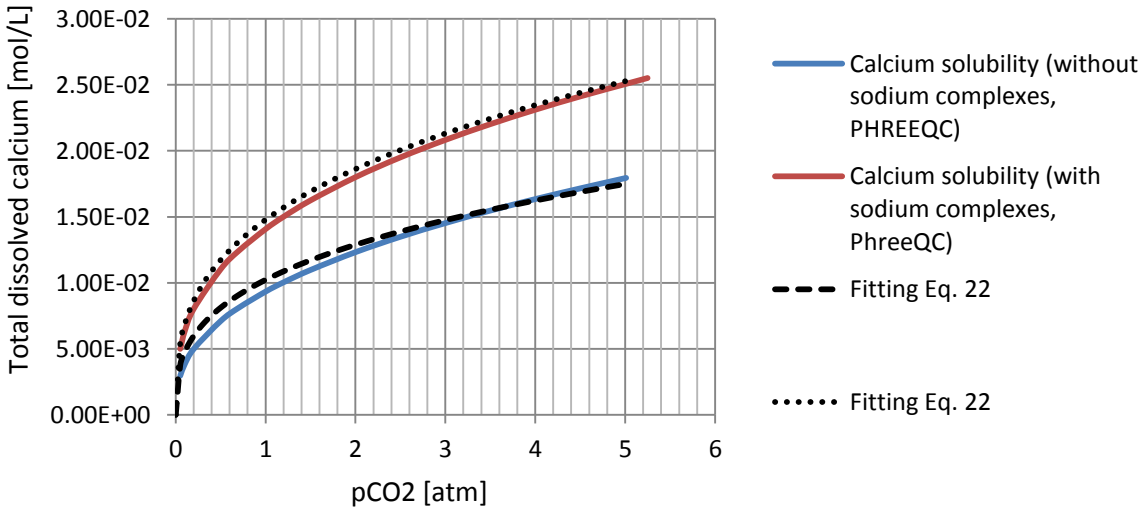

Fig. 3. *The solubility of calcite in water as a function of pCO_2. The curved lines indicates equilibrium with calcite according to PHREEQC calculations, where the blue line represent solubility assuming no salts are present and the red line represents solubility assuming in a solutions containing 0.375 mol/L of NaCl. The dashed lines are fitting lines obtained from Eq. 22.*

Figure 3 shows that the solubility of calcite increases if the salinity of the mixture is taken into account. The formation of complexes with sodium cations results in higher calcite solubility at

a given pCO_2. The large amount of required aqueous species and equilibrium reactions to describe this system will increase complexity of the STOMP model and therefore a different approach was used.

A relationship between the solubility of calcite and the partial pressure of CO_2 is described by the mass action equation of Eq. 1 using the equilibrium constants of Eqs. 3 and 6-9 (*see table 1*).

$$\frac{[Ca^{2+}][HCO_3^-]^2}{pCO_2} = \frac{K_1^2}{K_{sp}K_H K_2} \qquad \text{(Eq. 21)}$$

Assuming that $[Ca^{2+}]$:$[HCO_3^-]$ ratio of the injected ECOgrout solutes is 1:2, Eq. 13 is simplified (Appelo et al., 2005):

$$[Ca^{2+}] = \sqrt[3]{10^{\left(-\frac{0.0031}{k_{sp}}\right)}\, pCO_2} \qquad \text{(Eq. 22)}$$

Using the solubility product of calcite for normal water, $K_{sp} = 10^{-8.48}$ mol^2/L^2, the relationship fits well with the data obtained from PHREEQC. Fitting of Eq. 22 on the calcite solubility from the PHREEQC data, with the salinity of the solution taken into account, results in a K_{sp} of $10^{-8.00}$ mol^2/L^2.

2.4 EcoGrout solutions at calcite supersaturation

Injection of an EcoGrout mixture which is supersaturated with respect to calcite, might also be an option. E.g.: a solution of 0.1875 mol/L $CaCl_2$ and 0.375 mol/L $NaHCO_3$ is directly injected into the porous medium. The species assemblage of this mixture is shown in table 3. The initial pCO_2 of this mixture is 0.3801 atm, which implies that injecting this mixture at depth, the hydrostatic pressure is much higher than the pCO_2 of this solution and precipitation of calcite without degassing of CO_2 occurs (Eq. 13). Only when a sufficient supply of CO_2 is added to the system due to removal of carbonate ions by calcite precipitation, slow degassing kinetics of CO_2 will start controlling the precipitation rate of calcite.

The bicarbonate concentration is the most abundant carbon species in this mixture. Studies have shown that under these conditions CO_2 degassing from aqueous solutions proceeds by bicarbonate dehydration [$HCO_3^- + H^+ \rightarrow CO_2$ (aq) + H_2O] and dehydroxylation [$HCO_3^- \rightarrow CO_2$ (aq) + OH^-] (Dreybrodt et al., 1997 and Guo et al., 2007). These mechanisms are the rate limiting step in the reaction process and not the mass transfer between the aqueous and gaseous CO_2.

Table 3. *EcoGrout species assemblage immediately after mixing 0.1875 mol/L $CaCl_2$ and 0.375 mol/L $NaHCO_3$*

pH	7.476	
pCO2 [atm]	0.3801	Log [pCO_2] = -0.42
Ωcalc	1288,25	Log [Ωcalc] = 3.11
Species	**Concentration [mol/l]**	**Activity [mol/l]**
HCO3-	2.53E-01	1.70E-01
CO2	1.10E-02	1.30E-02
CO3-2	1.17E-03	2.38E-04
Ca+2	9.93E-02	2.47E-02
CaHCO3+	7.98E-02	5.35E-02
CaCO3	8.36E-03	9.89E-03
CaOH+	1.60E-07	1.20E-07
Na+	3.53E-01	2.50E-01
NaHCO3	2.02E-02	2.39E-02
NaCO3-	1.47E-03	1.11E-03
NaOH	4.09E-08	4.84E-08
Cl-	3.75E-01	2.32E-01

The initial calcite saturation index for the solution described in table 3 is 1288. According to Eq. 15, fast calcite kinetics can be expected at a solution far from equilibrium conditions. Deltares has done column experiments with injection of Ecogrout solutions of 0.750 mol/L $NaHCO_3$ and 0.375 mol/L $CaCl_2$. The cementation length in the column was short due to fast calcite precipitation (Van der Star et al., 2012). This yields that the kinetics of calcite precipitation are limiting the radius of influence during solute transport and high Damköhler numbers are expected.

Lower reaction rates are expected if kinetic degassing from water supersaturated with CO_2 solely controls calcite precipitation. Using the k_g found by Zhao et al. (2011), a quantitative estimation of the radius of influence can be made using the Damköhler number (Eq. 14). Assuming that Darcy velocities range between 0.2 to 0.00025 m/s during injection in porous medium, the k_g equals 0.001 s^{-1} and the desired injection length is 2 meters, the following Da values are calculated (*see table 4*). This yields that the controlling factor on calcite precipitation is sufficient to obtain considerable injection radii.

Table 4. *Damköhler numbers at different flow velocities at k_g = 0.001 s^{-1} and L = 2 m.*

Darcy Velocity [m/s]	**Da [-]**
0.2	0.015
0.1	0.03
0.05	0.06
0.01	0.3
0.005	0.6
0.001	3
0.00025	8

Adding acid to the mixture will increase the pCO_2 and decrease the carbonate concentration of the solution (*see Fig. 1*). This might be an interesting option, because with sufficient pH decrease the most abundant carbon species in the injected solution becomes aqueous CO_2. When the solution is supersaturated with aqueous CO_2, the control of CO_2 degassing on the calcite precipitation increases. In Fig. 4 is shown what the influence on the saturation index of calcite and pCO_2 of the mixture is after adding HCl. In the cases with significant pH lowering, CO_2 becomes the most abundant carbonate species. The mixture of 0.1875 mol/L $CaCl_2$, 0.375 mol/L $NaHCO_3$ and 0.3 mol/L HCl has a calcite saturation index of 4.6 and pCO_2 of 9.8 atm (*see table A3.7)*. This implies that under these conditions we might assume that the kinetic mass transfer between the aqueous and gaseous CO_2 largely controls the calcite precipitation and not the kinetics of calcite precipitation, or dehydration and dehydroxylation. Note that for an injection mixture in equilibrium with calcite 0.338 mol/L of HCl must be added.

The positive effect on the cemented length whilst using solutions with added acid is also shown at Deltares (Van der Star et al., 2012). Column experiments using solutions of 0.750 mol/L $NaHCO_3$, 0.375 mol/L $CaCl_2$ and 0.125 mol/L HCl increased the cemented length in the column compared to the situation with no HCl added. Flow rates were increased from 0.00025 to 0.001 m/s for all experiments. This implies that the Damköhler number is significantly lowered, due to slower calcite precipitation kinetics for the cases where HCl was added and the pCO_2 increased. Therefore, this study will mainly focus on the precipitation of calcite solely controlled by degassing from high pCO_2 solutions as discussed in paragraph *2.3* to obtain sufficient injection radii.

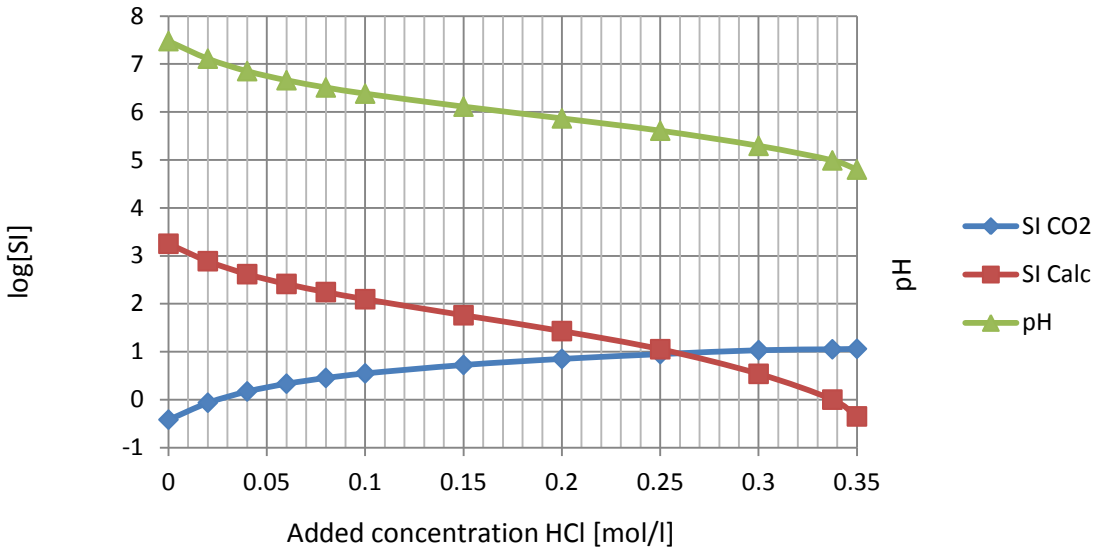

Fig. 4. *The saturation indices for both CO_2, calcite and the pH of 0.1875 mol/L $CaCl_2$ and 0.375 mol/L $NaHCO_3$ solutions with different added concentration of acid.*

3. Methods

3.1 STOMP-WNE-R

The *Subsurface Transport Over Multi Phases, Water-N component gas-Energy* (STOMP) simulator is a scientific modelling tool for analyzing single or multiple phase flow and transport in the subsurface. The hydrology group of the Pacific Northwest National Laboratory (PNNL) developed STOMP to produce numerical simulations of multiphase flow and transport in porous media. Data from analytical solutions and other existing multiphase flow simulators have been used for validation (White et al., 2006).

Variable operational modes of the STOMP simulator have been released, e.g. water-air, water-oil, water-salt, water-energy, water-CO_2 and combinations of above mentioned modes. The development of the STOMP-CO_2 operational mode was designed for CO_2 sequestration modelling. Chemical precipitation reactions are an important sequestration mechanism for CO_2 and to model this behaviour PNNL included a batch chemistry module Equilibrium-Conservation-Kinetic Equation Chemistry (ECKEChem). The ECKEChem module is written to allow implementation in all other operational modes.

An *input* file is required for executing the STOMP-simulator and basically translates the physical system description into a computational system. The input format consists of different cards grouping the needed input parameters to increase readability and usability of the input file. The STOMP User Guide lists all cards that can be used in the different operational modes and explains its formats. The source code of the STOMP-simulator is written in mixed Fortran 77/90 form and uses dynamic memory allocation. The solution of the governing partial differential equations that describe the multiphase flow processes in the porous medium are solved by using the integral volume finite difference method (White et al., 2000 and 2006).

The STOMP-WNE-R simulator has been designed to solve multiphase flow of multiple gas components and aqueous water combined with reactive transport problems in given porous media. This new code is still in development at PNNL and not released officially. PNNL ensured STOMP-WNE is validated at a wide range of experimental data in both unsaturated and saturated porous media. The source code used different variables and equations compared to the earlier officially released operational modes. This simulator describes transport and flow of energy, mass of the aqueous and gaseous phase. Multiple gas component species can be defined in the STOMP-WNE simulator and batch chemistry is simulated by including the ECKEChem module. Since the simulator is not released officially an user guide for this β-version was not yet available.

Figure 5 shows the flow path of the STOMP-WNE simulator. The flow path for the STOMP-WNE simulator with the ECKEChem module for one time step can be described by the following steps. The STOMP-simulator solves the coupled flow of the aqueous and gaseous phase and the transport system by calculating the associating non-linear governing mass conservation equations for multiphase flow and transport. These equations are discretized on defined grids in the model domain using finite difference approach. The non-linearities from

constitutive equations, e.g. the permeability-saturation-capillary pressure relations, are solved using Newton-Raphson iteration. The process is executed by three sequential components in the main program: initializing, iteration and closure. The initialization stage is executed once by loading the input data from the input file. Sequentially, the iteration is executed by using nested loops for both time stepping and for Newton-Raphson linearization. Closure is executed after successful convergence or convergence failure and the obtained data are written to plot and output files (White et al., 2006).

Sequentially from the multiphase flow and transport, the reactive transport equations are solved. The reactive transport system uses an operator splitting scheme, which computes the reactive species transport separately from the batch chemistry. The reactive transport solution first computes the transport of aqueous species. This is not the case for the reactive gaseous component species, which are transported by above mentioned coupled flow and transport mechanism. To reduce the number of transported species, the species are lumped into mobile component species and kinetic species, which implies that transport properties like dispersion and diffusion are species independent. Eventually the component and kinetic species passes the batch chemistry solver, computing the new species concentration at the given time step by using kinetic or equilibrium reaction equations. The ECKEChem equations are also non-linear and Newton-Raphson iteration is used to solve the batch chemistry system (White et al., 2005).

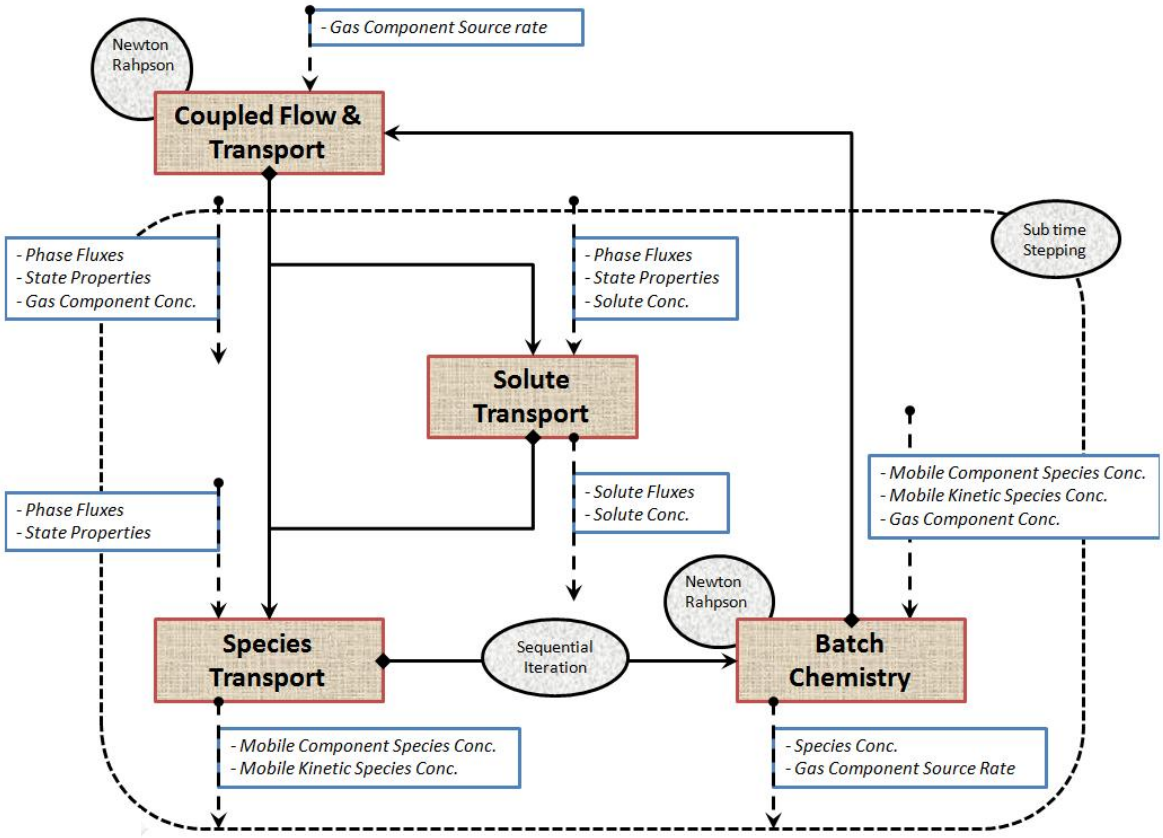

Fig. 5. *Flowpath of STOMP-WNE simulator and ECKEChem module.*

The used equations in the STOMP-WNE simulator and the batch chemistry are listed below. The model is extended with the kinetic degassing of CO_2 and the porosity and permeability alteration due to solid phase formation. Solving this set of non-linear equations results in complex model calculations. Consequently, this model requires long running times. Therefore a good balance in computational efficiency and accuracy of the model results was attempted during this study.

3.2 Batch chemistry

The ECKEChem module in the STOMP simulator can be used to describe the geochemical reaction processes in porous media. The approaches of Fang et al. (2003) are used for the ECKEChem module. Sufficiently fast reactions are described by equilibrium reactions and slow reactions are described by kinetic reactions. The batch chemistry in the STOMP simulator is translated in a system with equilibrium, conservation and kinetic equations. Equilibrium equations are based on the equilibrium constant and the related species activities:

$$a_j = K_{eq\,j} \prod_{N^s_{eq\,j}} a_i^{e_i}\ (i \neq j) \quad for: j = 1, N_{eq} \qquad \text{(Eq. 23)}$$

Chemical activities are deduced from the concentration by an activity factor calculated Debye-Hückel equation (*see A.1*)

In the batch chemistry system the component species defines a set of species, whose collective stochiometrically weighted summed concentration is constant over time. In other words, the mass conservation of the component species is invariant over time:

$$\frac{d \sum_{N^s_{tc\,j}} (f_i C_i)}{dt} = 0: \quad for\ j = 1, N_{cn} \qquad \text{(Eq. 24)}$$

The $\sum(b_i\ C_i)$ term equals the component species concentration.

The kinetic equations are defined in the same way as the conservation equations, but the stochiometrically weighted summed concentration is not constant over time:

$$\frac{d \sum_{N^s_{tk\,j}} (b_i C_i)}{dt} = \sum_{N^R_{tk\,j}} \beta_k R_k: \quad for\ j = 1, N_{kn} \qquad \text{(Eq. 25)}$$

In the batch chemistry system four reaction rate models are available. For modelling the EcoGrout process two kinetic reaction rate models are used. Further on (*see 3.5*) the adaption of these reaction rate models is briefly explained.
The Smith-Atkins forward-backward reaction rate model:

$$R_k = k_f \prod_{i=1}^{Nreactants} C_i\ - k_b \prod_{j=1}^{Nproducts} C_j \qquad \text{(Eq. 26)}$$

Dissolution-precipitation kinetics of a solid mineral can be described by the dissolution-precipitation equation of Steefel et al. (1994):

$$R_k = k_{calc} A[1 - \Omega_{calc}] \quad \text{Eq. (27)}$$

3.3 The governing equations

The STOMP-WNE simulator solves three coupled mass conservation equations: water mass, gas component mass and aqueous component species mass. Also a coupled conservation equation for thermal energy is included, but energy fluxes are neglected during modelling, because the temperature is considered constant during the EcoGrout process.

The advective fluxes of the mobile phase: water mass, gaseous and aqueous component mass are computed according to Darcy's law:

$$V_y = \frac{k_{ry}\,\kappa}{\mu_y}\left(\nabla P_y + \rho_y g z\right) \quad for\ y = l, g \quad \text{(Eq. 28)}$$

Water mass exist in both aqueous (l) and gas (g) phase under equilibrium conditions. The mass conservation equation for the water mass considers advection. Molecular diffusion is neglected, assuming advection is the main transport mechanism.

$$\frac{\partial}{\partial t}\sum_{y=l,g}\left(s_y\,\rho_y\,\omega_y^{H_2O}\,\theta_d\right) = -\sum_{y=l,g}\left(\rho_y\,\omega_y^{H_2O} V_y\right) + \sum_{y=l,g}\left(\omega_y^{H_2O} m_y\right) \quad \text{(Eq. 29)}$$

Substituting Darcy's law into the mass conservation equation yields Richard's equation:

$$\frac{\partial}{\partial t}\sum_{y=l,g}\left(s_y\,\rho_y\,\omega_y^{H_2O}\,\theta_d\right) = -\sum_{y=l,g}\left(\frac{\rho_y\,\omega_y^{H_2O} k_{ry}\,\kappa}{\mu_y}\left(\nabla P_y + \rho_y g z\right)\right) + \sum_{y=l,g}\left(\omega_y^{H_2O} m_y\right) \quad \text{(Eq. 30)}$$

The modelled gas component species CO_2 and N_2 exist in the aqueous and gas phase, assuming the equilibrium conditions described by Henry's law. The mass conservation equation for both CO_2 and N_2 considers advection:

$$\frac{\partial}{\partial t}\sum_{y=l,g}\left(s_y\,\rho_y\,\omega_y^{g_{Comp}}\,\theta_d\right) = -\sum_{y=l,g}\left(\rho_y\,\omega_y^{g_{Comp}} V_y\right) + \sum_{y=l,g}\left(\omega_y^{g_{Comp}} m_y\right) \quad \text{(Eq. 32)}$$

Combining the mass conservation equation and Darcy's law yields Richards equation:

$$\frac{\partial}{\partial t}\sum_{y=l,g}\left(s_y\,\rho_y\,\omega_y^{g_{Comp}}\,\theta_d\right) = -\sum_{y=l,g}\left(\frac{\rho_y\,\omega_y^{g_{Comp}} k_{ry}\,\kappa}{\mu_y}\left(\nabla P_y + \rho_y g z\right)\right) + \sum_{y=l,g}\left(\omega_y^{g_{Comp}} m_y\right) \quad \text{(Eq. 33)}$$

The mass transport of the component species is driven by advection and hydrodynamic dispersion through the diffusive pore space. The effectiveness ratio between mass transport by advection and hydrodynamic dispersion can be used to indicate which is the main transport mechanism for the solute mass. This dimensionless ratio is called the Peclet number (Pe):

$$Pe = \frac{V_l \Delta x}{D} \quad \text{(Eq. 34)}$$

The injection pressures of the reactive solutes during the EcoGrout process are high resulting in high Darcy velocities in the model domain. The grid dimension chosen in the model domain are small (0.1-0.05 meter) to obtain accurate model results and the corresponding realistic hydrodynamic dispersion values for these dimensions are generally a factor 10-10000 lower (Fetter, 1999). This yields that Peclet numbers in the order of 10-1000 are expected. In this model is assumed that the mass transport occurs solely by advection and mixing of solutes during flow is neglected (Pe → ∞)

To increase the computational efficiency of the STOMP-WNE simulator the mobile species fractions of the total component species and the total kinetic aqueous species are transported:

$$\frac{\partial [C_{tc\,j}]}{\partial t} = -\sum_{y=l,g} \left(\nabla \left(C^m_{tc\,j}\, V_y \right) \right) + \sum_{i=1}^{N^s_{tc\,j}} m_i + \sum_{k=1}^{N^R_{tc\,j}} R_{tc\,j,k} \quad \text{(Eq. 35)}$$

$$\frac{\partial [C_{tk\,j}]}{\partial t} = -\sum_{y=l,g} \left(\nabla \left(C^m_{tk\,j}\, V_y \right) \right) + \sum_{i=1}^{N^s_{tk\,j}} m_i + \sum_{k=1}^{N^R_{tk\,j}} R_{tk\,j,k} \quad \text{(Eq. 36)}$$

Combining Darcy's law with the mass conservation equations yields:

$$\frac{\partial [C_{tc\,j}]}{\partial t} = -\sum_{y=l,g} \left(\nabla \left(C^m_{tc\,j}\, \frac{k_{ry}\,\kappa}{\mu_y} \left(\nabla P_y + \rho_y g z \right) \right) \right) + \sum_{i=1}^{N^s_{tc\,j}} m_i + \sum_{k=1}^{N^R_{tc\,j}} R_{tc\,j,k} \quad \text{(Eq. 37)}$$

$$\frac{\partial [C_{tk\,j}]}{\partial t} = -\sum_{y=l,g} \left(\nabla \left(C^m_{tk\,j}\, \frac{k_{ry}\,\kappa}{\mu_y} \left(\nabla P_y + \rho_y g z \right) \right) \right) + \sum_{i=1}^{N^s_{tk\,j}} m_i + \sum_{k=1}^{N^R_{tk\,j}} R_{tk\,j,k} \quad \text{(Eq. 38)}$$

Note that the source and production rate for both the total kinetic and total component species are determined as a summation of the mobile fractions of the total component species and the total kinetic aqueous species. The immobile fractions are not transported by these flow equations. This means that the mass balance equation for solid minerals, which is calcite in the EcoGrout process, is only described by its reaction rate:

$$\frac{\partial [C_{tk\,j}]}{\partial t} = \frac{\partial CaCO_3(s)}{\partial t} = R_{CaCO_3} \quad \text{(Eq. 39)}$$

3.4 The constitutive relations

The gas-aqueous capillary pressure (P_c) is determined by the difference between gas and aqueous pressure (P_g and P_l):

$$P_c = P_g - P_l \quad \text{(Eq. 40)}$$

The total gas pressure is the sum of the water vapor pressure and the total component vapor pressure.

$$P_g = P_g^w + P_g^{comp} \quad \text{(Eq. 41)}$$

The water vapor pressure (P_g^w) is computed in the model (White et al., 2000). The total component pressure (P_g^{comp}) is defined by the sum of the component pressures: $P_g^{comp} = P_g^{CO_2} + P_g^{N_2}$
The partial pressure of the component species are computed by Henry's law and the mole fraction of the component in the aqueous phase:

$$P_g^j = \omega_l^j M_l^j * H^j \quad for\ j = CO_2, N_2 \quad \text{(Eq. 42)}$$

The component vapor densities (ρ_g^j) are computed from the water vapor and gas component pressures by the ideal gas law:

$$\rho_g^j = \frac{P_g^j}{RT} \quad for\ j = w, CO_2.N_2 \quad \text{(Eq. 43)}$$

The gas phase mass fraction for water, CO_2 and N_2 (ω_g^j) are calculated from the ratio between the component vapor density and the total vapor density:

$$\omega_g^j = \frac{\rho_g^j}{\sum_j \rho_g^j} \quad for\ j = w, CO_2.N_2 \quad \text{(Eq. 44)}$$

The effective water (s_{el}), effective gas (s_{eg}) and the effective total saturation (s_{et}) are defined:

$$s_{el} = \frac{s_l - s_m}{1 - s_m} \quad \text{(Eq. 45)}$$

$$s_{et} = \frac{s_t - s_m}{1 - s_m} = s_{eg} + s_{el} \quad \text{(Eq. 46)}$$

The effective water saturation is modelled by relating the gas-aqueous capillary pressure to the effective aqueous saturation with the van Genuchten function (Van Genuchten, 1980):
.

$$s_{el} = \begin{cases} \left[1 + \alpha \left[\frac{P_c}{\rho_l g}\right]^n\right]^{-m} & if\ P_c > 1 \\ 1 & if\ P_c \leq 1 \end{cases} \quad \text{(Eq. 47)}$$

The parameters of the van Genuchten function (α and n) depend on the soil texture. These functions are fitted to a large amount of experimental data to establish a good estimation of the capillary pressure-saturation function for a given soil. Assuming that the behaviour of multiphase flow of water and CO_2 is comparable with water and air, the parameters found by Carsel et al. (1988) are used for modelling with the STOMP simulator (*see A.2*).

The STOMP-WNE simulator lacks the ability to model hysteresis effects at the moment and consequently entrapment of gas. Most operational modes of STOMP are equipped with this feature by the method introduced by Parker et al. (1987) and Kaluarachchi et al. (1992). It is likely that the operational mode WNE will be equipped with this feature when it is officially released. However, in this study the saturation-pressure relationship can only be described assuming non-hysteresis effects.

The relative permeability of the aqueous and gaseous phase is calculated as a function of the aqueous and gaseous saturation from the van Genuchten function and the pore distribution model of Mualem:

$$k_{rl} = {s_{el}}^{1/2}\left[1-\left(1-{s_{el}}^{\frac{1}{m}}\right)^{m}\right]^{2} \qquad \text{(Eq. 48)}$$

$$k_{rg} = {s_{eg}}^{1/2}\left[1-\left(1-{s_{el}}^{\frac{1}{m}}\right)^{m}\right]^{2} \qquad \text{(Eq. 49)}$$

3.5 Model setup for the batch chemistry

The approach of Fang et al. (2003), which is described in section 3.2, is applied to describe the EcoGrout process (*see Eqs. 3, 6-9*). The rate limiting step in the EcoGrout reaction mechanism must be described kinetically. The kinetic rate limiting step of the EcoGrout injection mixture depends on the composition of the injected solute mixture. For mixtures close to calcite equilibrium, the kinetics of CO_2 degassing will control the calcite precipitation. For mixtures which are supersaturated with regard to calcite, precipitation can be controlled by different kinetic reactions.

For the case that the degassing of CO_2 is rate limiting, the following procedure is followed to model calcite precipitation. For this, the main challenge in using the STOMP-WNE simulator is that it uses Henry's law to determine equilibrium between the aqueous and gaseous phase for the defined component species. For gaseous flow transport in the main program the total gas is transported and sequentially the different gas component concentrations are computed using Henry's law. (*see Eqs. 41-44*). The mole fractions in the aqueous phase are used to calculate the partial pressure of the gas species. Therefore replacing Henry's law for CO_2 partitioning by a kinetic degassing equation of CO_2 described by Zhao et al. (2011) cannot be done, because it will ruin the basics of the STOMP-WNE simulator. This means that we can only model kinetic reactions from aqueous to aqueous or solid phase and vice versa. To describe the kinetic reaction at the gas-aqueous phase transition is impossible and therefore the following approach in the STOMP-WNE simulator was developed to allow the simulation of kinetic CO_2 degassing.

To simulate the kinetic degassing of CO_2, Eq. 3 is modified to the following reaction process in the STOMP simulator, by including a fictional aqueous species CO_2gas. This species is

formed by kinetic degassing of aqueous CO_2 and the CO_2gas is considered to be in equilibrium with gaseous CO_2 described by Henry's law:

$CO_2\,(aq) \rightarrow CO_2gas\,(aq) \leftrightarrow CO_2(g)$ (Eq. 50)

The kinetic degassing of CO_2 equation described by Zhao et al. (2011) is implemented in the ECKEChem module of the STOMP-WNE simulator by rewriting the kinetic forward-backward equation in the source code (*see Eq. 26*):

$$R_k \begin{cases} \frac{d[CO_2 gas]}{dt} = k_g([CO_2(aq)] - P_l\ 0.0003355) & if\ [CO_2(aq)] > 0.034\ mol/L \\ 0 & if\ [CO_2(aq)] \leq 0.034\ mol/L \end{cases} \quad \text{(Eq. 51)}$$

Note that the overall aqueous pressure is used. The overall aqueous and gas pressure are primary variables and implemented easily in the different subroutines using dynamic memory allocation. This choice is also defensible, due to the fact that the aqueous mole fractions of CO_2 are close to 1 in the injected EcoGrout solutes during the modelling. Henry's constant at a temperature of 25 ^{0}C is considered at a value of 0.0003355 mol/m^3 Pa. This means that temperature has no effect on Henry's constant in our model. Since we are mainly interested in degassing of CO_2, the dissolution of gaseous CO_2 into the aqueous phase is not modelled to increase the computational efficiency. Therefore the reaction rate is set to zero if the aqueous CO_2 concentration is lower than 0.034 mol/L.

The mole fraction of the fictional species CO_2gas concentration in the aqueous phase is linked with the gaseous phase by using Eq. 42:

$$P_g^j = \omega_l^j M_l^j * H^j \quad for\ j = CO_{2gas}, N_2 \quad \text{(Eq. 52)}$$

Henry's constant for the fictional CO_2gas species is chosen to be a fraction of 0.1 lower than the actual Henry's constant of CO_2. This means that a small fraction of the carbon species is stored as fictional aqueous CO_2gas species. Lower fractions are also tried, but results in convergence failure due to problems with the amount of gas volume formed in given grid cells.

This two step reaction mechanism is used to describe kinetic degassing of CO_2 with taken into account whether a solution is supersaturated or undersaturated with respect to aqueous CO_2.

Using the approach of Fang et al. (2003) it is not possible to define calcite equilibrium reaction for calcite: $\mathrm{K_{sp}} = (\mathrm{a_{Ca^{2+}}}\,\mathrm{a_{CO3^{2-}}})$. In this equilibrium reaction the solid phase is not defined in the equilibrium reaction because it is set to one. This means the calcite concentration cannot be declared in the batch chemistry using equilibrium reactions and kinetics are needed to describe the precipitation of calcite. In the STOMP-WNE simulator calcite precipitation can be described by dissolution-precipitation kinetics and assuming sufficiently fast kinetic calcite precipitation (*see Eq. 27*). The reactive surface area of calcite is irrelevant, because fast calcite nucleation kinetics are considered. Therefore this equation is simplified to the following precipitation-dissolution equation:

$$R_k = \frac{dCaCO_3(s)}{dt} = k_{calc}'[\Omega_{calc} - 1] \quad \text{(Eq. 53)}$$

Using the equilibrium reactions described by Eqs. 3-5 and 7 and the kinetic degassing, one could define the reaction mechanism of the EcoGrout process. Using the approach of Fang et al. (2003), the equilibrium reactions are described (*see Eq. 22*):

$$[a_{OH^-}] = \frac{10^{-14}}{[a_{H^+}]}$$
$$\left[a_{HCO_3^-}\right] = \frac{[a_{CO_2(aq)}]10^{-6.352}}{[a_{H^+}]}$$
$$\left[a_{CO_3^{2-}}\right] = \frac{[a_{CO_2(aq)}]10^{-16.681}}{[a_{H^+}]^2}$$
$$\left[a_{CaHCO_3^+}\right] = \frac{[a_{Ca^{2+}}]\,[a_{CO_2(aq)}]10^{-5.246}}{[a_{H^+}]}$$

The conservation equations for the total-component species Ca^{2++}, $CO_2(aq)$ and H^+ are described by Eq. 23:

$$\frac{d([Ca^{2+}]+[CaHCO_3^+]+CaCO_3(s)}{dt} = 0$$
$$\frac{d([CO_2]+[HCO3^-]+[CO3^{2-}]+CaCO_3(s)+[CO_2 gas]+[CaHCO_3^+])}{dt} = 0$$
$$\frac{d([H^+]-[OH^-]-[HCO3^-]-2[CO3^{2-}]+[CaHCO_3^+])}{dt} = 0$$

3.6 Porosity and permeability alteration

The STOMP-WNE simulator lacks the ability to change the porosity and permeability over time as a result of the precipitation of solid species.

The goal of the EcoGrout process is to reduce porosity and thereby increasing the strength and reducing the conductivity of the soil. In the voids of the soil the calcite will precipitate leading to a decrease in porosity. Assuming that all calcite formed in one grid cell is not transported by advection to the next grid cell and causes in-situ porosity reduction, the change in porosity is linked to the immobile calcite.

The porosity is, by definition, the pore volume per total volume:

$$\theta = \frac{V_{pores}}{V_{total}} \quad \text{(Eq. 54)}$$

The change in calcite pore volume is described by the following equation:

$$\frac{d\theta}{dt} = -\frac{dV_{pores}}{V_{total}\,dt} = \frac{-\mathrm{d}(\mathrm{C_{CaCO3}})}{\mathrm{m}\rho_{\mathrm{CaCO3}}\,dt} \quad \text{(Eq. 55)}$$

This differential equation is solved with θ at t = 0 is θ_0:

$$\theta(t) = \theta_0 - \frac{\mathrm{C_{CaCO3}(t) - C_{CaCO3}(0)}}{m\rho_{\mathrm{CaCO3}}} \quad \text{(Eq. 56)}$$

Where the molar density of calcite at a temperature of 25 ^{0}C is 27086.4 mol/m^3.

It is possible to link the intrinsic permeability to the porosity by the Kozeny-Carmen equation. This empirical correlation for granular materials accounts for the spread of grain sizes in porous media. Assuming a homogenous isotropic porous media, the intrinsic permeability alteration over time is modelled (Bear, 1972):

$$\kappa_{x,z}(t) = \frac{\theta(t)^3}{(1-\theta(t))^2}\frac{(d_{50})^2}{180} \qquad \text{(Eq. 57)}$$

In the STOMP simulator the intrinsic permeability is multiplied with a permeability factor throughout the code.

3.7 Model setup

The model domain is considered to be a two-dimensional homogeneous, isotropic vertical cross section of an unconfined aquifer. The length (X) and depth (Z) of the domain are respectively 6.00 and 3.00 meter. The width of model domain (Y) is 0.05 m. The simulated domain is divided in several blocks with different grid dimensions to increase the model accuracy in the injection region (*see Fig. 6*). The porous medium is considered to be fine sand and its physical properties are presented in table 5. A median grain diameter of 0.15 mm is assumed, which is the average median diameter for fine sand (Shepherd, R.G., 1989). The van Genuchten parameters are in the range of loamy sand to sandy loam based on average values found by Carsel et al., (1988) (*see A.2*).

Table 5. *Mechanical, hydrological and capillary pressure-saturation function properties*

Mechanical Properties		**Van Genuchten parameters**	
Bulk density porous media	2,600 [kg/m^3]	α	0.045 cm^{-1}
Initial porosity	0.4 [-]	n	1.68 [-]
Hydrological Properties		**Saturation Properties**	
Median grain diameter	1.5e-4 [m]	Residual water content	0.045 [-]

The borehole at the west boundary and the east and bottom boundary of the model domain are considered impermeable. At the west boundary the EcoGrout mixture is injected at 1.5 meter depth, assuming the grid cell located at the west boundary [X=0, 1.45<Z<1.50] is the injection point. The injection point is shown by the red arrow in Fig. 6. An injection pulse is modelled with a Dirichlet boundary condition, which is a constant injection pressure of 10 atm for our cases.

Initially, a vertical hydrostatic pressure distribution is assumed: $P_l(X,Z,t,) = P_l(X,0,t) - \rho_w gz$. Where the aqueous pressure at the bottom of the model (Z=0) is given in table 6. A small unsaturated layer is modelled, hence the aqueous pressure in the model domain is smaller than the gas pressure for the upper layer of the domain. The unsaturated zone is required to degassed CO_2 to leave the model domain.

Table 6. *Initial primary variables.*

Primary variable	**Pressure**	**Gradient**
Gas pressure	101325 [Pa]	
Component pressure	95000 [Pa]	
Aqueous pressure	126700 [Pa] for [x,0,t]	-9810 [1/m]
Mole fraction gaseous N_2	1.0 [-]	
Mole fraction gaseous CO_2	0.0 [-]	

The species properties for the batch chemistry are shown in table 7. The initial concentration of the species in the model domain is shown in table 8 and is considered as natural groundwater. The pCO_2 of the water is 0.13 atm and the water is slightly undersaturated with respect to calcite (ICP = $10^{-8.7}$). As mentioned above, Henry's constant relating the fictional aqueous CO_2gas species and gaseous CO_2 is considered to be 10% of Henry's constant for CO_2. Smaller Henry's constants causes convergence failure during the modelling.

Table 7. *Species properties for the batch chemistry*

Gaseous Species	**Molar mass [kg/kmol]**	**Henry's constant [Pa]**
CO_2	44.01	1.652e9
N_2	28.013	9.197e9
Aqueous Species	**Molar mass [kg/kmol]**	
H^+	1.00079	
OH^-	17.0073	
CO_2(aq)	44.01	
HCO_3^-	61.171	
CO_3^{2-}	60.0092	
Ca^{2+}	40.078	
$CaHCO_3^+$	101.0951	
CO_2gas (fictional)	44.01	
Solid Species	**Molar mass [kg/kmol]**	**Density [kg/m^3]**
$CaCO_3$(s)	100.0872	2.711

Table 8. *Initial species concentration of the groundwater*

Species	**Initial Concentration (t=0)**
pH	6.46
CO_2(aq)	4.66e-3 [mol/L]
HCO_3^-	5.97e-3 [mol/L]
CO_3^{2-}	8.06e-7 [mol/L]
Ca^{2+}	2.23e-3 [mol/L]
$CaHCO_3^+$	1.70e-4 [mol/L]
CO_2gas (fictional)	0.0 [mol/L]
$CaCO_3$(s)	0.0 [mol/L]

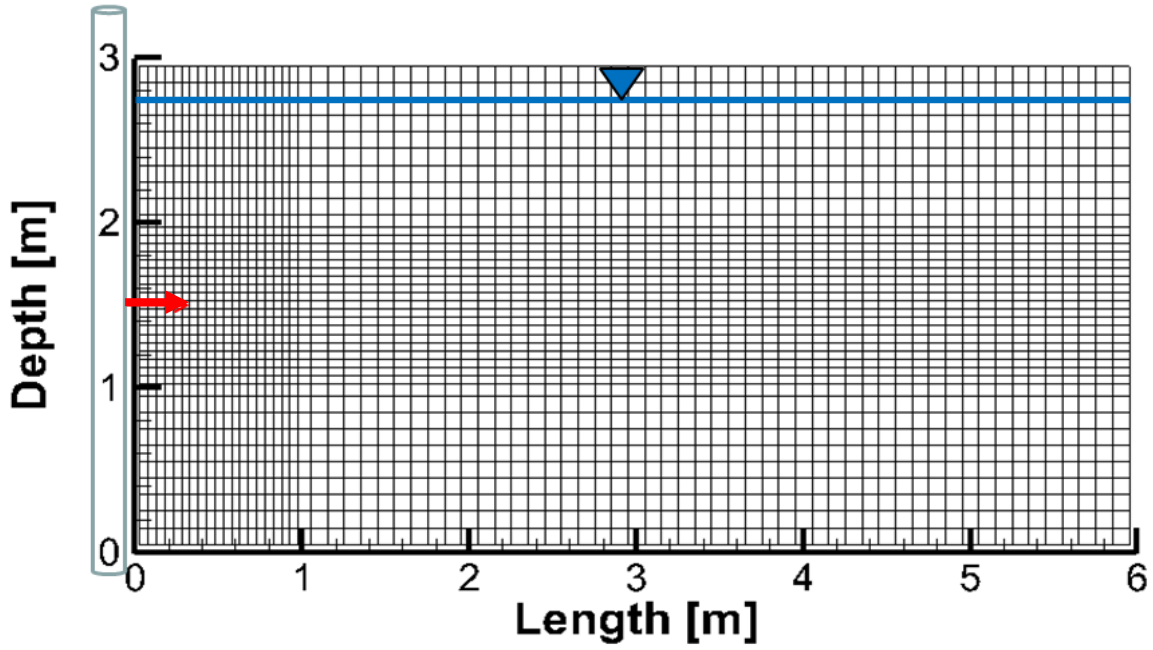

Fig. 6. *Model domain, where the red arrow indicates the injection point and the blue line the initial groundwater level.*

4. Results

Several cases were modelled to investigate the control of CO_2 degassing on calcite precipitation from an EcoGrout solution. The STOMP-WNE code is adapted for modelling kinetic degassing of CO_2 (*see 3.5*) and porosity and permeability alteration (*see 3.6*), and therefore validation of these processes is required. The modelled cases are listed below:

- **Case 1:** This is the reference scenario. An injection pulse of an EcoGrout solution at calcite equilibrium and a pCO_2 of 5.15 atm is injected at a pressure of 10 atm for 5 seconds.
- **Case 2:** The effect of increasing the solubility product of calcite is modelled to account for the salinity of the EcoGrout solution.
- **Case 3:** The effect on the control of CO_2 degassing on calcite precipitation using 3 different mass transfer coefficients for degassing.
- **Case 4:** The effect of solute transport in cemented porous medium with significant porosity reduction is investigated.
- **Case 5:** Injection pulse of an EcoGrout solution with a calcite saturation index of 1.2 and a pCO_2 of 5.15 atm is modelled.
- **Case 6:** Injection pulse of an EcoGrout solution with a calcite saturation index of 0.66 and a pCO_2 of 11.03 atm is modelled.

4.1 Case 1

In this case the precipitation of calcite is modelled from a solution in equilibrium with calcite and a pCO_2 of 5.15 atm. Initially the same species configuration as found in PHREEQC was used (*see table A3.1*). This resulted in a solution with an erroneously high supersaturation, resulting in fast calcite precipitation from t = 0 (*see A.8*). In table 9 the slightly adapted injection concentrations are shown to establish a solution in equilibrium with calcite according to the batch chemistry of the STOMP simulator. Note that the total calcium concentration is kept equal compared to the PHREEQC calculations.

The injection time is 5 seconds and the injection pressure is 10 atm. The Darcy velocities of the aqueous water mass during injection range up to 0.18 m/s in the vicinity of the injection point. After injection closure, 2.29 L of the EcoGrout solution is injected into the porous medium. The kinetic constants used for CO_2 degassing and calcite precipitation are shown in table 10.

In table 9 the concentrations of the EcoGrout solution are shown in the vicinity of the injection point at [X=0.225, Z=1.525]. No calcite precipitation and aqueous CO_2 removal occur in the injection region during injection. Figure 7 shows the system pressure and the aqueous CO_2 concentration at [X=0.125, Z=1.525] during the first time steps. The system pressure drops from 6.7 atm to an hydrostatic pressure of 1.1 atm after injection closure. Consequently, the pCO_2 of the injected solution becomes higher than the system pressure and the slow kinetics of aqueous CO_2 removal starts (*see Eq. 51*).

Table 9. *Initial and pulse species concentrations at grid cell [X=0.225, Z=1.525]*

Species	Input pulse concentration	Pulse concentration at t = 5 s	Concentration at t = 600 min
pH	-	5.4	6.0
CO_2(aq)	0.175 [mol/L]	0.175 [mol/L]	3.8e-2 [mol/L]
HCO_3^-	2.0e-2 [mol/L]	1.942e-2 [mol/L]	2.23e-2 [mol/L]
CO_3^{2-}	9.8e-8 [mol/L]	2.273e-7 [mol/L]	1.38e-6 [mol/L]
Ca^{2+}	1.5e-2 [mol/L]	1.442e-2 [mol/L]	2.39e-3 [mol/L]
$CaHCO_3^+$	3.0e-3 [mol/L]	3.580e-3 [mol/L]	6.81e-4 [mol/L]
CO_2gas (fictional)	-	0.0 [mol/L]	3.75e-3 [mol/L]
$CaCO_3$(s)	-	0.0 [mol/L]	1.49e-2 [mol/L]
PV calcite	-	-	2.2e-4 [-]

Table 10. *Kinetic constants for degassing and precipitation*

Kinetic constant	Value
k_f for CO_2 (aq) → CO_2gas (aq)	0.00278 [s^{-1}]
k for Ca^{2+}(aq) + CO_3^{2-}(aq) ↔ $CaCO_3$ (s)	1.39e-6 [mol/ m^3 s]

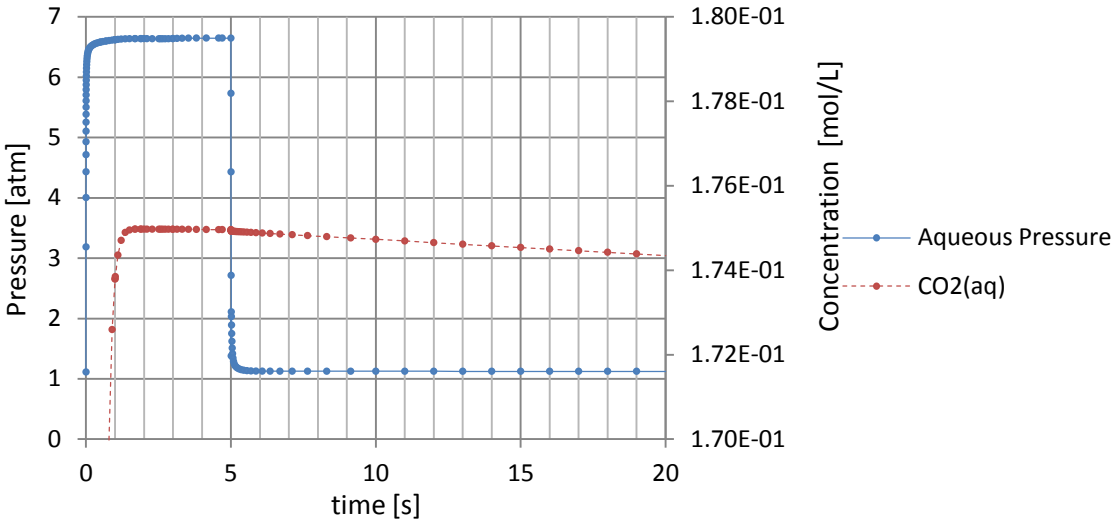

Fig. 7. *The system pressure and aqueous CO_2 concentration over time at [X=0.125,Z=1.525].*

Figures 8 and 9 show respectively the gas saturation and calcite precipitation in the domain at different times. During injection of the EcoGrout mixture a primary water table rise is determined. Gaseous CO_2 formation starts after 1.8 minutes. Note that the kinetic removal of aqueous CO_2 from the solution does not result in equimolar degassing of CO_2. Initially, the fictional aqueous CO_2gas species is formed and degassing will start when the solution becomes supersaturated with respect to the aqueous CO_2gas described by its Henry's constant (Eq. 52). Vertical flow of gaseous CO_2 is driven by buoyancy forces and causes net transport of CO_2 from the injection area to the unsaturated zone. At t = 600 min the degassing rate of CO_2 is very low and the aqueous CO_2 concentration is decreased to 0.038 mol/L. This results in a pCO_2 that equals the hydrostatic pressure at 1.1 atm, implying equilibrium conditions can be assumed.

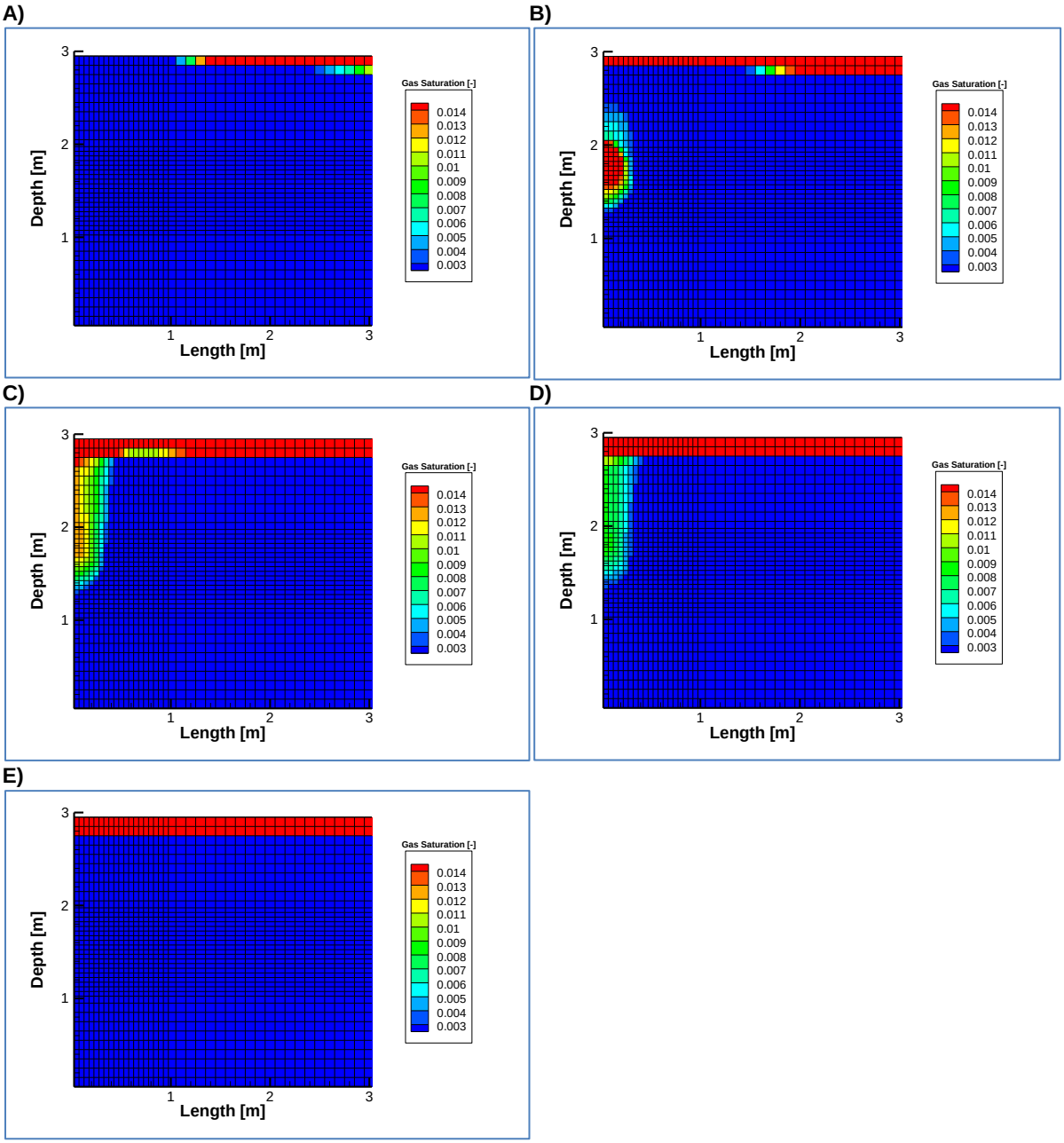

Fig. 8. *Gas saturations at respectively: A) 5 s, B) 3 min, C) 20 min, D) 50 min and E) 600 min.*

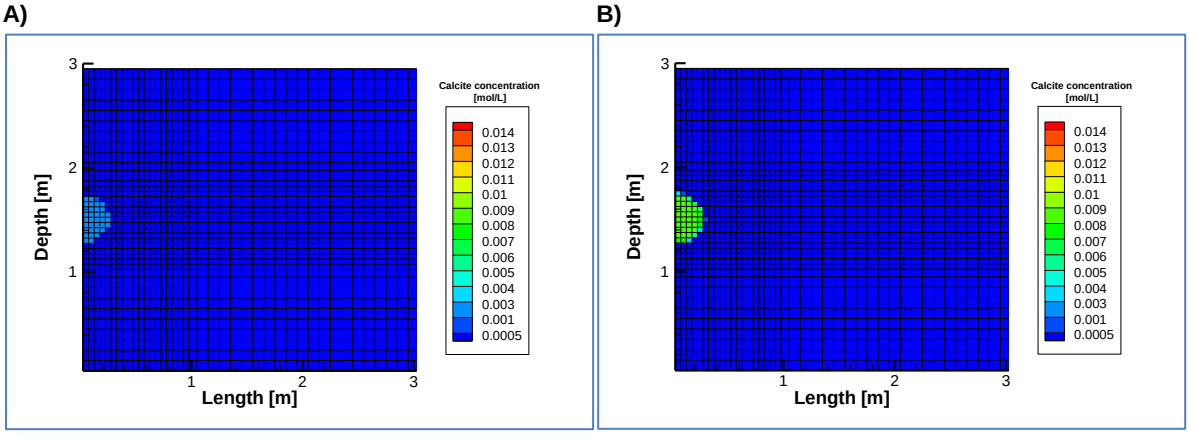

C)

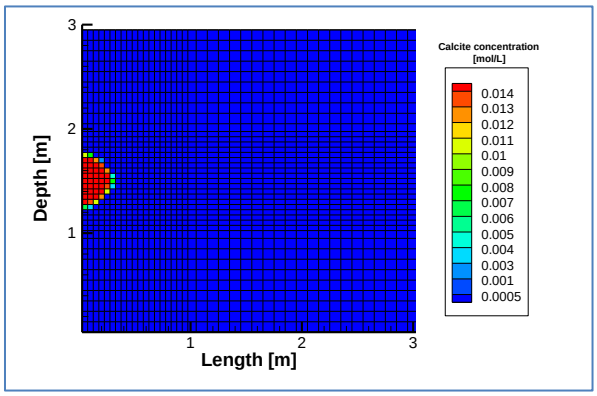

Fig. 9. *Calcite concentrations [mol/L] at respectively: A) 20 min, B) 50 min and C) 600 min.*

The cumulative loss of gas volume at the top boundary is shown in Fig. 10A. Due to the primary water table rise during injection a volumetric gas release of 2.21 L is modelled, corresponding quite well with the injected volume of 2.29 L. This primary gas release can be considered as air mass in the unsaturated zone leaving the model domain. From 1.8 min the volumetric gas release starts to increase sufficiently, representing the secondary water table rise due to the start of gaseous CO_2 formation in the porous medium (*see Fig. 8B*). Figure 10B shows the breakthrough curve of the gas saturation at the injection point. The CO_2 gas mole fraction is approximately 0.98 for the cases that gas saturation in the porous medium is present. Therefore the volumetric gas release at the top boundary is supposed to be solely due to CO_2 degassing when the gas plume contacts the unsaturated zone (*see Fig. 8C)*. Assuming the loss of gaseous air mass is negligible between 5 and 600 minutes, the net volume of gaseous CO_2 loss equals 9.44 L. This yields 0.399 moles of CO_2, according to the ideal gas law: $\frac{PV}{RT} = \frac{101325 * 0.00944}{8.314 * 288} = 0.399\, mol$. The total mol mass of injected aqueous CO_2 is 0.4. Assuming that from t = 1.8 min solely gaseous CO_2 degasses at the top boundary the CO_2 loss due to degassing is 0.399 mol, implies that the moles of CO_2 that remains in the batch chemistry system equals 0.01 mol. Nevertheless, a given amount of CO_2 is stored in the system as residual CO_2 concentration by the fictional aqueous species CO_2gas after degassing. During the initial stage of CO_2 gas formation the water table also rises and sufficient loss of air mass at the top boundary occurs. This implies that the total moles of 0.399 degassed CO_2 is slightly overestimated.

The coupled process of kinetic degassing and calcite precipitation and its effect on the species configuration of the solution is shown in Fig. 10C and D. The initial pCO_2 of the solution is 5.15 atm. When the system pressure drops, degassing starts and the removal of aqueous CO_2 increases the pH from 5.4 to 6.0 and consequently the alkalinity of the solution (*see Fig. 10C*). The carbonate concentration increases and thereby the ICP increases (*see Fig. 10D*). This implies that the solution becomes supersaturated with respect to calcite, resulting in fast calcite precipitation rates described by the kinetic Eq. 53. Due to degassing of CO_2 the saturation index for calcite increases up to 1.2 within 30 minutes, causing also an increase in precipitation rates since calcite kinetics depends on its saturation index. When the formation of carbonate decreases due to slower degassing rates, the removal of calcite species by calcite precipitation is so high that the ICP and thereby the calcite precipitation rates decreases until equilibrium conditions are reached. This yields that most of the calcite

precipitates in the time range of 10 to 50 minutes when the CO_2 degassing rates are high. Figures 10C and D show that the calcite precipitation is sufficiently fast and hardly any time lag between CO_2 degassing and calcite precipitation is modelled.

A)

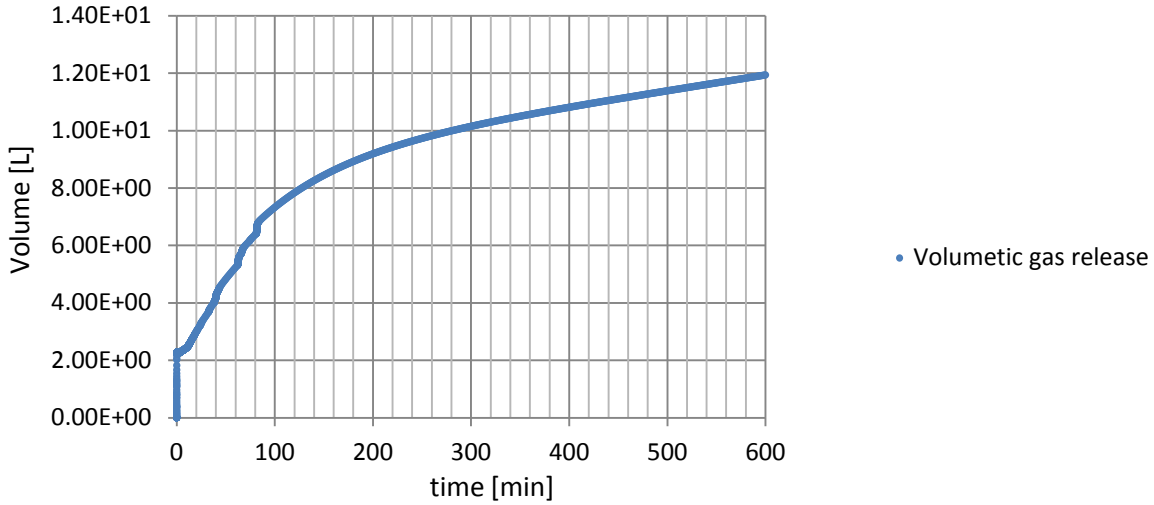

B)

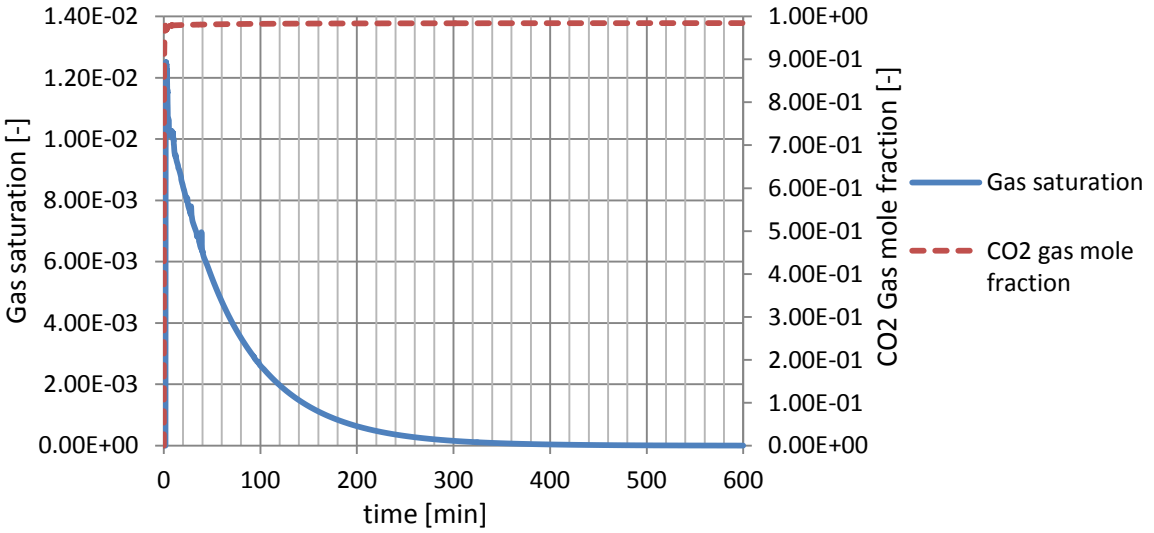

C)

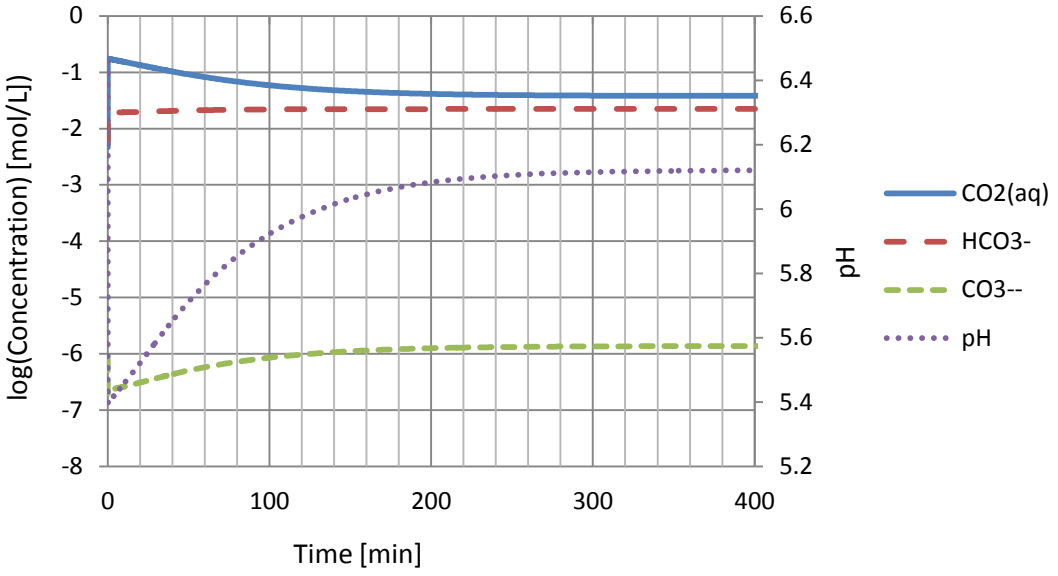

D)

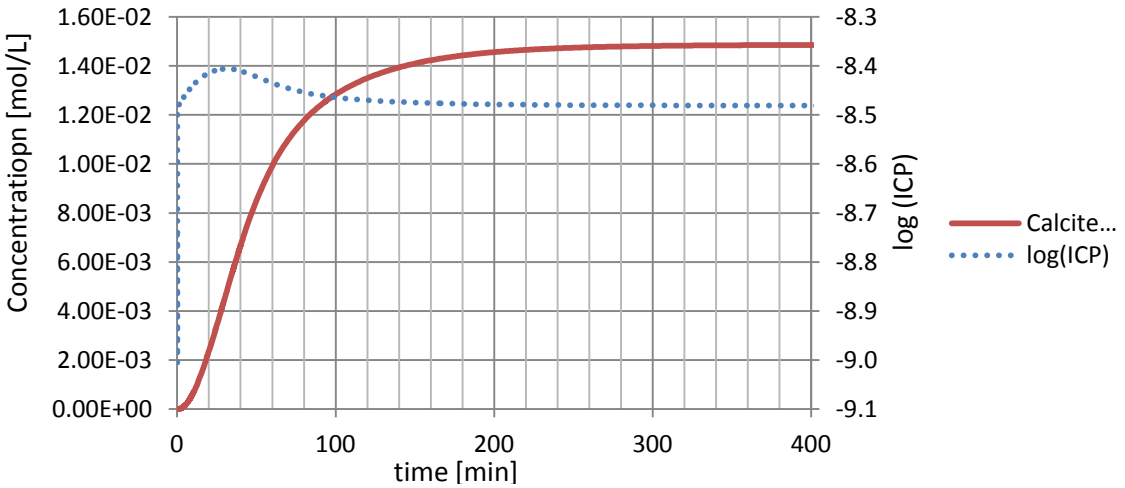

Fig. 10. *A) Gaseous volumetric gas release at the top boundary [X, Z=0, t]. B) Gas saturation and CO_2 gas mole fraction breakthrough curve at [X=0.025, Z= 1.525, t], C) The log concentrations of CO_2(aq), HCO_3^-, CO_3^- and the pH over time at [X=0.225, Z=1.525, t]. D) Precipitated calcite and ICP over time at [X=0.225, Z=1.525, t].*

4.2 Case 2

In this case the same conditions are assumed as in Case 1, but with taking into account the salinity of the solution. The injected concentration assemblage of the solution is shown in table 11 and is based on the species configuration according to PHREEQC (*see table A3.3*). The relationship described by Eq. 22 is used to determine the different calcite solubility of $10^{-8.00}$ mol^2/L^2 to allow for salinity, instead of modelling the formation of sodium complexes.

Table 11. *Initial and pulse species concentrations at grid cell [X=0.225, Z=1.525]*

Species	Input pulse concentration	Pulse concentration at t = 5 s	Concentration at t = 300 min
pH	-	5.6	6.3
CO_2(aq)	0.175 [mol/L]	0.175 [mol/L]	3.8e-2 [mol/L]
HCO_3^-	3.3e-2 [mol/L]	2.92e-2 [mol/L]	3.50e-2 [mol/L]
CO_3^{2-}	9.7e-7 [mol/L]	5.14e-7 [mol/L]	3.32e-6 [mol/L]
Ca^{2+}	2.2e-2 [mol/L]	1.82e-2 [mol/L]	3.00e-3 [mol/L]
$CaHCO_3^+$	3.0e-3 [mol/L]	6.79e-3 [mol/L]	1.33e-3 [mol/L]
CO_2gas (fictional)	-	0.0 [mol/L]	3.75e-3 [mol/L]
$CaCO_3$(s)	-	0.0 [mol/L]	2.05e-2 [mol/L]
PV Calcite	-	0.0 [-]	3.0e-4 [-]

In Fig. 11A is shown that the pH increases from 5.6 to 6.3 due to degassing of CO_2, resulting in an increase of the alkalinity. Consequently, the ICP increases up to $10^{-7.9}$ causing an increase in calcite precipitation rates. Equilibrium conditions are reached within the same time range as found for Case 1. The final alkalinity of the final solution is higher than found for Case 1. Also the concentration of precipitated calcite is increased with 5.1e-3 mol/L. If equilibrium conditions are assumed after 300 minutes, 0.0197 mol/L calcite is precipitated due to degassing of CO_2 and a pore volume reduction of 3.0e-4 is obtained.

A)

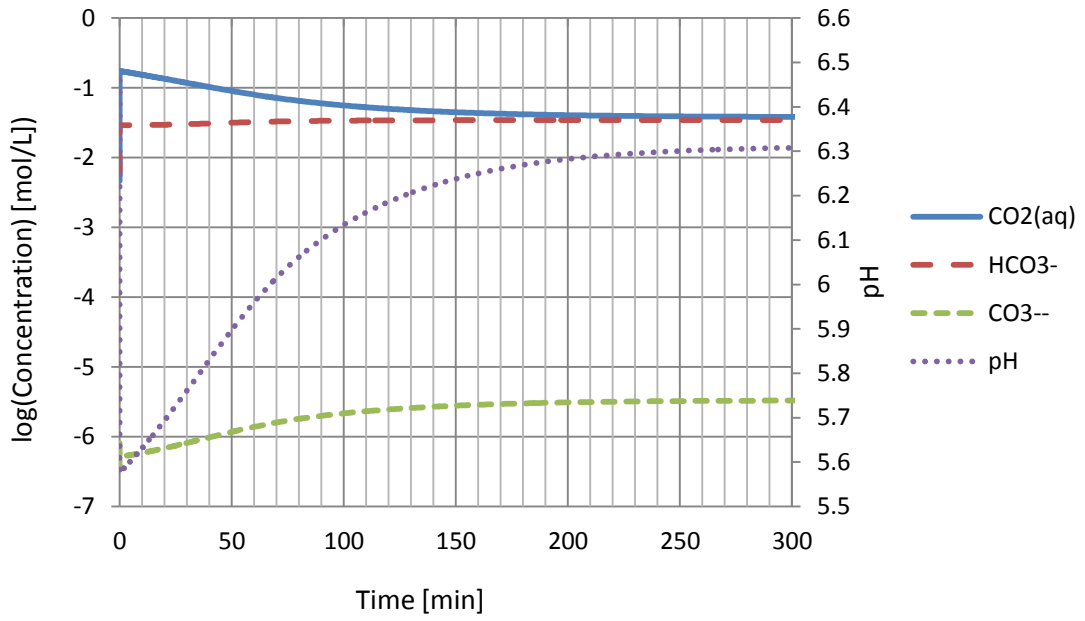

B)

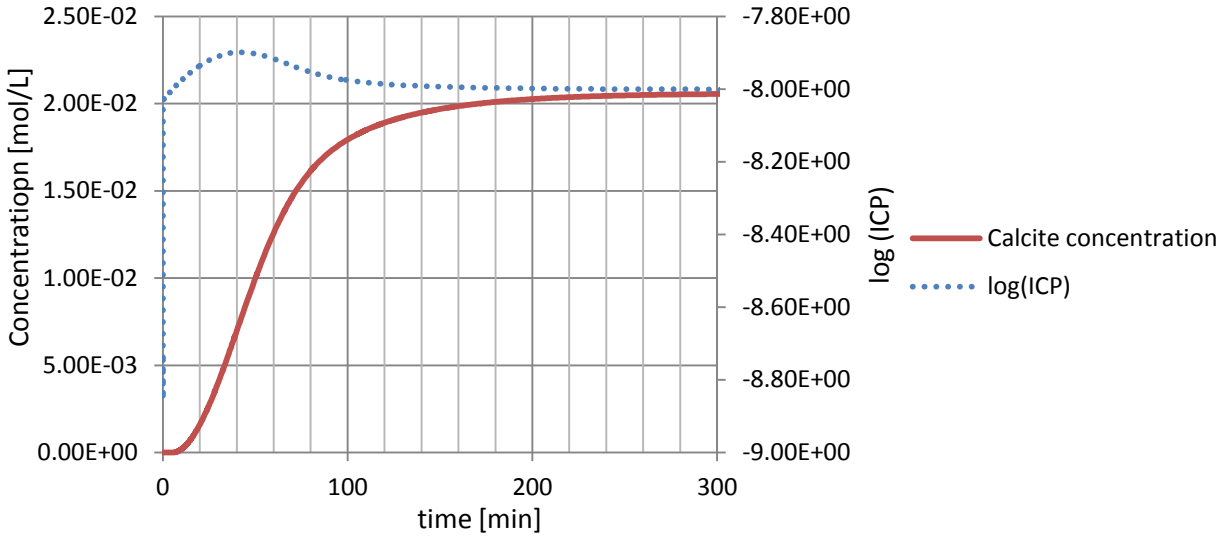

Fig. 11. *A) The log concentrations of CO_2(aq), HCO_3^-, CO_3^- and the pH over time at [X=0.225, Z=1.525]. B) Precipitated calcite and ICP over time at [X=0.225, Z=1.525].*

4.3 Case 3

According to Zhao et al. (2011) the mass transfer coefficient for degassing of CO_2 is related to the gas saturation (*see Fig. 2*). In our model only one value of k_g can be used to describe the whole degassing process, whilst the gas saturation in the degassing plume is significantly lowered due to decreasing degassing rates over time (*see Fig. 8 and Fig. 11B*). In this case is tested whether the use of different k_g values and its corresponding modelled gas saturations can be represented by the data of Zhao et al. (2011). This is done to verify which k_g is required to model the kinetic degassing of CO_2.

To assess the effect of different CO_2 degassing rates on calcite precipitation, 3 cases with different mass transfer coefficients are tested. The mass transfer coefficient used in Case 1 is compared with the k_g determined by Zhao et al. (2011) and for a k_g which is factor two higher than in Case 1, corresponding to a value of 0.0044 s^{-1} (Case 3.1). The relation between the mass transfer coefficient and gaseous saturation is shown in Fig. 2. According to this data the k_g used for Case 1 is slightly higher than found by their coefficients at low gas saturation. The sensitivity of CO_2 degassing on calcite precipitation is determined using constants of 0.0011 s^{-1} (Case 3.2) and 0.00036 s^{-1} (Case 3.3), corresponding to gas saturations of 0.1 and 0.025 respectively. Figure 12 shows the calcite and aqueous CO_2 concentration if degassing proceeds after the injection pulse. Half of aqueous CO_2 concentration is degassed at 41 minutes for Case 1, whilst for Case 3.1-3.3 this has occurred at 38, 60 and 350 minutes respectively.

Figures 13-15 show the gas saturation in the domain at a reference time of t = 20 min for the given cases. Also the gas saturation is showed when more than half of the initial aqueous CO_2 concentration is removed. Gas saturations up to 0.014 are found for Case 3.1, whilst for Cases 3.2 and 3.3 the gas saturations are respectively 0.01 and 0.003 at t = 20 min.

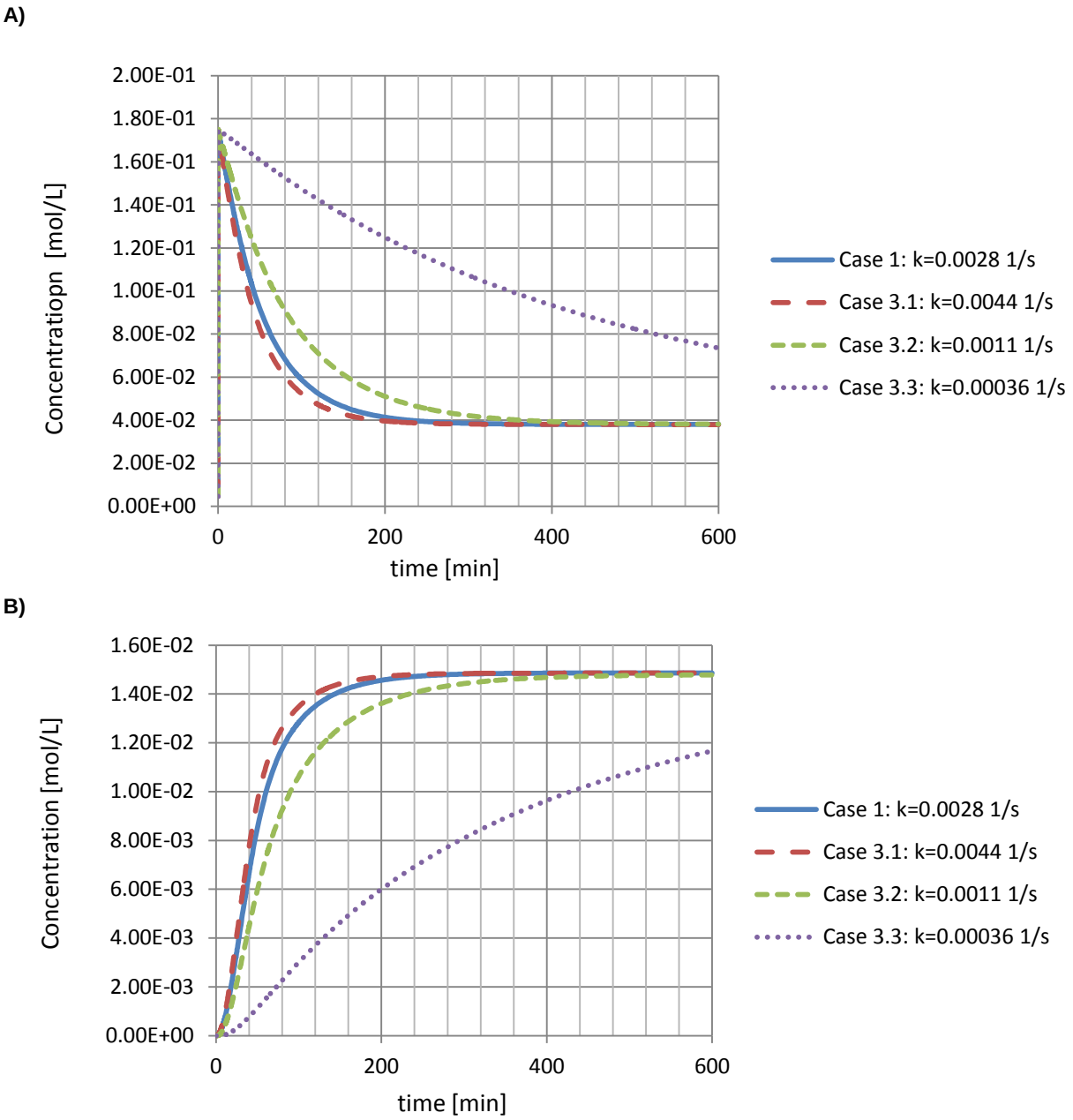

Fig. 12. *The concentration over time for A) aqueous CO_2, B) precipitated calcite at [X=0.225, Z=1.525]*

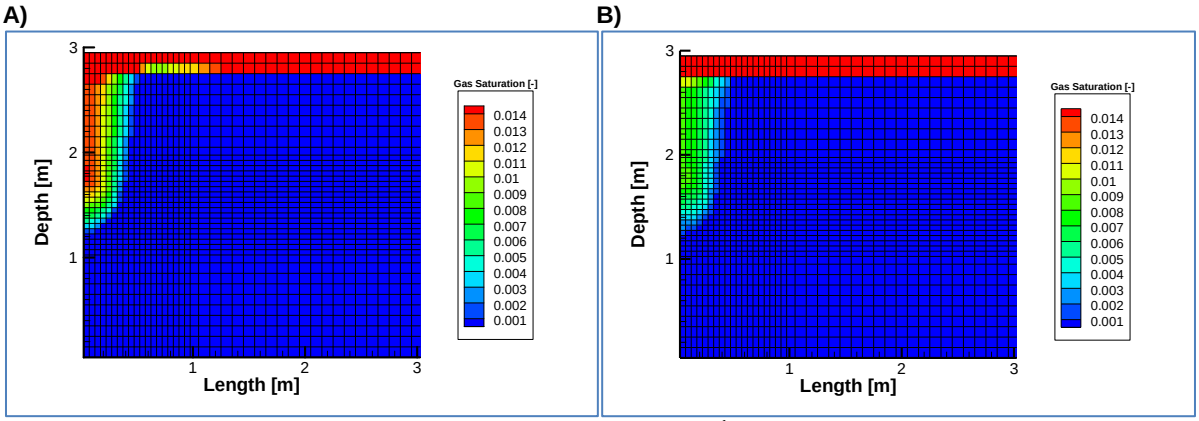

Fig. 13. *Degassing at mass transfer coefficient (k_g) 0.0044 s^{-1} at A) 20 min and B) 50 min for Case 3.1.*

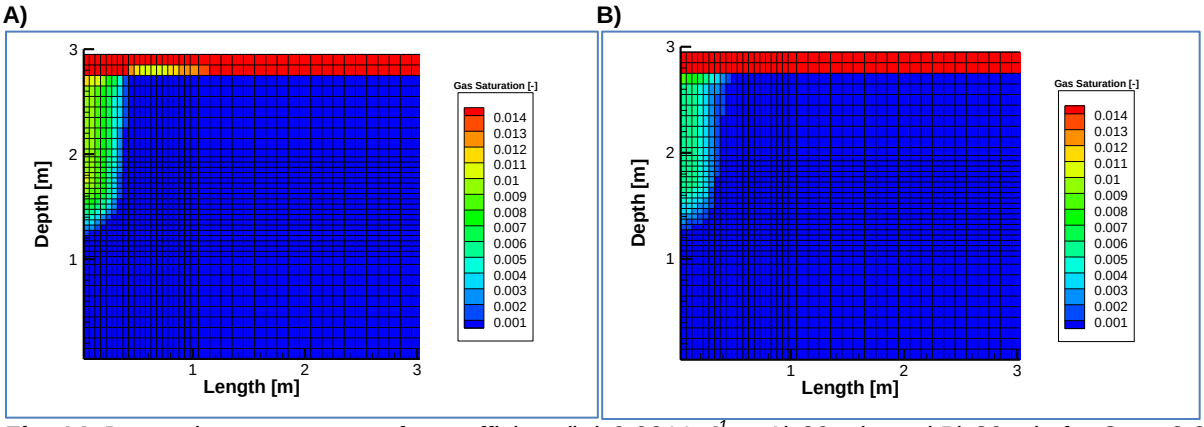

Fig. 14. *Degassing at mass transfer coefficient (k_g) 0.0011 s^{-1} at A) 20 min and B) 80 min for Case 3.2.*

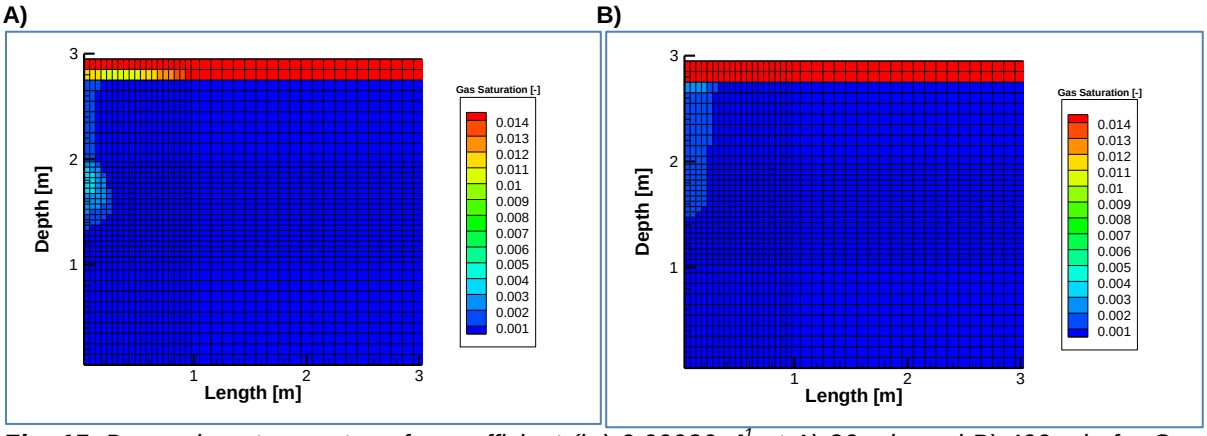

Fig. 15. *Degassing at mass transfer coefficient (k_g) 0.00036 s^{-1} at A) 20 min and B) 400 min for Case 3.3.*

4.4 Case 4

The precipitated calcite concentration after one injection pulse is low and therefore its effect on porosity reduction is small. Modelling of multiple injections to obtain the wanted reduction of porosity requires excessive long run times due to the complexity of the model calculations. A simple approach was adapted to investigate the effect of porosity reduction on permeability to validate the adaptations in the STOMP-WNE code for permeability reduction described by the Kozeny-Carmen relationship (Eq. 57).

In the model domain the porosity in the injection area, located at 0.0<X<0.4 and 1.6<Z<2.4, is manually decreased to 0.3, 0.2 and 0.1 for respectively Case 4.1, Case 4.2 and Case 4.3. The required injection time to attain the same injection volume as modelled in Case 1 can be determined using the Kozeny-Carmen relation and Darcy's law (*see A.6*). In table 12 the used injection times are shown and the resulting total injected aqueous volume after injection closure. For all cases the expected amount of volume injection was modelled using the given injection times. Due to the reduction of the pore space during cementation, the formed pore volume calcite is reduced per injection pulse. Also the injection radius is increased with decreasing porosity. In Fig. 16-18 the porosity and permeability reductions are shown for respectively Case 1, Case 4.1 and Case 4.2.

Table 12. *The injection time and total injected aqueous volume after injection closure.*

Cases	Porosity [-]	Injection time [s]	Total injected volume [L]	Pore volume calcite [-] at t = 600 min
Case 1	0.4	5	2.29	2.2e-4
Case 4.1	0.3	13	2.27	1.6e-4
Case 4.2	0.2	47	2.44	1.1e-4
Case 4.3	0.1	500	2.44	5.1e-5

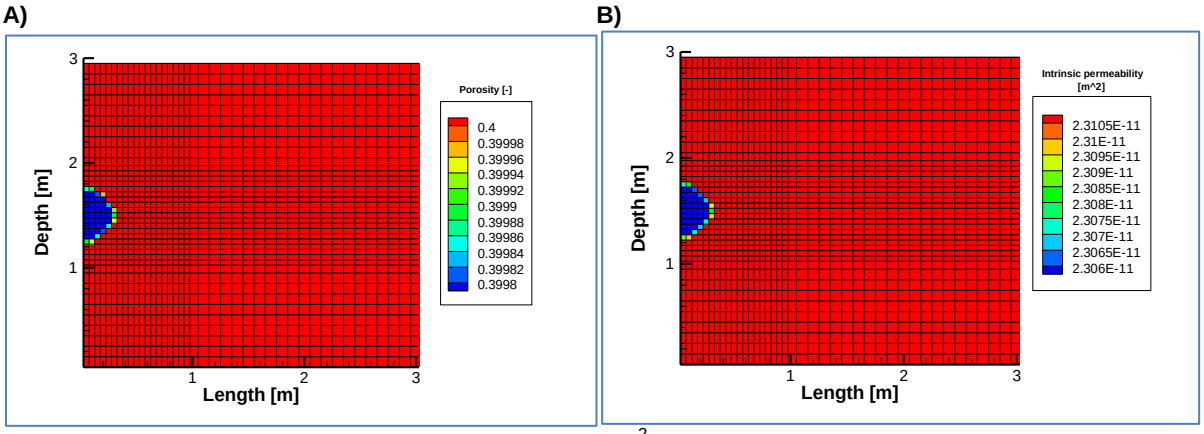

Fig. 16. *A) Porosity [-] and B) Intrinsic permeability [m^2] at t = 600 min for Case 1.*

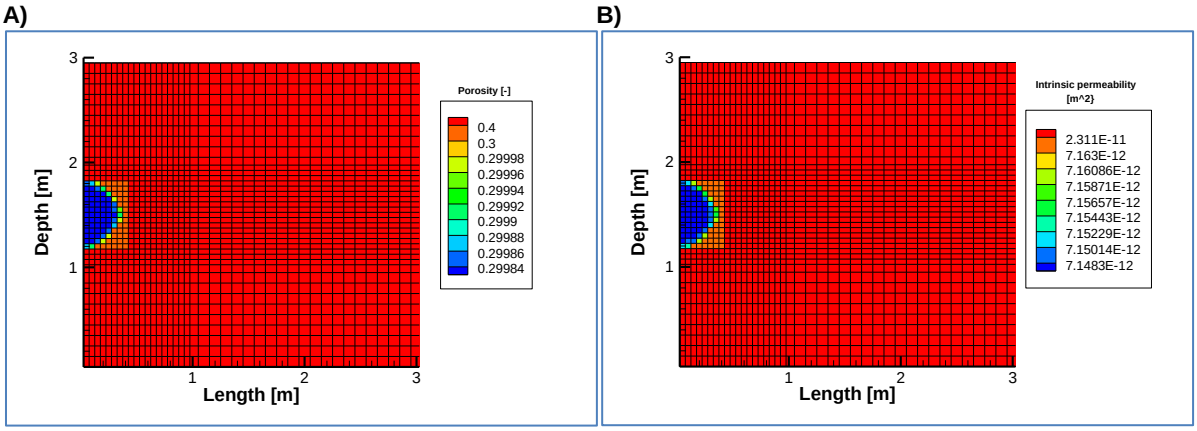

Fig. 17. *A) The porosity and B) intrinsic permeability at t = 600 min for Case 4.1*

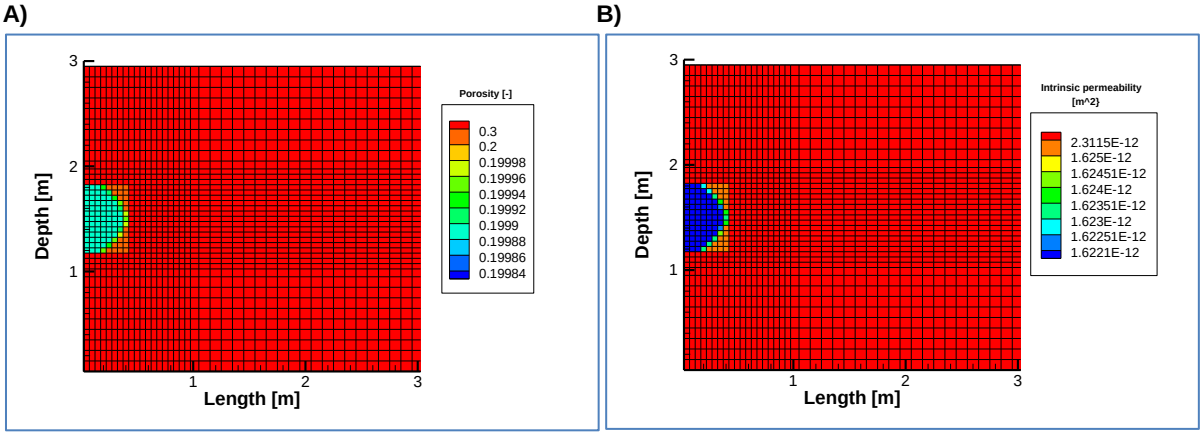

Fig. 18. *A) The porosity and B) intrinsic permeability at t = 600 min for Case 4.2*

In Fig. 19 the breakthrough curves of aqueous CO_2 for the different cases at point [0.225,1.525] are shown. Note that the breakthrough curve of aqueous CO_2 for Case 4.3 is not modelled as a sharp breakthrough front, whilst this should be expected since only advective transport is modelled and no mixing during transport of the aqueous CO_2 is taken into account. This is due to numerical dispersion (*see 5.1)*

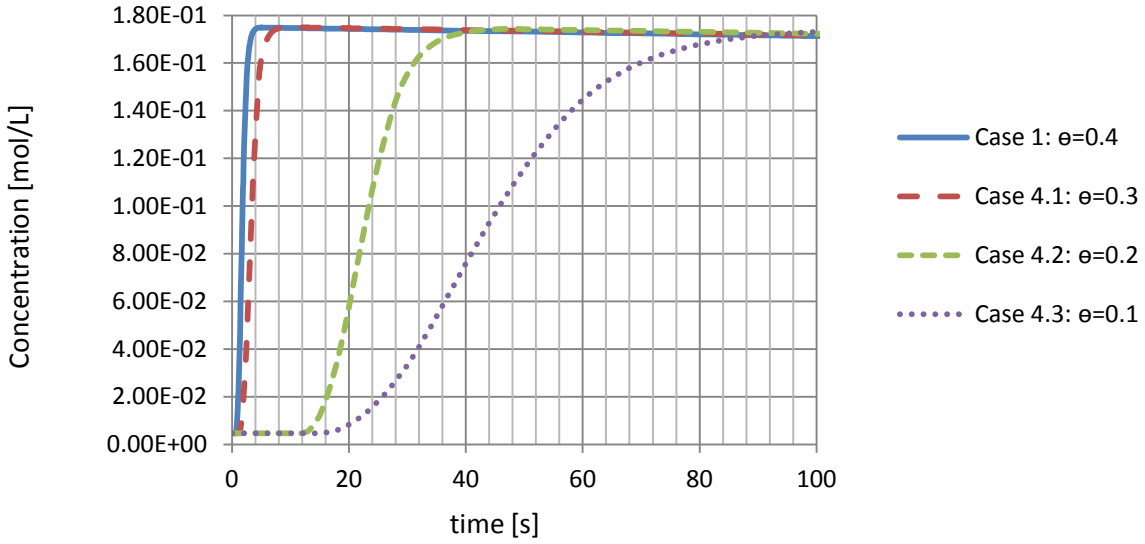

Fig. 19. *Breakthrough curves of aqueous CO_2 at [X=0.225, Z=1.525,t] for different porosities.*

Figures 20 and 21 show the gas plume for respectively Case 4.1 and 4.2. Due to decreased permeabilities within the cemented soil the gas flow is restricted. This implies that the residence time of formed gaseous CO_2 in the cemented porous medium is increased, due to decreased gaseous Darcy velocities within the grouted soil.

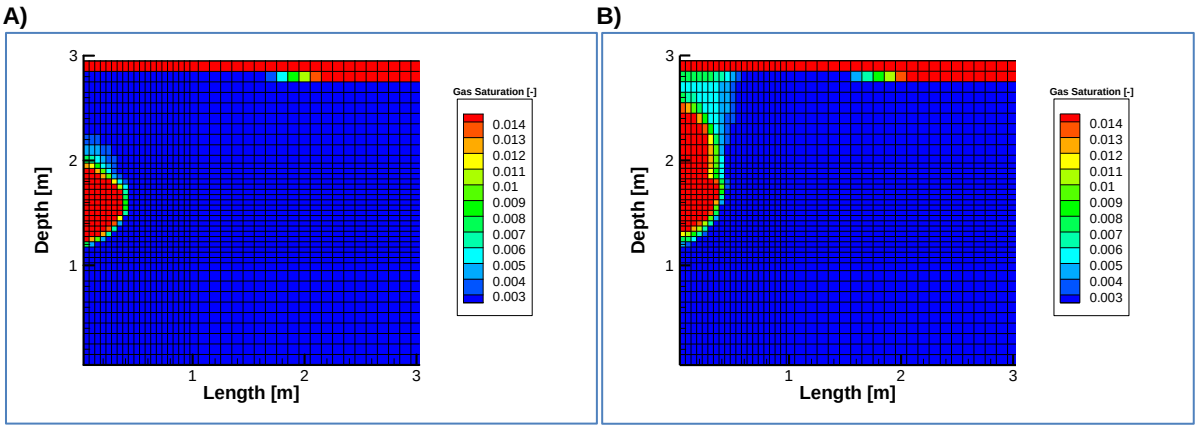

Fig. 20. *Gas saturations at respectively: A) 3 min and B) 5 min for Case 4.1*

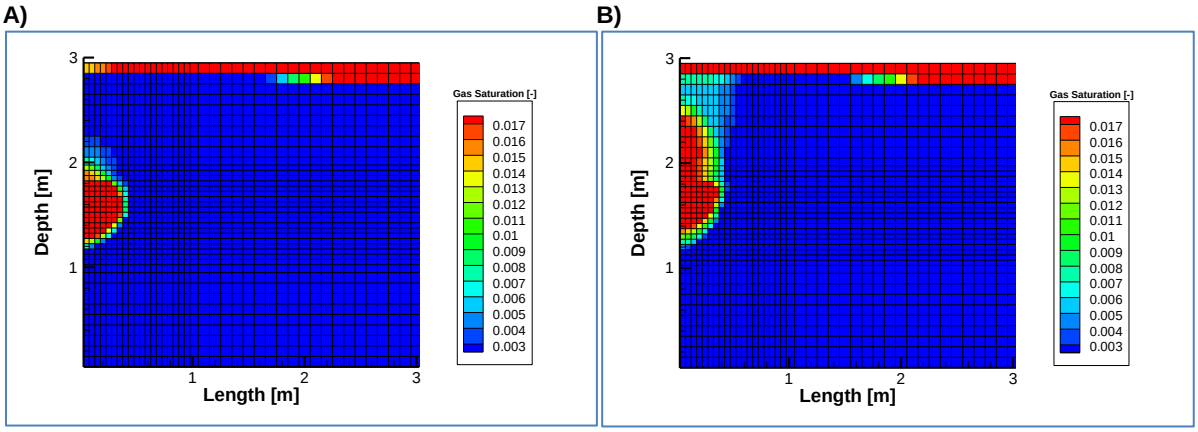

Fig. 21. *Gas saturations at respectively: A) 3 min and B) 5 min. for Case 4.2*

4.5 Case 5

An initial EcoGrout solution slightly supersaturated with respect to calcite at a pCO_2 of 5.1 atm is proposed (*see table 13)*. In Fig. 22B is shown that the initial calcite saturation index is 1.8, resulting in immediate precipitation of calcite during injection of the solution. The ICP is increased in the first 20 minutes due to degassing of CO_2, whilst the maximum ICP peak for Cases 1 and 2 was reached around 30 min. The high saturation index of calcite results in fast calcite precipitation rates described by Eq. 53, which causes a faster supply of CO_2 to the solution. This implies that sub-sequentially the degassing rates of CO_2 are also increased (*see Fig. 22A)* . Consequently, the equilibrium conditions are reached in a smaller timeframe than found for Case 1. At equilibrium conditions 4.97e-2 mol/L calcite is precipitated, resulting in a pore volume reduction of 7.3e-4. This implies that erroneous calcite precipitation occurs, since the initial total injected calcium concentration is 2.5e-2 mol/L.

Table 13. *Initial and pulse species concentrations at grid cell [X=0.225, Z=1.525]*

Species	**Input pulse concentration**	**Pulse concentration at t = 1.5 s**	**Concentration at t = 600 min**
pH	-	5.3	6.3
CO_2(aq)	0.175 [mol/L]	0.175 [mol/L]	3.8e-2 [mol/L]
HCO_3^-	3.3e-2 [mol/L]	1.46e-2 [mol/L]	2.23e-2 [mol/L]
CO_3^{2-}	9.7e-7 [mol/L]	1.29e-7 [mol/L]	1.38e-6 [mol/L]
Ca^{2+}	2.2e-2 [mol/L]	4.4e-2 [mol/L]	2.39e-3 [mol/L]
$CaHCO_3^+$	3.0e-3 [mol/L]	6.79e-3 [mol/L]	1.33e-3 [mol/L]
CO_2gas (fictional)	-	0.0 [mol/L]	3.75e-3 [mol/L]
$CaCO_3$(s)	-	0.0 [mol/L]	4.97e-2 [mol/L]
PV Calcite	-	0.0 [-]	7.3e-4 [-]

A)

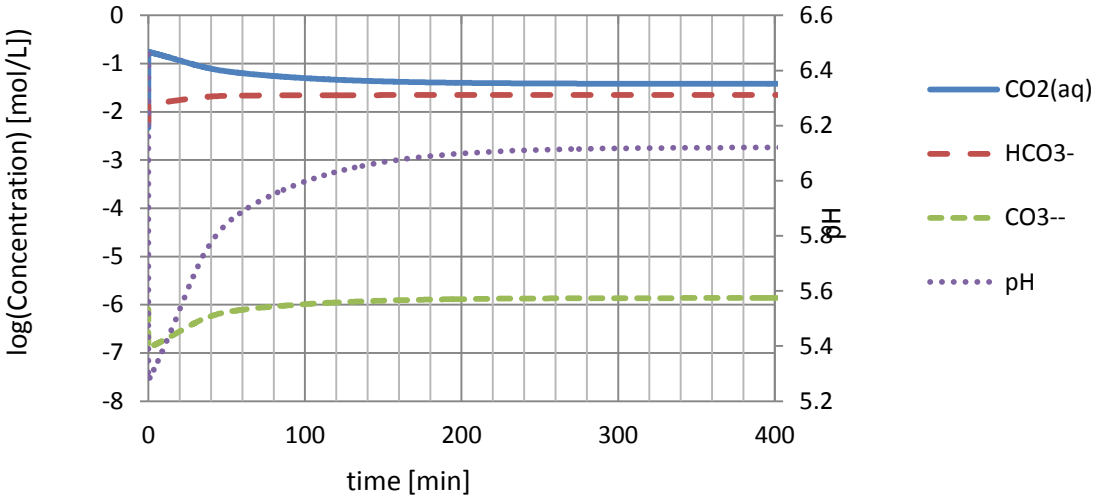

B)

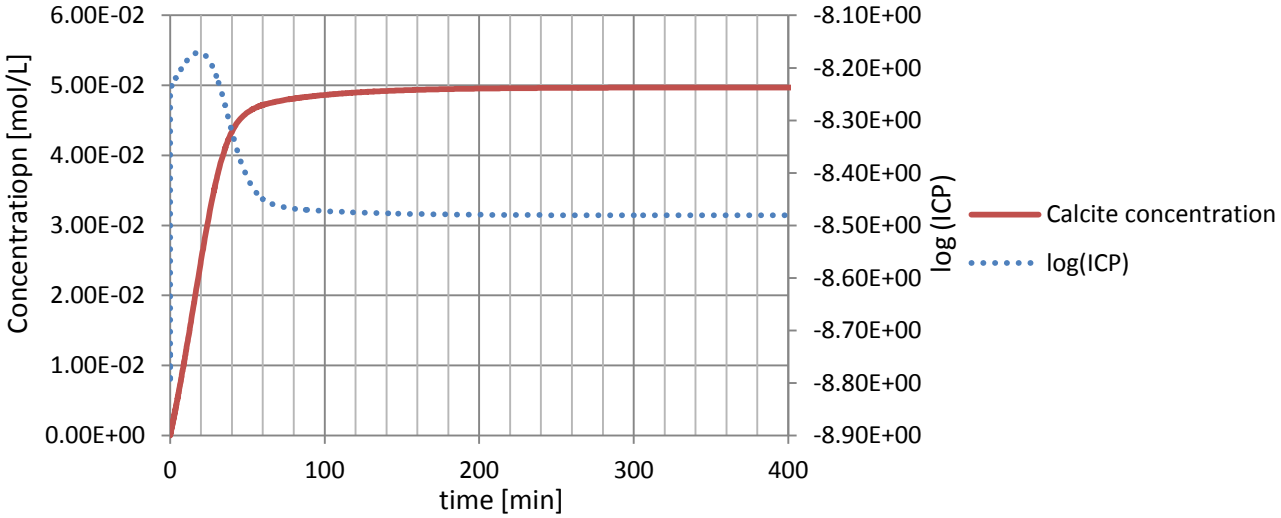

Fig. 22. *A) The log concentrations of $CO_2(aq)$, HCO_3^-, CO_3^- and the pH over time at [X=0.225, Z=1.525]. B) Precipitated calcite and ICP over time at [X=0.225, Z=1.525,] for Case 6.*

4.6 Case 6

Injection of an initial EcoGrout solution slightly undersaturated with respect to calcite and with a pCO_2 of 11.0 atm is modelled. The species configuration of this solutions is shown in table 14 and is based on PHREEQC data (*see table A3.6*). The calcite saturation index of this solution is 0.665.

Table 14. *Initial and pulse species concentrations at grid cell [X=0.225, Z=1.525]*

Species	**Input pulse concentration**	**Pulse concentration at t = 5 s**	**Concentration at t = 600 min**
pH	-	5.1	6.2
CO_2(aq)	0.375 [mol/L]	0.375 [mol/L]	3.8e-2 [mol/L]
HCO_3^-	2.0e-2 [mol/L]	2.00e-2 [mol/L]	2.44e-2 [mol/L]
CO_3^{2-}	9.7e-7 [mol/L]	1.13e-7 [mol/L]	1.65e-6 [mol/L]
Ca^{2+}	1.95e-2 [mol/L]	1.95e-2 [mol/L]	2.00e-3 [mol/L]
$CaHCO_3^+$	5.0e-3 [mol/L]	5.00e-3 [mol/L]	6.25e-4 [mol/L]
CO_2gas (fictional)	-	1.01e-4 [mol/L]	3.75e-3 [mol/L]
$CaCO_3$(s)	-	0.0 [mol/L]	2.17e-2 [mol/L]
PV Calcite	-	0.0 [-]	3.21e-4 [-]

The initial pCO_2 of the solution is a factor 2 higher than for the solution described in Case 1. An injection pressure of 10 atm was used. This results in system pressures that are sufficiently lower than the pCO_2 of the solution during the injection and causes immediate removal of CO_2 during injection due to the formation of aqueous CO_2gas. When equilibrium conditions are reached the pH is increased from 5.1 to 6.2 and the alkalinity is increased (*see Fig. 23A*). Figure 23B shows that calcite precipitation starts after 35 min. This is at the point when the ICP is increased above $10^{-8.48}$ due to the degassing of CO_2.

Figure 24 shows that the gas saturations in this case are up to a factor 4 higher compared to Case 1 due to increased degassing rates. Gas saturations up to 0.04 are modelled for the initial stage of CO_2 gas formation at time 3 min (*see Fig. 24A*). The cumulative loss of gas volume at the top boundary is 36.2 L at t = 600 min. Using the same method as described for Case 1, a loss of 1.42 moles gaseous CO_2 at the top boundary is determined, whilst 0.86 moles are injected. Note that the initial gas saturations are much higher than found for Case 1. This will result in a higher secondary water table rise and thereby a larger amount of volumetric air mass release at the top boundary. This might explain the discrepancy between the two values.

A)

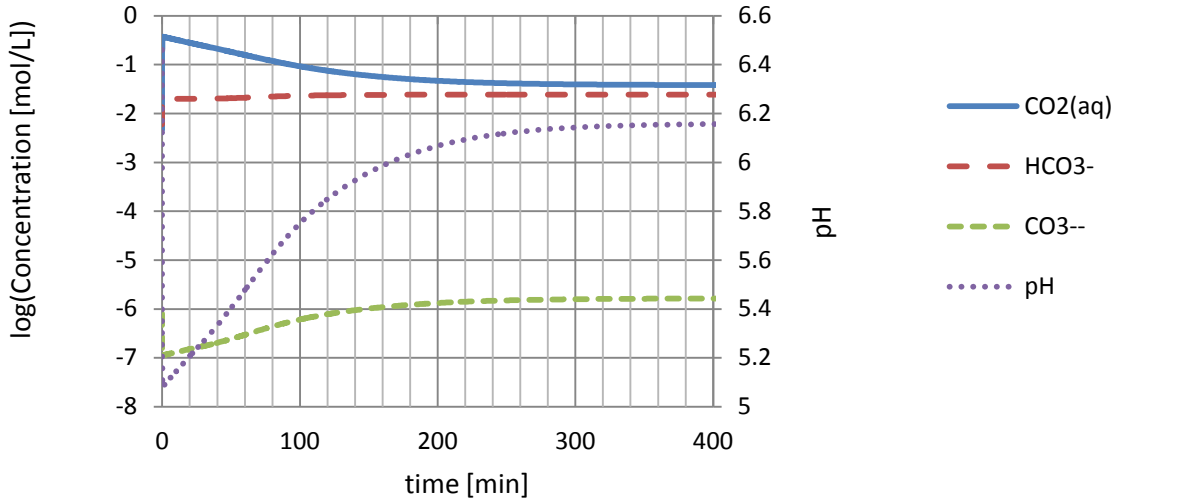

B)

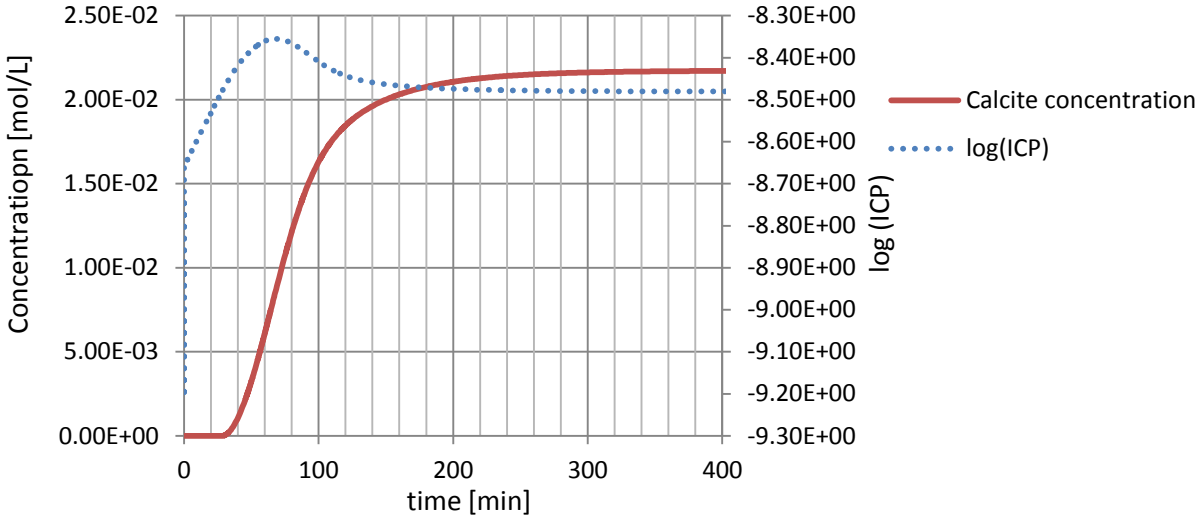

Fig. 23. *A) The log concentrations of $CO_2(aq)$, HCO_3^-, CO_3^- and the pH over time at [X=0.225, Z=1.525]. B) Precipitated calcite and ICP over time at [X=0.225, Z=1.525] for Case 6.*

A)

B)

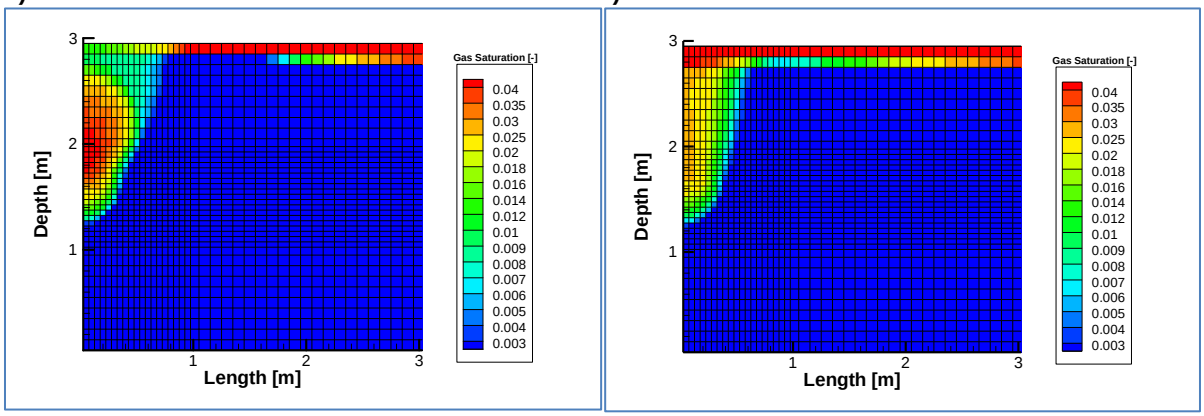

C) D)

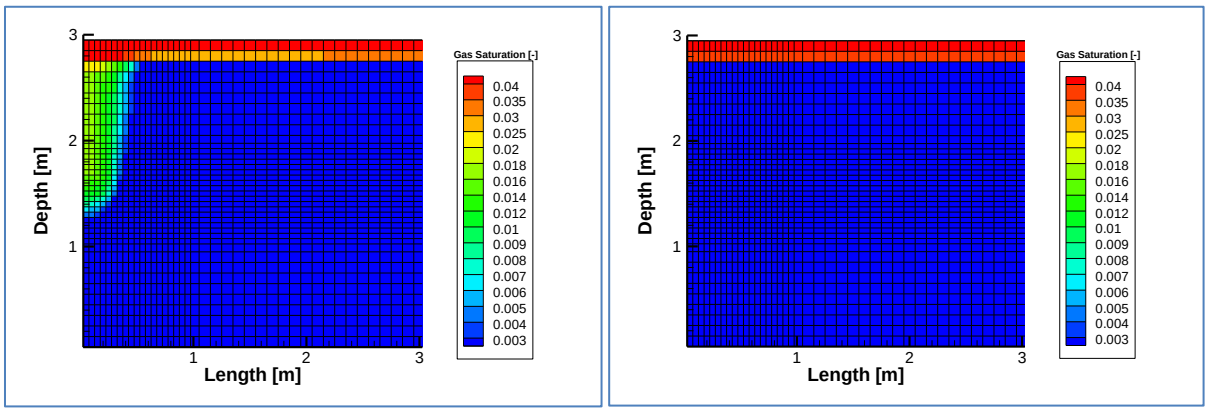

Fig 24. *Gas saturations at respectively: A) 3 min, B) 20 min, C) 50 min and D) 600 min.*

4.7 STOMP data versus PHREEQC data

The calcite precipitation per injection pulse is also calculated with PHREEQC. In A.3 the species assemblages of the initial and final EcoGrout solutions are shown. In table 15 the discrepancies between the calcite precipitation from our model and from PHREEQC are shown. For all cases the calcite precipitation in our model is higher than according to the PHREEQC calculations. These discrepancies are discussed below.

Table 15. *Discrepancies of net calcite precipitation after equilibrium conditions are reached at a hydrostatic pressure of 1.1 atm between our model and the PHREEQC model.*

Case	**STOMP calcite precipitation [mol/L]**	**PHREEQC calcite precipitation [mol/L]**
Case 1	1.49e-2	8.2e-3
Case 2	2.05e-2	1.09e-2
Case 5	4.97e-2	1.58e-2
Case 6	2.17e-2	1.12e-2

5. Discussion

In this study a model has been built to describe the EcoGrout process. An intricate complex model was built to model multiphase flow of gaseous CO_2 in the aqueous phase as well as kinetic degassing CO_2 from a solution that is supersaturated with respect to CO_2. Also the coupled process of CO_2 degassing and calcite precipitation is modelled with taking into account porosity and permeability alteration due to calcite formation. This is the first study that presents a model which describes the EcoGrout process.

The model was built to obtain insight into different aspects of the EcoGrout process and its influence on the properties of the unconsolidated soil. In this study an Ecogrout solution is injected into the porous medium for 5 seconds at an injection pressure of 10 atm. The used EcoGrout solution is initially in equilibrium with calcite at a high pCO_2 value. Due to high injection pressures, no degassing occurs during injection. When the injection pulse stops the kinetic degassing of CO_2 starts. The model results show that during the kinetic degassing of CO_2 the pH and thereby the carbonate concentration increase. Consequently, the solution becomes supersaturated with respect to calcite and fast calcite precipitation kinetics occurs. Calcite precipitation from a solution in equilibrium with calcite at a pCO_2 of 5.15 without and with taken into account the salinity (Case 1 and Case 2 respectively) and from a solution slightly undersaturated with calcite at a pCO_2 of 11 atm (Case 6) were modelled. This resulted in low calcite precipitation concentrations of respectively 1.49e-2, 2.05e-2 and 2.17e-2 mol/L for an injection pulse in porous medium with at an initial porosity of 0.4. These results imply that multiple injection pulses are required to attain the desired cementation of the soil in the field. The model was created under several assumptions, which are discussed below. The model should be validated using experiments to indicate whether these assumptions are plausible or not. Also the main aspects of modelling of the EcoGrout process are discussed.

5.1 Numerical dispersion

The solute transport of the injected species in the STOMP-simulator may produce numerical errors. Especially transport of low concentrations is susceptible to this behaviour and could result in erroneous results. A well known phenomenon is that the solute tends to disperse more than described by its physical transport processes. When solute transport is mainly controlled by advection, the numerical dispersion could have a significant influence on the model results (Aimo et al., 1997). During the EcoGrout modelling in STOMP, dispersion is assumed negligible and advection is considered to be the main transport mechanism ($Pe \rightarrow \infty$). This means that significant numerical dispersion can be expected in our model. The spreading front of the injected solutes should be sharp, because no dispersion is modelled. The breakthrough curves of aqueous CO_2 whilst using different porosities are shown in Fig. 19. No sharp concentration fronts are modelled for low flow rate conditions, like in Case 4.3. This can be explained by significant numerical dispersion during modelling.

Numerical dispersion might also be an issue for gaseous flow in our model domain. The buoyancy force driving the gaseous CO_2 to the surface is very large compared to the mixing of gaseous CO_2 with the aqueous phase by diffusion. Therefore advection for the gaseous mass transport is also the main transport mechanism for gas flow. This yields that high

Peclet numbers for gaseous flow might cause a significant numerical dispersion in our model. The numerical dispersion in our model might result in much wider and larger gas plumes in the model compared to plumes in the field. For the low porosity cases the effect of numerical dispersion on gas flow was high, resulting in erroneous gas plumes for Case 4.3 within the reduced porosity region.

5.2 Dissolution of gaseous CO_2

The STOMP-WNE simulator lacks the ability to model hysteresis effects at the moment and consequently entrapment of gas. This means that the net CO_2 flux to the unsaturated zone is higher in a case assuming non-hysteresis effects as described in this study than in a case which takes into account gaseous CO_2 entrapment. In this model, the fictional aqueous CO_2gas accounts for residual CO_2 in the gas plume. During degassing of CO_2, the transported CO_2 and also the trapped gaseous CO_2 will have a considerable influence on the local carbonate system. Gaseous CO_2 in the plume region above the injection point dissolves into groundwater which is undersaturated with respect to CO_2. The alkalinity of the groundwater increases and pH decreases until equilibrium between gaseous CO_2 and the carbonate system is reached. Also the calcite solubility increases due to the dissolution of CO_2 in the water, which implies that calcite dissolution in the degassing plume will occur when initial calcite concentrations in the soil are sufficiently high. However, the model is only applied with kinetic degassing by Eq. 51 and therefore the dissolution of CO_2 and its impact on the carbonate system is not modelled.

5.3 Discrepancy between STOMP and PHREEQC data

Calcite precipitation from solutions with a high calcite saturation index are not successfully modelled by the STOMP simulator. Fast kinetic precipitation rates described by Eq. 53 cause significant errors in the species concentration configuration or even convergence failure in the batch chemistry of ECKEchem. In Case 5 the calcite precipitation is shown from a solution where the ICP increases up to $10^{-8.2}$ mol^2/L^2 due to degassing of CO_2. This results in a calcite saturation index of 1.91, whilst for the other cases maximum values of the Ω_{calc} range from 1.2 to 1.35. The calcite precipitation rates were thereby increased with a factor 4.5 for Case 5 compared to Case 1. These fast rates might explain the erroneous results from Case 5 due to the use of relative large time steps to calculate the calcite precipitation. A thorough understanding of the calcite precipitation without the control of CO_2 degassing is needed to model this process realistically.

The understanding of the kinetic formulation of calcite precipitation by polynuclear processes from solutions with high calcite saturation indices is low. Calcite precipitations rates were considered to be fast compared to kinetics of CO_2 degassing and were described by Eq. 17 with u equals 1 (*see Eq. 53*). Other studies have fitted their data on high n^{th}-order reactions to describe the kinetics of polynuclear calcite precipitation from solutions with different calcite saturation indices (e.g. Sheikholeslami et al., 2003, Lioliou et al., 2007 and Rosa et al., 2011). This study focuses mainly on the control of CO_2 degassing on calcite precipitation and therefore sufficiently fast calcite precipitation rates are modelled. Calcite precipitation from solutions with high calcite saturation indices might also be modelled, but a sufficient amount of experimental data is needed for model calibration. For these cases it is important to know

whether polynuclear calcite formation or CO_2 degassing controls the EcoGrout reaction whilst the solution composition is changing over time.

In all cases the total calcite precipitation after one injection is overestimated compared to the PHREEQC data (*see table 15*). The same calcite precipitation should be expected from the STOMP simulator, since the equilibrium constants from the PHREEQC database are used for the equilibrium reactions in ECKEchem. Initially, the species configuration according to PHREEQC was injected for Case 1 (*see A.8*). This yields that the solution is supersaturated with respect to calcite. Therefore kinetic calcite precipitation starts immediately during injection without the control of CO_2 degassing. Hence, the initial concentrations of aqueous CO_2 were increased and those of CO_3^- lowered whilst keeping the total calcium concentration constant to obtain a solution in equilibrium with calcite. The batch chemistry of the ECKEchem module does not take into account the charge balance of the charged aqueous species. This results in slightly positively charged aqueous solutions, because the alkalinity is reduced and the whole system is balanced with its equilibrium constants. The fact that the species configuration of initial solutions in STOMP-WNE does not match with PHREEQC using the same equilibrium constants indicates a discrepancy between both models.

Both the activities and molalities of the species are shown in table A3.2. The solubility product of calcite equals the IAP at $10^{-8.48}$ mol^2/L^2, since the solution is in equilibrium with calcite at a pCO_2 of 1.1 atm. The ICP of the solution is $10^{-7.96}$ mol^2/L^2. That is much higher than the IAP, implying that the solubility product based on the concentrations instead of activities is also higher. The activities in PHREEQC are calculated by the extended Debye-Hückel equation (*see A.1*) (Parkhurst et al., 1999), just as in the ECKEchem module. In table A3.2 is shown that the activity coefficients based on PHREEQC for both carbonate and calcium are considerably low.

The same result must be expected from the batch chemistry described by the ECKEchem module, but this is not the case. Figure 8B shows that the ICP stabilizes at $10^{-8.48}$ mol^2/L^2, whilst stabilization at $10^{-7.96}$ mol^2/L^2 should be expected at equilibrium conditions, assuming the batch chemistry of ECKEchem matches with PHREEQC. From these results can be concluded that the solubility product of calcite based on both activities and concentrations are the same in the STOMP simulator. This implies that the activity coefficients for both carbonate and calcium are one and consequently the activity equals the concentration in the STOMP simulator. This is an indication that the activity calculations are not fully implemented throughout the code in this β-version of STOMP-WNE and this might be adapted in the final version of STOMP-WNE. However, in this study it has a large influence on the chemistry calculations. The CO_3^{2-} concentration of the final solution equals 1.38e-6 mol/L for Case 1 (*see table 9*) and only slightly differs with the CO_3^{2-}concentration of 1.27e-6 mol/L from the PHREEQC data (*see table A3.2).* The Ca^{2+} concentration of the final solution equals 2.39e-3 mol/L for Case 1, whilst the Ca^{2+} concentration calculated with PHREEQC is 8.59e-3 mol/L. The significant lower calcium concentrations calculated in the STOMP simulator, due to a lower calcite solubility product based on concentrations result in a significant overestimation of kinetic calcite precipitation. This explains the overestimation of calcite precipitation and the discrepancy of the species configuration in the carbonate system comparing the STOMP data with the PHREEQC data.

These discrepancy problems can be prevented in future studies by: 1) adapting the STOMP code to obtain the same activities as found by PHREEQC, 2) or using the ICP for a given solution at calcite equilibrium from the PHREEQC database to determine the solubility product and use this solubility product instead of the $K_{sp} = 10^{-8.48}$ mol^2/L^2. E.g., for Case 1 this should imply $K_{sp} = 10^{-7.84}$ mol^2/L^2 (*see table A3.1)*. Nevertheless, we should also account for the calcium bicarbonate complex, which is also susceptible to the discrepancy between the ICP and IAP of the calcium ion. Note that the ICP for calcite is not constant at calcite equilibrium for different species assemblages (*see A.3*). This makes it complicated to apply the second method properly. Appendix 9 shows the attempt to model Case 1 with the right species configuration and a K_{sp}' that equals the ICP of the initial EcoGrout solution at $10^{-7.84}$ mol^2/L^2. The formation of calcium bicarbonate complexes are not taken into account and the total concentration of calcium is thereby set to 1.8e-2 mol/L. The net calcite precipitation concentration is still overestimated compared to the PHREEQC data at 1.39e-2 mol/L and the final species configuration does not balance the charged species. Note that the initial pH is 5.7, whilst 5.5 is expected.

In Case 1 and 6 the pH of the initial solutions are respectively 5.4 and 5.2 in our model and matches quite well with the species configuration found by PHREEQC (*see tables A3.1 and A3.6*). However, the carbonate concentration of the solution is significantly lower, e.g.: 2.27e-7 versus 9.7e-7 for Case 1 and 1.14e-7 versus 6.04e-7 mol/L for Case 6. Small discrepancies between the two models are significant at these low concentrations of protons and carbonate ions and might have a considerable impact on the ICP and thereby the kinetic modelling of calcite precipitation. Numerical errors during the kinetic modelling of calcite precipitation might also explain the erroneous results from the STOMP simulator. This might be obviated by significantly reducing the time steps during modelling to attain more accurate results.

The total calcium concentrations for Case 1, 2 and 6 are respectively 4.1e-3, 4.3e-3 and 2.6e-3 mol/L when equilibrium conditions are reached at a pCO_2 of 1.1 atm. According to PHREEQC the total calcium concentration is 9.7e-3 mol/L at this pCO_2 (*see table A3.2)*. Figure 3 shows that these calculated calcium solubilities are reached when the pCO_2 has dropped below 0.2 atm if the PHREEQC data is used.

5.4 Kinetic degassing of CO_2

The mass transfer coefficient accounting for kinetic degassing is set to 0.0028 s^{-1} for Case 1 to have sufficiently fast degassing. Nevertheless, also lower coefficients were found by Zhao et al. (2011). The k_g in the range between 0.0011 and 0.00036 s^{-1} affects the degassing rate considerably. According to Zhao et al. (2011), these values correspond to gas saturations of 0.04 and 0.1 respectively (*see Fig. 2)*. The corresponding gas saturations determined in our model are much lower for a k_g of 0.0011 and 0.00036 s^{-1} at respectively 0.01 and 0.0013 at t = 20 min. The k_g values at gas saturations lower than 0.025 are not determined by Zhao et al. (2011). Extrapolating the relationship shown in Fig. 2, results in increased k_g values with decreasing gas saturation. This implies that the k_g used for Case 1 might be a good estimation for degassing in the first time interval, resulting in gas saturations up to 0.014 (*see Fig. 14)*. For Case 6 a k_g of 0.0028 s^{-1} results in gas saturations up to 0.04 (*see Fig. 24)*. This implies that for solutions with a high initial pCO_2 a lower k_g can be used, according to the data from Zhao et al. (2011).

Note that the results of Zhao et al. (2011) are based on degassing from water with a pCO_2 of 3.3 atm and a system pressure of 1.1 atm, whilst in our cases solutions with a pCO_2 of 5 and 10 atm are used. Experimental data of kinetic CO_2 degassing are needed to determine empirical mass transfer coefficients that account for degassing during the EcoGrout process. Only a fixed k_g to account for CO_2 degassing is assumed in the model, however the gas saturation and thereby k_g changes over time. A mean k_g is required to model the whole degassing process as accurate as possible. Calibration of the model using k_g values based on experimental data is required to verify scenarios.

5.5 Calcite precipitation efficiency per injection pulse

The chosen injection depth is 1.4 meter below the water table, whilst for geotechnical applications larger depths might also be required. This shallow depth was chosen in this model to ensure a significant amount of CO_2 degassing and thereby calcite precipitation. Figure 3 shows the relationship between calcite solubility and pCO_2. At larger depths the hydrostatic pressure will increase and thereby also the pCO_2 of the final solution will increase. This implies that using the same EcoGrout solution in the deeper subsurface will result in less calcite precipitation. Increasing the initial pCO_2 of the injected solution will increase the initial calcite solubility of the solution and thereby the net calcite precipitation after one injection. Nevertheless, the efficiency will decrease with increasing pCO_2 since the relationship between calcite equilibrium and pCO_2 is described by a 0.33^{th} order equation (*see Eq. 22*). In Case 6 the pCO_2 is increased up to twice the pCO_2 of Case 1, but this resulted only in 3e-3 mol/L calcite precipitation increase according to PHREEQC.

Figure 3 shows that the calcite solubility decreases significantly within the range of 1 to 0 atm pCO_2. Inexpensive methods to reduce the pCO_2 of the EcoGrout solution close to 0 atm can be considered to increase the calcite precipitation that can be obtained from an injected solution. E.g. the solution can be stripped from aqueous CO_2 to lower the pCO_2 using air sparging. If the CO_2 concentration of the sparged air is lower than the CO_2 concentration in groundwater, stripping occurs (Hasson et al., 2008).

According to Fig. 12, equilibrium conditions are reached after 200 minutes for Cases 1, 3.1 and 3.2. This implies that long time intervals of no injection are required to precipitate all calcite. Techniques to enhance the rate of pCO_2 lowering during the EcoGrout process should be investigated to increase calcite precipitation if slow kinetics are an issue. E.g.: aforementioned technique of CO_2 stripping during EcoGrout injection by simultaneous injection of air might increase the rate of aqueous CO_2 removal from the solution.

Increasing the solubility of calcite by increasing the salinity of the EcoGrout solution might be considered to obtain more calcite precipitation during one injection pulse. In Fig. 3 is shown the effect of sodium ions on the solubility of calcite at a sodium concentration of 0.375 mol/L. This effect is investigated in Case 2. Adding NaCl to an EcoGrout solution at a given pCO_2 will result in even higher calcite solubility. Also inhibitors, like magnesium (Mg^{2+}) or sulfate (SO_4^{2-}), can be used to reduce calcite solubility and to decrease kinetic calcite precipitation rates (Morse et al., 2007 and Sheikholeslami et al., 2003).

5.6 Porosity and permeability alteration

The pore volume reduction due to calcite precipitation is successfully modelled. The intrinsic permeabilities determined by the STOMP simulator are slightly higher than expected using intrinsic permeabilities solely based on the Kozeny-Carmen relation. This is due to permeability factors which are used in the entire source code. At porosities of 0.4, 0.3, 0.2 and 0.1, the intrinsic permeabilities determined in the STOMP-WNE simulator are respectively a factor 2.3, 1.9, 1.5 and 1.2 higher than expected.

In this study it is assumed that the Kozeny-Carmen relation is a representative relation to describe the permeability reduction due to changing porosity during the EcoGrout process. It is questionable if this relation which is mainly used for cohesionless soil is correct for this cementation process. Also the used mean grain size diameter (d_{50}) might alter over time. If the formed calcite particles are attached to the soil particles the d_{50} increases. If the calcite particles are formed without attaching to the soil particles and are significantly smaller than the grain particles of the soil, the d_{50} decreases.

Table 12 shows that the total injected volumes of EcoGrout solution for Cases 1 and 4.1-4.3 are equal. This validates the flow velocity reduction in our model on the analytical calculations done in A6 with decreasing porosity. The injection radii are increased for Cases 4.1 and 4.2 (*see Fig. 17 and 18*), which is also expected since the pore volume in the injection area is reduced. Only the porosity is manually adapted for the Cases 4.1-4.3. In reality the entry pressure for gaseous CO_2 will increase, when cementation of the pore throats occurs. Therefore different van Genuchten parameters should be used to define the capillary pressure-saturation function at given porosities.

5.7 Maximum injection pressure

In all cases an injection pressure of 10 atm is used at a depth of 1.4 meter to ensure that no degassing occurs during injection. In reality, injection into the soil is restricted due to liquefaction and soil fracturing whilst using high injection velocities. Darcy velocities of ~0.18 m/s are modelled in the vicinity of the injection point, resulting in volumetric rates of ~27 L/min (*see A.7*). According to Powers et al. (2007) the normal range of injection flow rates of permeation grouts are between 2 and 11 L/min and therefore liquefaction of the soil might be an issue in our modelled cases. For field applications it is necessary to account for the maximum injection pressure.

5.8 Calcite precipitation and strengthening of the soil

The formation of calcite in STOMP is modelled as in-situ precipitation, implying no transport of the calcite particles occurs. However, the concentration of the precipitated calcite after one injection pulse is very low and it is likely that colloidal transport of the small solid calcite nuclei through the pore space will occur. A consecutive process of multiple injection pulses, especially when using high injection pressures, might cause a considerable high advective flow for calcite nuclei transport. This implies that the modelled in-situ calcite precipitation overestimates the net precipitated calcite in one grid cell during one injection. These effects need to be studied thoroughly during experiments, to obtain insight in the transport of calcite nuclei by advective flow.

Geotechnical strenghening is an important potential use of the EcoGrout process. Increase of the strength of the soil requires less precipitation and is thus easier to achieve than reduction of the porosity and permeability for groundwater control. A sufficient amount of pore volumes calcite is needed to reduce permeability, whilst this is not necessarily needed to increase the strength of the soil (Parker et al., 2007). For these cases it is important that the cohesion of grain particles and thereby the shear strength of the soil is increased. It is likely that the formed calcite nuclei will clog the small pore throats of the porous medium first, resulting in an increased cohesion between the grain particles. The required pore volume reduction by calcite precipitation to increase the strength of the soil is determined for the BioGrout process (Van Wijngaarden et al., 2011). Assuming these values are comparable to the EcoGrout process an estimate of the required injection pulses can be made. In most geotechnical applications for strength increase, low strength cementation up to 1.5 MPa is sufficient. This corresponds to a calcite content of 250 kg/m^3 in the BioGrout process (van der Ruyt et al., 2009). Extrapolating these data to our modelled cases a pore volume reduction of approximately 0.09 is required. To prevent liquefaction of the soil, much lower cementation strength, up to 0.15 MPa is required, yielding a calcite content of only 80 kg/m^3 in the BioGrout process (Whiffin et al., 2007). This corresponds to a pore volume reduction of approximately 0.09 in our model. However, for strengthening of the soil it is important where the calcite precipitates during the EcoGrout process. Calcite precipitation that connects the soil particles at the pore throats will result in sufficient increase in strength, whilst loose calcite particle formation will hardly cause an increase in strength. Therefore experimental tests need to be done to determine the strength of EcoGout cemented soil at different calcite contents

The required injection pulses for our modelled cases to obtain the pore volume reduction for prevention of soil liquefaction, low strength cementation and significant porosity reduction for groundwater control are shown in table 16. This implies that for geotechnical applications that require low pore volume reduction and large injection radii, EcoGrout methods based on calcite precipitation solely controlled by CO_2 degassing might be a considerable option, although it will be time-consuming.

Table 16. *Required injection pulses for calculated PV reductions from both STOMP and PHREEQC.*

Cases	**Required PV reduction**	**Required injection pulses (STOMP)**	**Required injection pulses (PHREEQC)**
1	0.03	142	268
1	0.09	464	874
1	0.3	2520	4753
2	0.03	103	194
2	0.09	337	634
2	0.3	1831	3445
6	0.03	99	190
6	0.09	319	617
6	0.3	1725	3341

5.9 Feasibility and further study

As shown above, the calcite precipitation solely controlled by CO_2 degassing by using an EcoGrout solution at calcite equilibrium at a high pCO_2 will be very time-consuming. This study shows that per injection pulse up to 200 minutes are required until equilibrium conditions are reached and all calcite is precipitated. In addition, the amount of required injection pulses to obtain sufficient cementation of the soil is high (*see table 16).* On the other hand, this study shows that the control on injection radii is high since no degassing occurs if the injection pressure is higher than the pCO_2. In addition, the degassing rates are sufficiently low to prevent clogging during injection.

The net calcite precipitation per injection pulse can be increased by using EcoGrout solutions that are slightly supersaturated with respect to calcite. When a relative acid EcoGrout solution with a high pCO_2 (*see Fig. 4*) is used, the degassing of CO_2 will largely control the precipitation process. It is important that during the injection of these EcoGrout solutions, which are initially supersaturated with respect to calcite, the system pressure is significantly lower than the pCO_2. Otherwise the calcite precipitation will occur without degassing of CO_2 and degassing will not control the calcite precipitation. The method of injection pulses as introduced in this study might be an interesting option. Tables A3.7-8 show that using an injection pulse of an EcoGrout solution of 0.1875 mol/L Ca^{2+} and 0.375 mol/L HCO_3^- with 0.3 mol/L HCl results in 3.2e-2 mol/L calcite precipitation assuming the system pressure drops to 1.1 atm. Note that the net calcite precipitation per injection pulse increases with decreasing acidity and pCO_2 of the initial solution. This implies that the control of CO_2 degassing on calcite precipitation also decreases, since the calcite saturation index increases.

A thorough understanding is required whether calcite nucleation or degassing of CO_2 is the rate limiting during calcite precipitation taking into account the change of the solutions configuration over time during the reaction process. Therefore lab experiments with EcoGrout solutions at different calcite saturation indices and pCO_2 values are needed to extent and validate the model. This study shows that the control of CO_2 degassing on calcite precipitation will enable us to attain large injection radii and prevent clogging in the vicinity of the well. The lab experiments with different EcoGrout solutions will show whether insufficient injection radii and clogging are obtained. The aim for further studies should be to establish a good balance between reducing the required timeframe to attain sufficient cementation and obtaining sufficient injection radii per injection pulse.

6. Conclusion

The STOMP-WNE simulator extended with the batch chemistry module ECKEchem has been used to describe the EcoGrout process. The kinetic degassing of gaseous CO_2 and the porosity and permeability alteration due to precipitating calcite were formulated in the source code. This model gives insight into the processes that play an important role during calcite precipitation. This study mainly focuses on control of CO_2 degassing on calcite precipitation using an initial EcoGrout solution in equilibrium with calcite and a pCO_2 of 5.1 atm. The main conclusions are listed below:

- Increase of pH and alkalinity is determined for all cases during CO_2 degassing. This results in an increase of the ICP, implying the solution becomes supersaturated with calcite and fast precipitation of calcite starts.
- Different mass transfer coefficients for CO_2 degassing have a significant control on the rate of calcite precipitation. Slow degassing conditions increase the required time to reach equilibrium conditions sufficiently.
- No degassing occurs during injection when the system pressure is higher than the pCO_2 of the solution. This implies that large injection radii can be achieved for geotechnical applications. In addition, the degassing rates of CO_2 are sufficiently low that continuous injection at CO_2 supersaturation is also feasible.
- The determined pore volume reduction per injection pulse is low and multiple injections are required for geotechnical applications. Pore volume reductions range from 2.2e-4 to 3.2e-4 for the cases modelled at a porosity of 0.4. During cementation of the soil the net pore volume reduction per injection pulse is decreased.
- The pore volume reduction was increased using EcoGrout solutions in equilibrium with calcite with 1) taking into account NaCl concentrations and 2) higher pCO_2.
- To attain the wanted injection volume in the cemented soil the required injection time increases drastically using a fixed injection pressure. This is due to the permeability reduction obtained from the precipitated calcite.
- Discrepancies in the batch chemistry between data from the STOMP-simulator and PHREEQC have been identified. The simulations in STOMP result in significant overestimation of the final precipitated calcite compared to the PHREEQC data. Therefore, improvement of the batch chemistry ECKEchem is required.

Recommendations

In this study a basic model was build for modelling calcite precipitation controlled by kinetic degassing of CO_2. Also, alteration of porosity and permeability due to formation of solid particles is modelled. Unfortunately, the STOMP-WNE code is still under construction and a not officially released β- version was used. Consequently, this version lacked the usual support. It is likely that the final code will feature more possibilities, e.g. modelling of non-hysteresis effects. Also the batch chemistry of the ECKEchem module might be improved. It is recommended to acquire the STOMP-WNE code from PNNL, when it is officially released. Implementation of the adapted parts of the source code done in this study, e.g. porosity and permeability alteration and kinetic degassing, could be used for the source code of the officially released STOMP-WNE simulator.

The main problem is that the activities of calcium and carbonate ions equals the concentrations in the batch chemistry of ECKEchem, whilst PHREEQC calculated activities a factor two lower. This causes a significant discrepancy in the calcite solubility product based on concentrations between both models. A thorough understanding of the used Debye-Hückel relationship in both models is needed and adaptations of the ECKEchem code are required.

The computational power of the used PC must be high to model cases with longer injection times and sufficient porosity reduction. The used models ran on the computer server of the Geophysics department of University of Utrecht on one node. Using more server nodes might increase the computational efficiency.

Experimental data from EcoGrout processes under field conditions is needed to calibrate the STOMP model for obtaining reliable results. It is recommended to start with simple experimental column tests to investigate the kinetic rate of CO_2 and the resulting calcite precipitation from EcoGrout solutions initially in equilibrium with calcite. The STOMP simulator can be used to simulate these experiments to determine the parameters accurately.

This model focuses mainly on the control of CO_2 degassing on calcite precipitation, whilst using solutions with high calcite supersaturations should also be considered. The potential for calcite precipiation per volume unit EcoGrout solution is much higher for solutions with increased calcite supersaturation (*see 2.4*). The rate limiting reaction that controls calcite precipitation could alter over time and therefore adaption of the source code is required. E.g.: according to experimental data the calcite precipitation is controlled by polynuclear calcite formation if the calcite saturation index higher than 5 and can be described by using Eq. 17 with u = 3. If the calcite saturation index lower than 5, CO_2 degassing controls the calcite precipitation. This can be easily implemented into the source code of ECKEchem using IF .. THEN statements.

The mass transfer of CO_2 between the gaseous and aqueous is described by using Eqs. 50-52. This is done because flow of multiple gas components is calculated using Henry's law (*see 3.4*). Initially, the STOMP-WNE model was recommended because the effect of stripping volatile organic compounds (VOC's) from contaminated groundwater due to CO_2

degassing during the EcoGrout process is also investigated at Deltares. The STOMP-WNE simulator can be used to insert a third gaseous compound, which is in this case VOC, to model the effect of stripping during CO_2 degassing. Modelling kinetic degassing as direct mass transfer between the gaseous and aqueous phase should be done in a model with one component gas. In this case Henry's law can be easily replaced by Eq. 18, without ruining the basics of the model. STOMP-CO_2-R can be used for this application (White et al., 2005).

The initial goal of this model was to obtain insight in the feasibility of the EcoGrout process. However, this basic model can also be used for different scenarios, where permeability and porosity alteration and gas formation are an issue. We can think about: 1) Modelling of well clogging at ATES systems due to thermodynamic effects on calcite solubility with using the heat flow option the STOMP-WNE simulator and the adoptions that are made in the code during this study. 2). Enhanced biodegradation of organic matter using Monod-kinetics and the associated formation of gaseous CO_2 in porous medium, whilst porosity is increasing.

Acknowledgement

I wish to thank some people for their contribution to this study:

Prof. dr. ir. S.M. Hassanizadeh: He could always find time to help me with solving problems I was facing. He was also a big help for establishing the contact with the PNNL laboratory. I also want to thank him for the interesting courses he has lectured during my Master.

Dr. N. Hartog: He guided me with patience and 'get-up-and-go' enthusiasm, whilst explaining the principles of carbonate chemistry and EcoGrout. He has taught me so much during the whole process.

Dr. A. Marsman: She helped me with the understanding and the use of the STOMP-simulator and guided me through the principles of modelling an programming in complex codes.

Dr. A. van der Berg and **mr. T. van Zessen:** They enabled me to run my STOMP models on the computer server of the department of Geophysics at Utrecht University. Running times were reduced from 1.5 weeks to a few days, resulting in this study gained momentum. Dr. van der Berg's detailed instructions how to model in Linux were very helpful.

PNNL Laboratory: They disposed their unreleased STOMP-WNE-R code for free use.

In addition, I have a word of thank to **dr. J. Valstar** from Deltares and **dr. C. Hofstee** from TNO, who have proposed suggestions during the programming in the STOMP-WNE code. I also want to thank **mrs. D. den Hamer** from Deltares for discussion on the EcoGrout process and fellow student, **mr. T. Sweijen**, for mutual discussion whilst modelling with STOMP and writing our theses.

References

Aimo, N.J. and Oostrom, M., 1997. *PMFCT-2D: A transport simulator for various grid Peclet numbers.* Groundwater, Vol. 35(1), P. 30-38.

Appelo, C.A.J. and Postma D., 2005. *Geochemistry, groundwater and pollution*. 2nd version, A.A. Balkema, Leiden, P. 105-141.

Arakaki T. and Mucci A., 1995. *A continuous and mechanistic representation of calcite reaction-controlled kinetics in dilute solutions at 25 ^{0}C and 1 atm total pressure*. Aquatic Geochemistry, Vol. 1(1), P. 105-130.

Bear, J.,1972. *Dynamics of Fluids in Porous Media*. Dover Publications, New York. P. 119-194.

Byle, M.J. and Borden R.H., 1995. *Verification of geotechnical grouting: a report from the ASCE Committee on Grouting of the geotechnical Engineering division and paper presented at the ASCE Convention in San Diego, California, October 23-27, 1995.* The American Society of Civil Engineers. P. 1-164.

Carsel, F.F. and Parrish, R.S., 1988. *Developing joint probability distributions of soil water retention characteristics.* Water Resources Research, Vol. 24(5), P. 755-769.

Dreybrodt, W., Eisenlohr, L., Madry, B. and Ringer, S., 1997. *Precipitation kinetics of calite in the system $CaCO_3$ - H_2O - CO_2: The conversion to CO_2 by the slow process $H^+ + HCO_3^- \rightarrow CO_2 + H_2O$ as a rate limiting step.* Geochimica et Cosmochimica Acta, Vol. 61(18), P. 3897-3904.

Enouy, R., Li, M. Ioannidis, M.A. and Unger, A.J.A., 2010. *Gas exsolution and flow during supersaturated water injection in porous media: 2. Column experiments and continuum modelling.* Advances in water resources, Vol. 34(1), P. 15-25.

Fang, Y., Yeh G.-T. and Burgos, W.D., 2003. *A general paradigm to model reaction-based biochemical processes in batch systems.* Water Resources Research, Vol. 34(4), P. 1083-1107.

Fetter, C.W., 1999. *Contaminant Hydrology.* 2nd version ,Waveland Press, Illinois, P. 170-263.

Guo, W., Daëron, M., Niles, P., Goddard, W.A. and Eiler., J.M., 2007. *Isotopic fractionations associated with degassing of CO_2 from aqueous solutions and implications for carbonate clumped isotope thermometry.* Eos, Transactions American Geophysical Union, Vol. 88(52), Fall meet. Suppl. Abstract, PP43B-1276.

Hasson D., Lisitsin, D. and Semiat, R., 2008. *The potential of CO_2 stripping for pretreating brackish and wastewater desalination feed.* Desalination, Vol. 222, P. 50-58.

Kaluarachchi, J.J. and Parker, J.C., 1992. *Multiphase Flow with a simplified model for oil entrapment.* Transport in porous media, Vol. 7(1), P 1-14.

Kashchiev, D. and Firoozabadi, A., 1993. *Kinetics of the initial stage of isothermal gas phase formation*. Journal of chemistry physics, Vol. 98(6), P. 4690-4699.

Kazemian, S., Huat, B.B.K, Prasad, A. and Barhchi, M., 2010. *A review of stabilization of soft soils by injection of chemical grouting*. Australian journal of basic and applied sciences, Vol. 4(12), P. 5862-5868.

Knapp, R.B. 1989. *Spatial and temporal scales of local equilibrium in dynamic fluid-rock systems*. Geochimica et Cosmochimica Acta, Vol. 53(8), P. 1955-1964.

Kühn, M, 2004. *Reactive flow modeling of hydrothermal systems*. Springer-Verlag Berlin Heidelberg, P. 91-91.

Lioliou M.G., Paraskeva, P.G., Koutsoukos, P.G. and Payatakes, A.C., 2007. *Heterogeneous nucleation and growth on calcite and quartz*. Journal of colloid and interface science, Vol.308(2), P. 421-428

Michaelis, J., Usdowski, E. and Menschel, G., 1985. *Partitioning of ^{13}C and ^{12}C on the degassing of CO_2 and the precipitaion of calcite - Rayleigh type fractionation and a kinetic model.* American Journal of Science, Vol. 285, P. 318 - 327.

Molins, S. Trebotich, D., Steefel, C.I., Shen, C., 2012. *An investigation of the effect of pore scale flow on average geochemical reaction rate using direct numerical simulation*. Water Resources Research, doi:10.1029/2011WR011404, in press.

Morse, J.W., Arvidson, R.S. and Lüttge, A., 2007. *Calcium carbonate formation and dissolution*. Chemical reviews, Vol. 107(2), P. 342-381.

Nambi, I.M. and Power, S.E., 2003. *Mass transfer correlations for nonaqueous phase liquid dissolution from regions with high initial saturations.* Water Resources Research, Vol 39., 1030, doi:10.1029/2001WR000667.

Noiriel, C., Steefel, C.I., Yang, L. and Ajo-Franklink, J., 2011. *Upscaling calcium carbonate precipitation rates from pore to continuum scale.* Chemical Geology, Vol. 318-319, P. 60-74.

Parker, J.C. and Lenhard, R.J., 1987. *A model for hysteric constitutive relations governing multiphase flow, 1. Saturation-pressure relations*. Water Resources Research, Vol. 23, P. 2187-2196.

Parkhurst, D. L. and Appelo, C.A.J., 1999. *User's Guide to PHREEQC (Version 2) A Computer Program for Speciation, Batch-Reaction, One-Dimensional Transport, and Inverse Geochemical Calculations.* Water Resources Investigations report 99-4259, P. 1-312.

Powers, J.P., Corwin, A.B., Schmall, P.C. and Kaeck, W.E., 2007. *Construction dewatering and groundwater control: New methods and applications*. Edition 3. John Wiley & Sons Inc. Hoboken, New Jersey, P. 410-491.

Rosa, S. and Lundager Madsen, H.E., 2011. *Kinetics of mass crystallization of calcium carbonate at 25, 30 and 37 ^{0}C*. Journal of crystal growth, Vol. 318(1), P. 99-102.

Sheikholeslami, R. and Ong, H.W.K., 2003 Kinetics and thermodynamics of calcium carbonate and calcium sulfate at salinities up to 1.5 M. Desalination, Vol. 157. P.217-234.

Sheperd, R.G., 1989. *Correlations of permeability and grain size.* Ground water, Vol. 27(5), P. 633-638.

Soil Survey Staff, 1998. *Keys to Soil Taxonomy*. Edition 8, United states Department of Agriculture. Natural Resources Conservation Service, P. 317.

Steefel C.I. and Lasaga, A.C., 1994. *A coupled model for transport of multiple chemical species and kinetic precipitation/dissolution reactions with application to reactive flow in single phase hydrothermal systems.* American Journal of Science, Vol. 294., P. 529 – 592.

Van Genuchten, M. Th., 1980. *A closed-form equation for predicting the hydraulic conductivity of unsaturated soils.* Soil Science Social American Journal, Vol. 44(5), P. 892-898.

Van Oss H.G. and Padovani, 2003. *Cement manufacture and the environment.* A.C. Journal of Industrial Ecology, Vol. 7(1), P. 93-126.

Van Paassen, L.A., Ghose, R., van der Linden, T.J.M., van der Star, W.R.L. and van Loosdrecht, M.C.M., 2010. *Quantifying biomediated ground improvement by ureolysis: Large-scale Biogrout experiment.* Journal of geotechnical and geoenvironmental engineering, Vol. 136(12), P. 1721-1728.

Van der Ruyt, M. and van der Zon, W., 2009. *Biological in situ reinforcement of sand in near-shore areas*. Proceedings of the Institution of Civil Engineers: Geotechnical Engineering, Vol 162, P. 81–83.

Van der Star, W.R.L. and Hartog, N., 2012 *EcoGrout: Feasibility of in situ calcium carbonate precipitation*. Confidential report of Deltares, P. 1-11.

Van Wijngaarden, W.K., Vermolen, F.J., van Meurs, G.A.M. and Vuik, C., 2011. *Modelling Biogrout: A new ground improvement method based on microbial induced carbonate precipitation.* Transport in porous media, Vol. 87, P. 397-420.

Van Wijngaarden, W.K., Vermolen, F.J., van Meurs, G.A.M. and Vuik, C., 2012. *A mathematical model and analytical solution for the fixation of bacteria in Biogrout.* Transport in porous media, Vol. 92, P. 847-866.

Whiffin, V.S., van Paassen, L.A. and Harkes, M.P., 2007. *Microbial carbonate precipitation as a soil improvement technique*. Geomicrobiology Journal, Vol. 24(5), P. 417–423.

White, M.D. and Oostrom, M., 2000. *STOMP: Subsurface transport over multiple phases. Version 2.0 Theory Guide.* Pacific Northwest National Laboratory, http://stomp.pnnl.gov.

White, M.D. and McGrail, B.P., 2005. *STOMP: Subsurface Transport Over Multiple Phases; Addendum: ECKEChem (Equilibrium-Conservation-Kinetic Equation Chemistry and Reactive Transport), Version 1.* Pacific Northwest National Laboratory, http://stomp.pnnl.gov.

White, M.D. and Oostrom, M., 2006. *STOMP: Subsurface transport over multiple phases. Version 4.0 User Guide.* Pacific Northwest National Laboratory, http://stomp.pnnl.gov.

Zhao, W. and Ioannidis, M.A., 2011. *Gas exsolution and flow during supersaturated water injection in porous media: 1. Pore network modelling.* Advances in water resources, Vol. 34(1), P 2-14.

Appendices

A.1 Debye-Hückel equation

The activity of the ions in the batch chemistry are determined by using the Debye-Hückel equation. The chemical activity of an ion is equal to the molal concentration of the ion times a factor known as the activity coefficient.

$$a_x = [X]\gamma_x$$

The activity coefficient varies with the total amount of cations and anions in a solution. The concentration and charge of these ions will determine the ionic strength of the solution. The Debye-Hückel equation is used to determine the activity coefficient.

$$-\log\gamma_i = \frac{Az_i^2\sqrt{I}}{1 + d_i B\sqrt{I}}$$

Where
γ_i = the activity coefficient of species i
z_i = the charge on ionic species i
d_i = the effective diameter of ion species i
A = 0.5085 at 25 ^{0}C
B = 0.3281 at 25 ^{0}C
I = ionic strength of the solution

The ionic strength is calculated:

$$I = \frac{1}{2}\sum m_i z_i^2$$

Where:
m_i = molality of species i

The charge of the ionic species and the effective diameter of the ion species used in our model are shown in table A1.

Table A1. *Values of the effective ionic diameter and ionic charge of the modelled species.*

Species	Ionic charge	Effective ionic diameter [Å]
H^+	+1	9
OH^-	-1	3.5
HCO_3^-	-1	4.5
CO_3^{2-}	-2	5
Ca^{2+}	+2	6

A.2 Capillary pressure-Saturation functions

The average van Genuchten soil parameters for the 12 soil textural groups of the USDA-SCS classification system are determined by Carsel et al. (1988). For a given soil the textural class can be determined by its sand, silt and clay content, using the texture triangle (*see Fig. A2.1*). Sandy soils consist mainly of coarse sand. The loamy soils can be considered as moderately coarse to moderately fine sand and contain many subdivisions in the textural triangle. In our model the van Genuchten capillary pressure-saturation characteristics of the soil are assumed to be loamy sand to sandy loam to account for fine sand. This is done by setting α to 0.045 cm^{-1} and n to 1.68 in the STOMP simulator. In Fig. A2.2 the soil retention curves are shown using the van Genuchten parameters of our model and the soil retention curves based on the experimental dataset of Carsel et al. (1988).

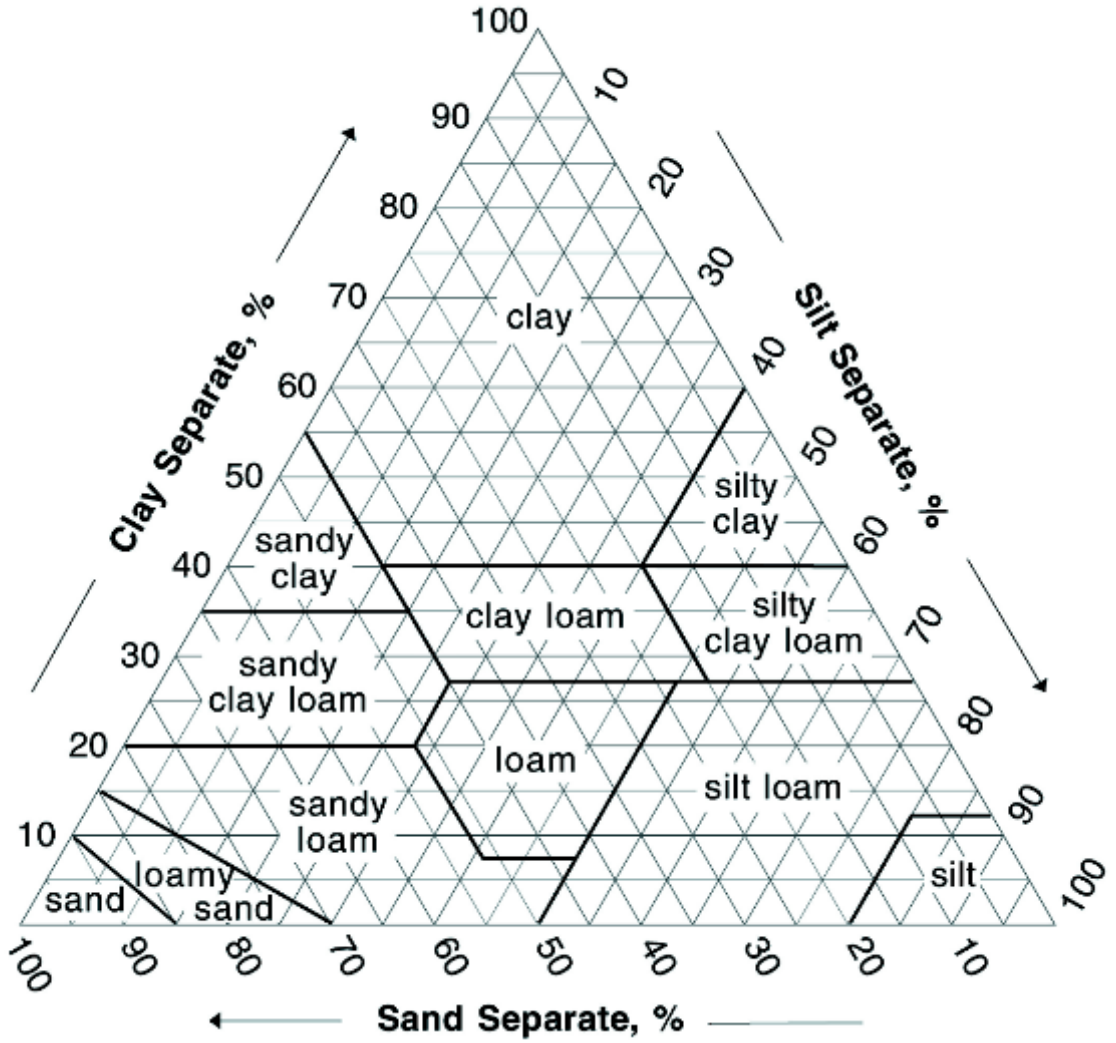

Fig. A2.1. *Soil textural classes in the U.S. texture triangle.(Soil Survey Staff, 1998)*

Table A2. *Average values of the van Genuchten soil parameters obtained by experimental means (Carsel et al.,1988)*

Soil texture	***Porosity [-]***	***Irreducible water content [-]***	***Saturated hydraulic conductivity [cm/hr]***	***α-parameter [1/cm]***	***n-parameter***
Clay Loam	0.41	0.095	0.26	0.019	1.31
Loam	0.43	0.078	1.04	0.036	1.56
Loamy sand	0.41	0.057	14.59	0.124	2.28
Silt	0.46	0.034	0.25	0.016	1.37
Silt loam	0.45	0.067	0.45	0.020	1.41
Sility clay	0.36	0.070	0.02	0.005	1.09
Silty clay loam	0.43	0.089	0.07	0.010	1.23
Sand	0.43	0.045	29.70	0.145	2.68
Sandy Clay	0.38	0.100	0.12	0.027	1.23
Sandy clay loam	0.39	0.100	1.31	0.059	2.68
Sandy loam	0.41	0.065	4.42	0.075	1.89

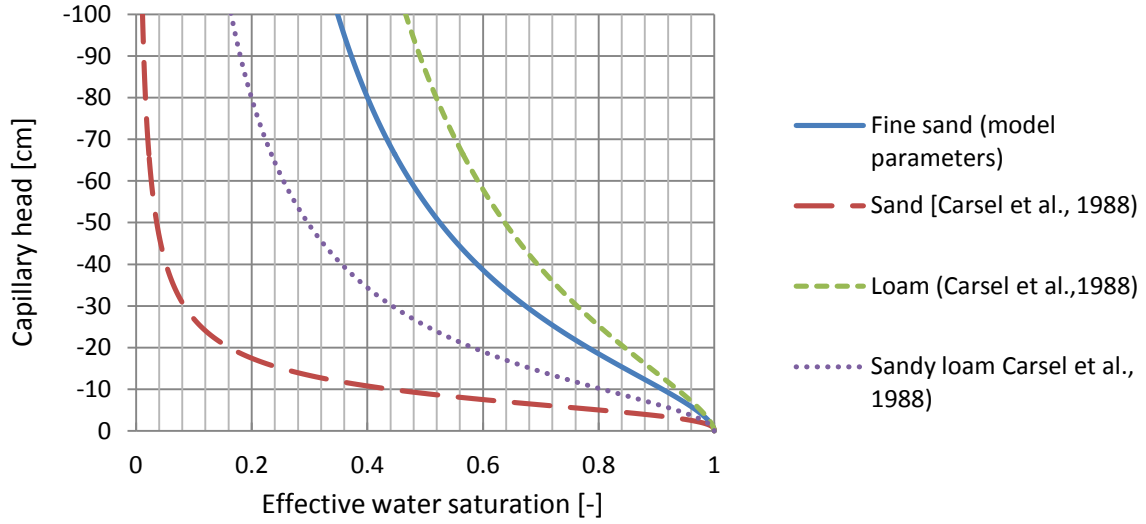

Figure A2.2. *The capillary pressure-saturation relationship using the van Genuchten function and the parameters listed in table A2. The model parameters are: α = 0.045 cm^{-1} , n = 1.68.*

A.3 PHREEQC calculations on species configuration of EcoGrout solutions

Case 1: Initial & final species assemblage of the EcoGrout solution

Table A3.1. *PHREEQC species assemblage for reacting 0.1875 mol/L Ca^{2+} and 0.375 mol/l HCO_3^-, assuming a closed system and calcite equilibrium.*

Species	Molality	Activity	log Molality	log Activity	Gamma
H+	3.24E-06	2.77E-06	-5.49	-5.558	-0.068
CO2	1.69E-01	1.71E-01	-0.772	-0.767	0.005
HCO3-	3.29E-02	2.73E-02	-1.483	-1.563	-0.08
CO3-2	9.70E-07	4.63E-07	-6.013	-6.334	-0.321
Ca+2	1.49E-02	7.15E-03	-1.826	-2.145	-0.32
CaHCO3+	3.00E-03	2.50E-03	-2.523	-2.603	-0.08
CaCO3	5.50E-06	5.57E-06	-5.259	-5.255	0.005
CaOH+	5.18E-10	4.27E-10	-9.285	-9.369	-0.084
Total Ca	1.76E-02				
	SI	**log(IAP)**	**log K_{sp}**	**log(ICP)**	
Calcite	0	-8.48	-8.48	-7.84	
CO2(g)	5.03 atm	-0.77	-1.47		

Table A3.2. *PHREEQC species assemblage for reacting 0.1875 mol/L Ca^{2+} and 0.375 mol/L HCO_3^-, assuming a pCO_2 of 1.1 atm and calcite equilibrium.*

Species	Molality	Activity	log Molality	log Activity	Gamma
H+	1.20E-06	1.06E-06	-5.92	-5.976	-0.056
CO2	3.72E-02	3.74E-02	-1.429	-1.427	0.003
HCO3-	1.83E-02	1.58E-02	-1.738	-1.803	-0.065
CO3-2	1.27E-06	7.00E-07	-5.896	-6.155	-0.259
Ca+2	8.59E-03	4.74E-03	-2.066	-2.325	-0.259
CaHCO3+	1.10E-03	9.52E-04	-2.957	-3.022	-0.065
CaCO3	5.53E-06	5.57E-06	-5.257	-5.255	0.003
CaOH+	8.69E-10	7.43E-10	-9.061	-9.129	-0.068
Total Ca	9.70E-03				
	SI	**log(IAP)**	**log K_{sp}**	**log(ICP)**	
Calcite	0	-8.48	-8.48	-7.96	
pCO_2	1.1 atm	-1.43	-1.47		

Case 2: Initial & final species assemblage of the EcoGrout solution

Table A3.3. *PHREEQC species assemblage for reacting 0.1875 mol/L $CaCl_2$ and 0.375 mol/L $NaHCO_3$, assuming a closed system and calcite equilibrium.*

Species	Molality	Activity	log Molality	log Activity	Gamma
H+	3.33E-06	2.56E-06	-5.478	-5.592	-0.114
CO2	1.61E-01	1.79E-01	-0.792	-0.748	0.044
HCO3-	4.36E-02	3.05E-02	-1.36	-1.515	-0.155
CO3-2	2.34E-06	5.59E-07	-5.631	-6.252	-0.621
Ca+2	2.22E-02	5.92E-03	-1.653	-2.228	-0.574
CaHCO3+	3.30E-03	2.31E-03	-2.482	-2.637	-0.155
CaCO3	5.03E-06	5.57E-06	-5.299	-5.255	0.044
CaOH+	5.16E-10	3.78E-10	-9.287	-9.423	-0.136
Na+	3.70E-01	2.63E-01	-0.432	-0.58	-0.148
NaHCO3	4.09E-03	4.52E-03	-2.389	-2.345	0.044
NaCO3-	3.75E-06	2.74E-06	-5.426	-5.562	-0.136
NaOH	6.04E-10	6.68E-10	-9.219	-9.175	0.044
Cl-	3.74E-01	2.44E-01	-0.427	-0.612	-0.185
Total Ca	2.55E-02				
	SI	**log(IAP)**	**log K_{sp}**	**log(ICP)**	
Calcite	0	-8.48	-8.48	-7.28	
pCO_2	5.25 atm	-0.75	-1.47		

Table A3.4. *PHREEQC species assemblage for reacting 0.1875 mol/L $CaCl_2$ and 0.375 molL $NaHCO_3$, assuming a pCO_2 of 1.1 atm and calcite equilibrium.*

Species	Molality	Activity	log Molality	log Activity	Gamma
H+	1.19E-06	9.16E-07	-5.925	-6.038	-0.113
CO2	3.41E-02	3.74E-02	-1.468	-1.427	0.041
HCO3-	2.55E-02	1.79E-02	-1.594	-1.747	-0.153
CO3-2	3.75E-06	9.17E-07	-5.426	-6.037	-0.612
Ca+2	1.34E-02	3.61E-03	-1.873	-2.442	-0.569
CaHCO3+	1.17E-03	8.26E-04	-2.93	-3.083	-0.153
CaCO3	5.06E-06	5.57E-06	-5.296	-5.255	0.041
CaOH+	8.82E-10	6.45E-10	-9.054	-9.19	-0.136
Na+	3.71E-01	2.65E-01	-0.43	-0.577	-0.147
NaHCO3	2.43E-03	2.67E-03	-2.615	-2.573	0.041
NaCO3-	6.20E-06	4.53E-06	-5.208	-5.344	-0.136
NaOH	1.71E-09	1.89E-09	-8.766	-8.725	0.041
Cl-	3.74E-01	2.46E-01	-0.427	-0.609	-0.182
Total Ca	1.46E-02				
	SI	**log(IAP)**	**log K_{sp}**	**log(ICP)**	
Calcite	0	-8.48	-8.48	-7.30	
pCO_2	1.1 atm	-1.43	-1.47		

Case 5: Initial species assemblage of the EcoGrout solution

Table A3.5. *PHREEQC species assemblage for reacting 0.1875 mol/L $CaCl_2$ and 0.375 mol/L $NaHCO_3$, assuming a fixed pCO_2 of 5.15 atm and slight calcite supersaturation at Ω_{calc} =1.8.*

Species	Molality	Activity	log Molality	log Activity	Gamma
H+	2.68E-06	2.27E-06	-5.572	-5.645	-0.073
CO2	1.73E-01	1.75E-01	-0.762	-0.756	0.006
HCO3-	4.19E-02	3.43E-02	-1.378	-1.465	-0.087
CO3-2	1.59E-06	7.09E-07	-5.8	-6.149	-0.349
Ca+2	1.87E-02	8.41E-03	-1.728	-2.075	-0.347
CaHCO3+	4.49E-03	3.68E-03	-2.347	-2.435	-0.087
CaCO3	9.88E-06	1.00E-05	-5.005	-4.999	0.006
CaOH+	7.57E-10	6.13E-10	-9.121	-9.212	-0.091
Total Ca	2.55E-02				
	SI	**log(IAP)**	**log K_{sp}**	**log(ICP)**	
Calcite	0.26	-8.22	-8.48	-7.53	
pCO_2	5.15 atm	-0.75	-1.47		

Case 6: Initial species assemblage of the EcoGrout solution

Table A3.6. *PHREEQC species assemblage for reacting 0.375 mol/L $CaCl_2$ and 0.1875 mol/L $NaHCO_3$, assuming a fixed pCO_2 of 11.0 atm and slight calcite undersaturation at Ω_{calc} = 0.66.*

Species	Molality	Activity	log Molality	log Activity	Gamma
H+	6.23E-06	5.30E-06	-5.205	-5.276	-0.071
CO2	3.71E-01	3.76E-01	-0.431	-0.425	0.006
HCO3-	3.80E-02	3.13E-02	-1.42	-1.504	-0.084
CO3-2	6.04E-07	2.77E-07	-6.219	-6.557	-0.338
Ca+2	1.71E-02	7.89E-03	-1.767	-2.103	-0.336
CaHCO3+	3.83E-03	3.15E-03	-2.417	-2.502	-0.084
CaCO3	3.63E-06	3.67E-06	-5.441	-5.435	0.006
CaOH+	3.01E-10	2.45E-10	-9.522	-9.61	-0.088
Total Ca	2.09E-02				
	SI	**log(IAP)**	**log K_{sp}**	**log(ICP)**	
Calcite	-0.18	-8.66	-8.48	-8.00	
pCO_2	11.00 atm	-0.43	-1.47		

Case: Initial & final species assemblage of an EcoGrout solution with 0.3 mol/L HCl

Table A3.7. *Initial PHREEQC species assemblage for 0.1875 mol/L Ca^{2+}, 0.375 mol/l HCO_3^- and 0.3 mol/L HCl.*

Species	Molality	Activity	log Molality	log Activity	Gamma
H+	5.72E-06	4.37E-06	-5.242	-5.359	-0.117
CO2	2.98E-01	3.35E-01	-0.525	-0.474	0.051
HCO3-	4.87E-02	3.36E-02	-1.313	-1.473	-0.16
CO3-2	1.58E-06	3.61E-07	-5.801	-6.443	-0.641
Ca+2	1.61E-01	4.17E-02	-0.794	-1.38	-0.585
CaHCO3+	2.59E-02	1.79E-02	-1.587	-1.747	-0.16
CaCO3	2.25E-05	2.53E-05	-4.648	-4.597	0.051
CaOH+	2.13E-09	1.56E-09	-8.672	-8.807	-0.134
Cl-	2.98E-01	1.92E-01	-0.525	-0.717	-0.192
Total Ca	1.87E-01				
	SI	**log(IAP)**	**log K_{sp}**	**log(ICP)**	
Calcite	0	-8.48	-8.48	-6.60	
pCO_2	9.8 atm	-0.47	-1.47		

Table A3.8 *PHREEQC species assemblage for reacting 0.1875 mol/L Ca^{2+} and 0.375 mol/L HCO_3^-, assuming a pCO_2 of 1.1 atm and calcite equilibrium.*

Species	Molality	Activity	log Molality	log Activity	Gamma
H+	3.98E-06	3.06E-06	-5.4	-5.515	-0.056
CO2	3.37E-02	3.74E-02	-1.472	-1.427	0.003
HCO3-	7.75E-03	5.40E-03	-2.111	-2.267	-0.065
CO3-2	3.51E-07	8.29E-08	-6.455	-7.081	-0.259
Ca+2	1.51E-01	4.00E-02	-0.821	-1.398	-0.259
CaHCO3+	3.95E-03	2.75E-03	-2.403	-2.56	-0.065
CaCO3	5.01E-06	5.57E-06	-5.3	-5.255	0.003
CaOH+	2.94E-09	2.15E-09	-8.532	-8.667	-0.068
Cl-	2.98E-01	1.94E-01	-0.525	-0.712	
Total Ca	1.55E-01				
	SI	**log(IAP)**	**log K_{sp}**	**log(ICP)**	
Calcite	0	-8.48	-8.48	-7.28	
pCO_2	1.1 atm	-1.43	-1.47		

A.4 Domain plots of modelled cases

Final residual CO_2 concentrations

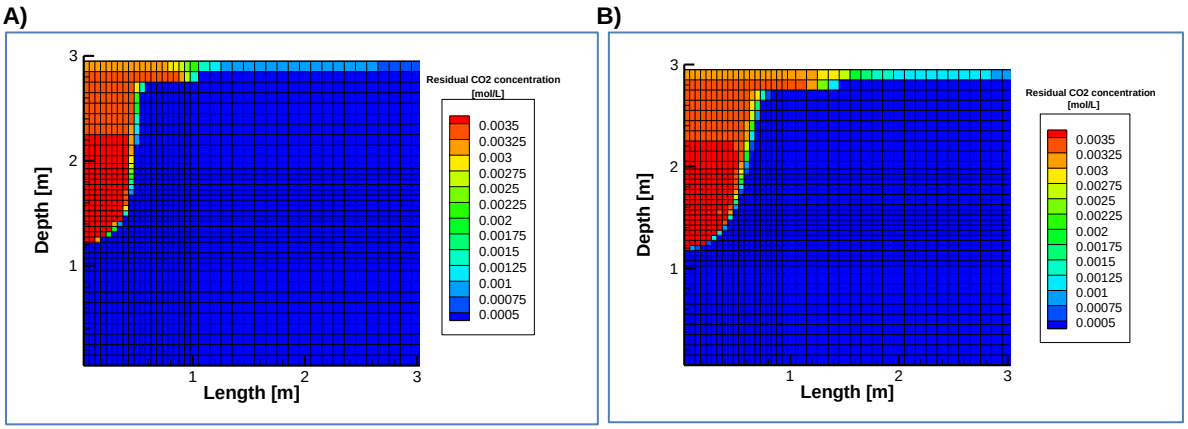

Fig. A4.1. *Residual CO_2 concentration [mol/L] at t = 600 min A) for Case 1 and B) for Case 6.*

Case 5: Gas saturation

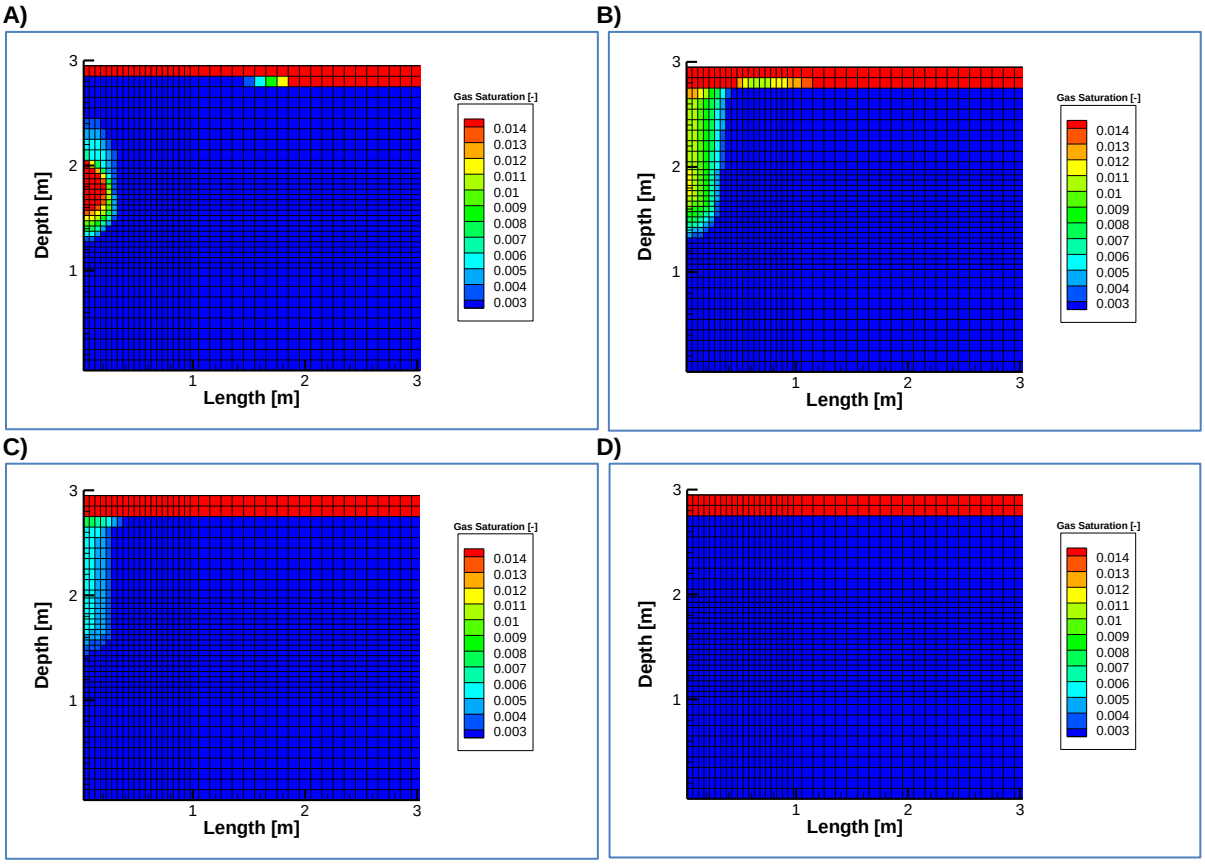

Fig. A4.2. *Gas saturations at respectively: A) 3 min, B) 20 min, C) 50 min and D) 600 min.*

Case 5: Calcite precipitation

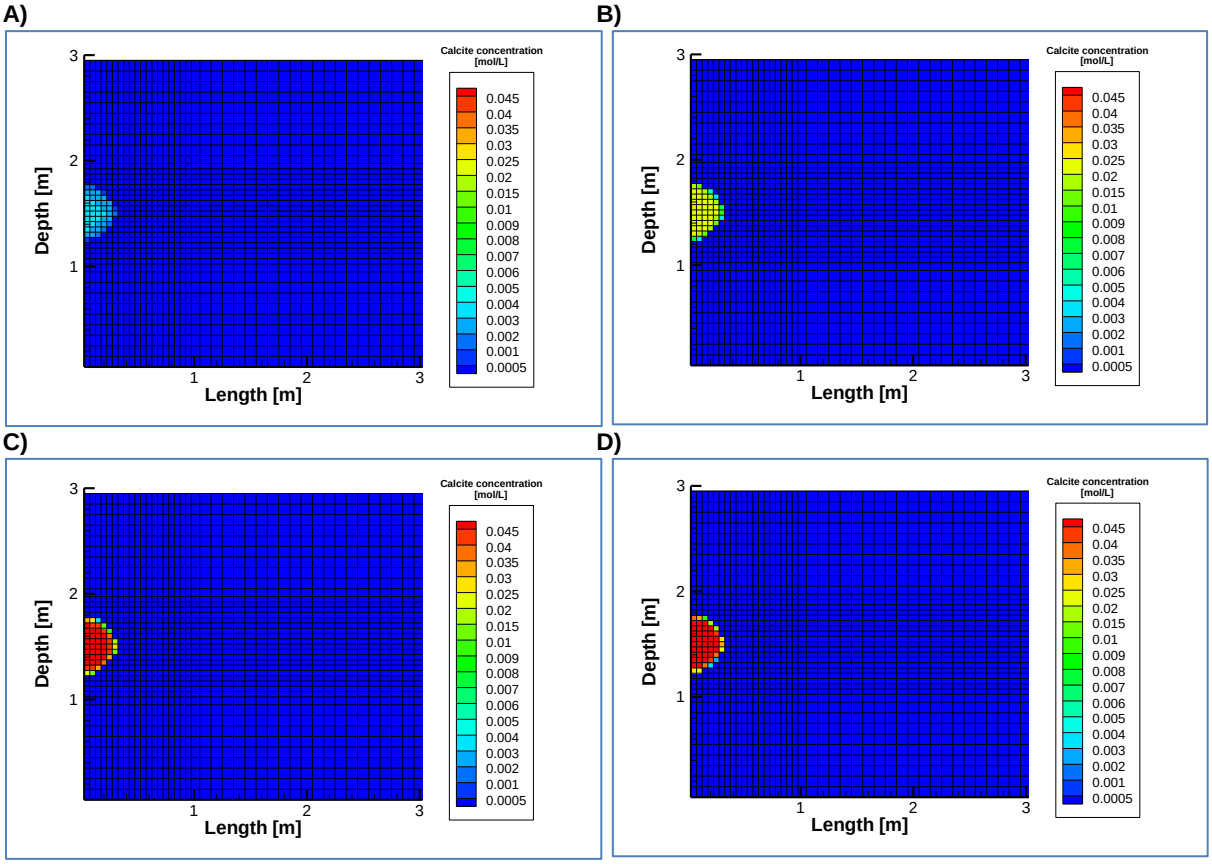

Fig. A4.3. *Calcite concentrations [mol/L] at respectively: A) 3 min, b) 20 min, C) 50 min and D) 600 min.*

Case 6: Calcite precipitation

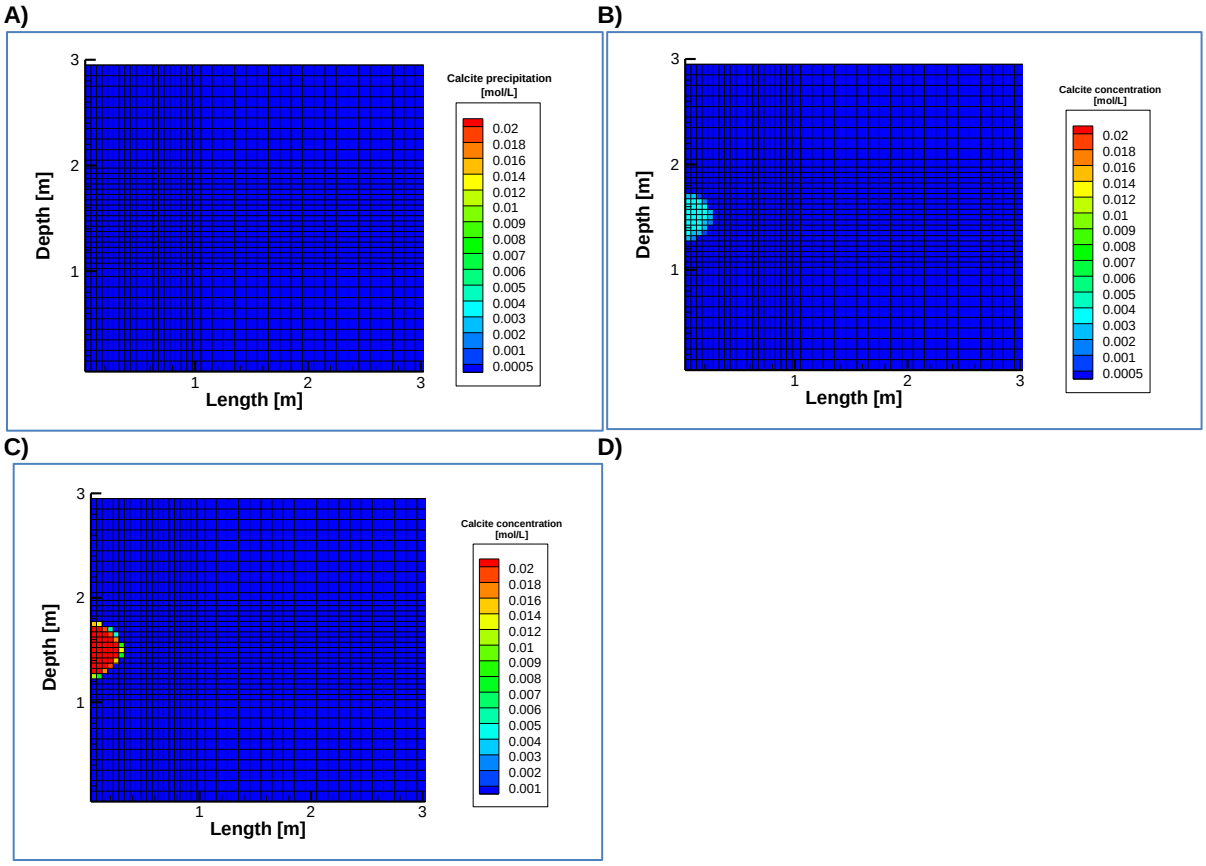

Fig. A4.4. *Calcite concentrations [mol/L] at respectively: A) 20 min, B) 50 min and C) 600 min. D) Residual CO_2 concentration [mol/L] at t = 600 min.*

A.5 Gas saturation and CO_2 gas mole fractions

A)

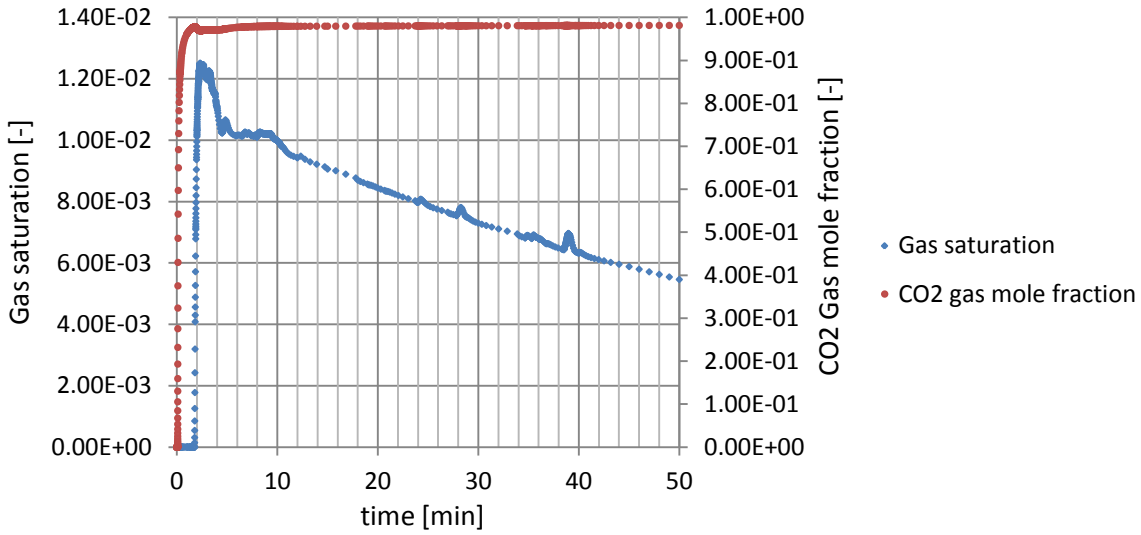

B)

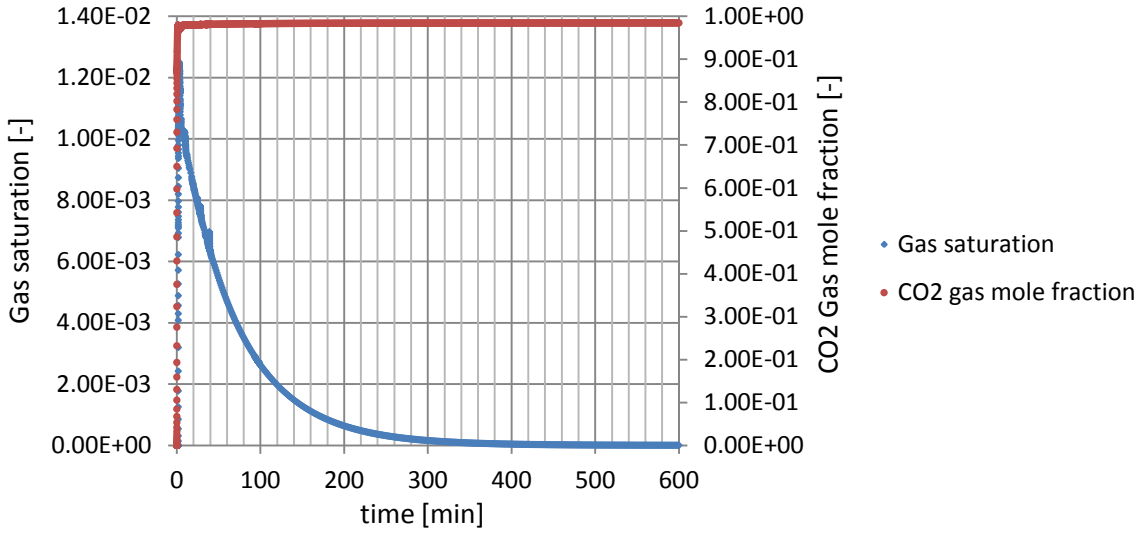

Fig. A5.1 *Gas saturation and CO_2 gas mole fraction breakthrough curve at [X=0.025, Z= 1.525, t] for Case 1 at A) the time interval 0<t<50 min and B) the time interval 0<t<600 min.*

A.6 Injection time for different porosities

The permeability of the porous medium will have a significant effect on the volumetric flow rate. In this model the Kozeny-Carmen relation (*see Eq. 57*) is used to describe the intrinsic permeability in terms of porosity. Darcy's law describes the flow rate in the STOMP simulator (Eq. 28):

$$V_l = \frac{k_{rl}\,\kappa}{\mu_l}(\nabla P_l + \rho_l g z)$$

To obtain the same injection volume as in Case 1 at reduced porosity, and thereby lower intrinsic permeability, the injection time should be increased. This is due to decreasing flow velocity whilst using the same injection pressure.

Assuming a fixed median grain diameter and injection pressure, the Kozeny-Karmen relationship can be used to estimate the injection time that is required to obtain the same injection radius:

$$\frac{\kappa_{\theta int}}{\kappa_\theta} = \frac{V_{\theta int}}{V_\theta} = \frac{t_{\theta int}}{t_\theta}$$

Starting with an injection time of 5 s and initial porosity of 0.4, the required injection time at different porosities can be calculated. In Fig. A.6 is shown the required injection time at a given porosity to obtain a constant volume of injected EcoGrout solution.

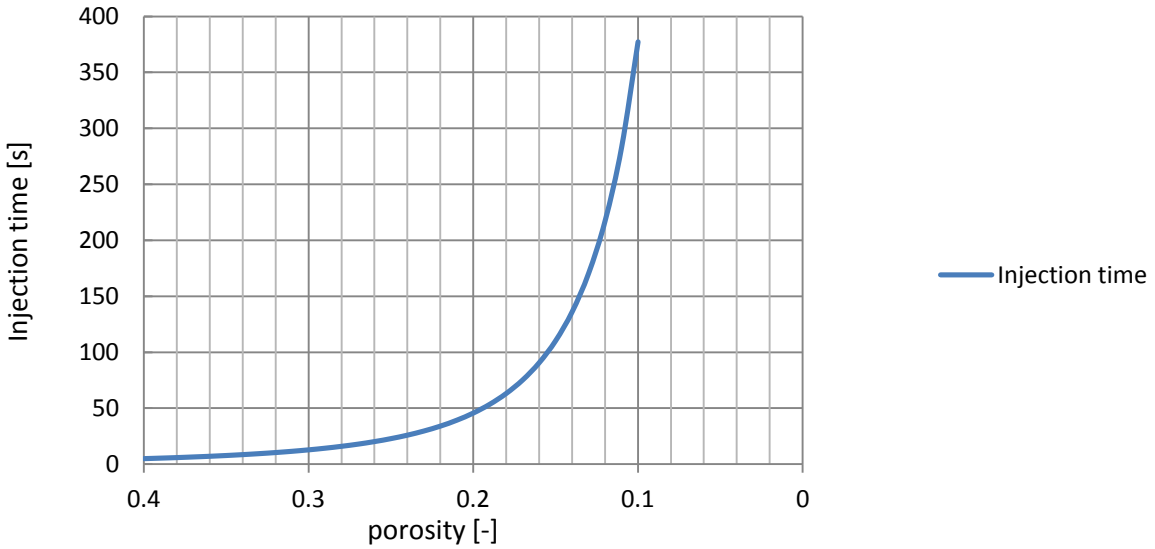

Fig. A6. *The injection time which is required to attain a constant volume of injected EcoGrout solution at different porosities.*

A.7 Darcy velocities during injection

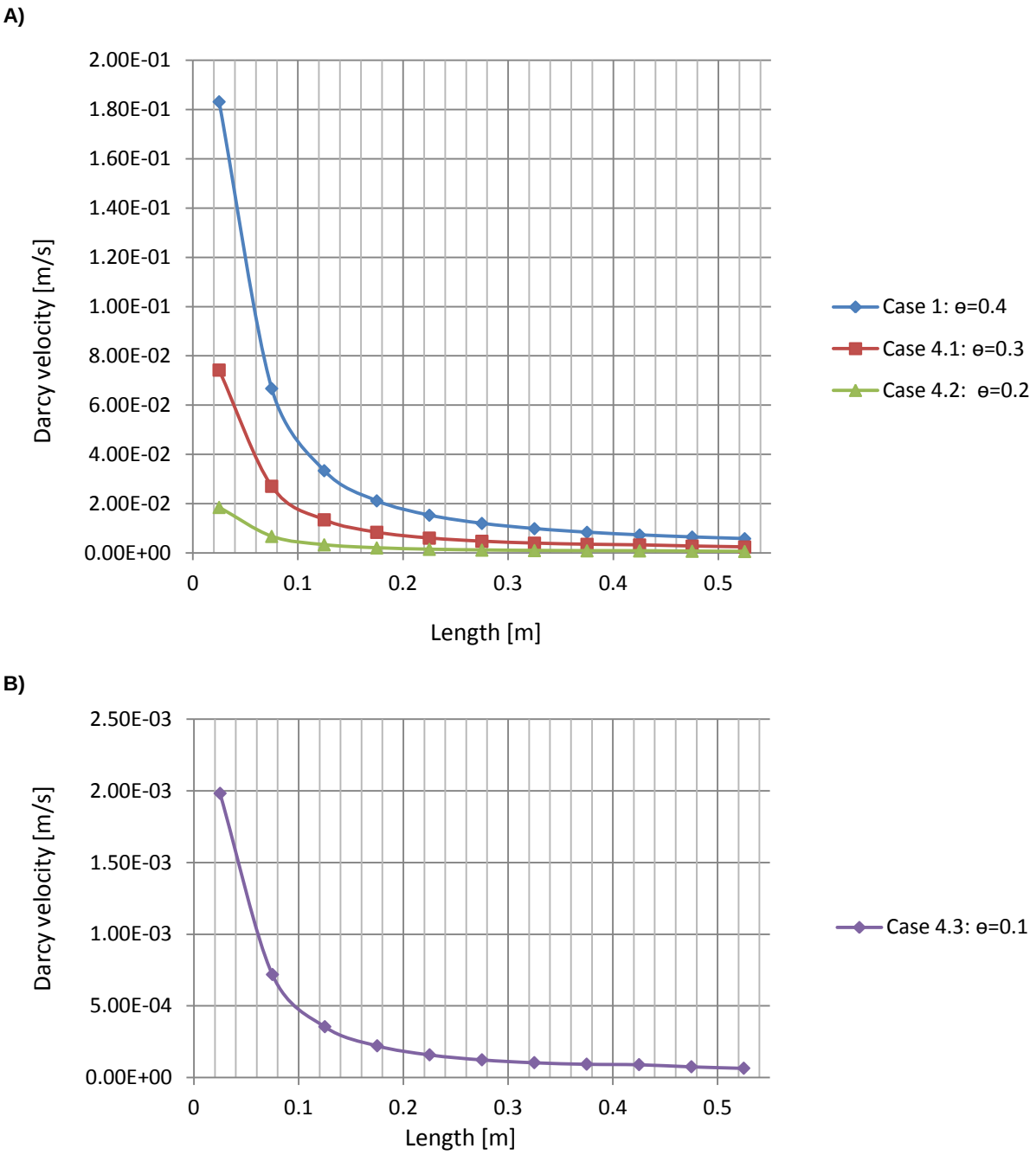

Fig. A7. *Darcy velocities modelled during the injection at [0.025<X<0.525, 1.5] for A) Cases 1, 4.1 and 4.2 at t = 2 s and B) Case 4.3.*

A.8 Case 1: Injection of a solution with the PHREEQC species configuration

Table A8. *Initial and pulse species concentrations at grid cell [X=0.225, Z=1.525]*

Species	Input pulse concentration	Pulse concentration at t = 1.5 s	Concentration at t = 100 min
pH	-	5.6	6.1
CO_2(aq)	0.169 [mol/L]	0.169 [mol/L]	5.90e-2 [mol/L]
HCO_3^-	3.3e-2 [mol/L]	3.090e-2 [mol/L]	3.53e-2 [mol/L]
CO_3^{2-}	9.8e-8 [mol/L]	5.959e-7 [mol/L]	2.23e-6 [mol/L]
Ca^{2+}	1.5e-2 [mol/L]	1.290e-2 [mol/L]	1.50e-3 [mol/L]
$CaHCO_3^+$	3.0e-3 [mol/L]	5.096e-3 [mol/L]	6.78e-4 [mol/L]
CO_2gas (fictional)	-	0.0 [mol/L]	4.09e-3 [mol/L]
$CaCO_3$(s)	-	4.156e-5 [mol/L]	1.58e-2 [mol/L]
PV calcite	-	-	2.33e-4 [-]

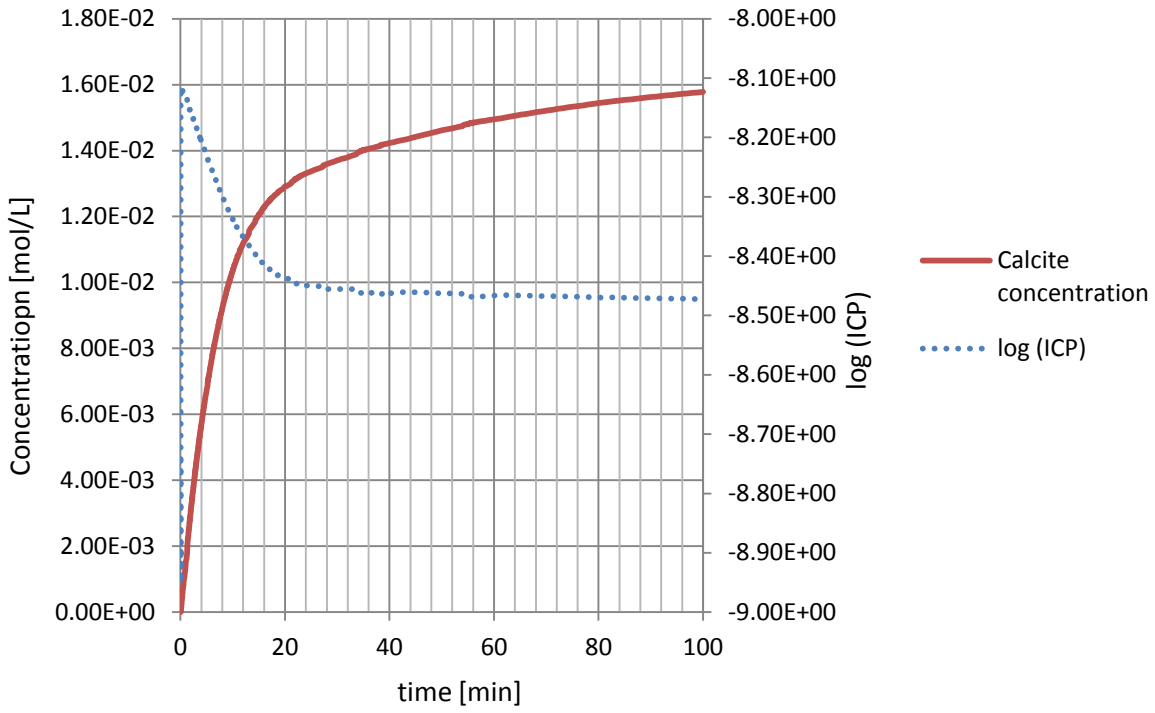

Fig. A8. *Precipitated calcite and ICP over time at [X=0.225, Z=1.525]*

A.9 Case 1: Injection of a solution with adapted K_{sp}

In this case the calcite solubility product was reduced to 7.84 mol^2/L^2, to model calcite precipitation from a solution with a balanced species configuration.

Table A9. *Initial and pulse species concentrations at grid cell [X=0.225, Z=1.525]*

Species	Input pulse concentration	Pulse concentration at t = 5 s	Concentration at t = 600 min
pH	-	5.7	6.3
CO_2(aq)	0.170 [mol/L]	0.170 [mol/L]	3.80e-2 [mol/L]
HCO_3^-	3.6e-2 [mol/L]	3.60e-2 [mol/L]	3.60e-2 [mol/L]
CO_3^{2-}	9.7e-7 [mol/L]	5.58e-7 [mol/L]	3.60e-6 [mol/L]
Ca^{2+}	1.8e-2 [mol/L]	1.80e-2 [mol/L]	4.02e-3 [mol/L]
$CaHCO_3^+$	Not modelled	Not modelled	Not modelled
CO_2gas (fictional)	-	0.0 [mol/L]	3.75e-3 [mol/L]
$CaCO_3$(s)	-	2.32e-8 [mol/L]	1.39e-3 [mol/L]
PV calcite	-	-	2.05e-4 [-]

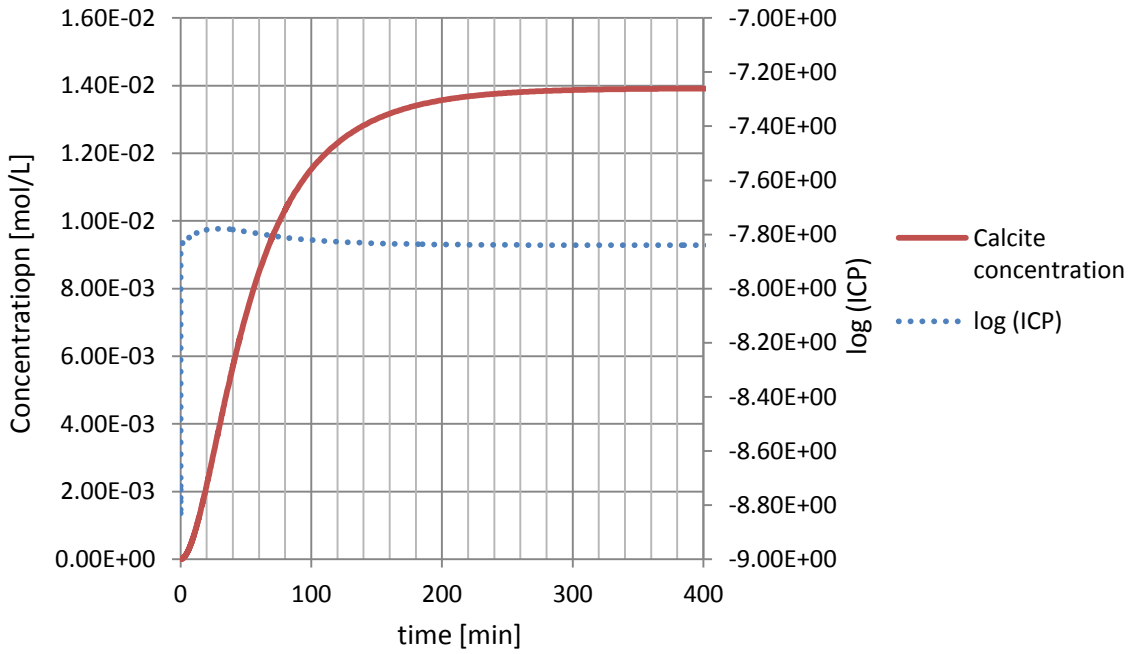

Fig. A9. *Precipitated calcite and ICP over time at [X=0.225, Z=1.525]*